AD-A182 741 A NUMERICAL MODEL FOR SHOALING AND REFRACTION OF SECOND-ORDER CNOIDAL WAV (U) COASTAL ENGINEERING RESEARCH CENTER VICKSBURG MS T A HARDY ET AL MAY 86 1/3

UNCLASSIFIED CERC-MP-87-9 F/G 20/4 NL

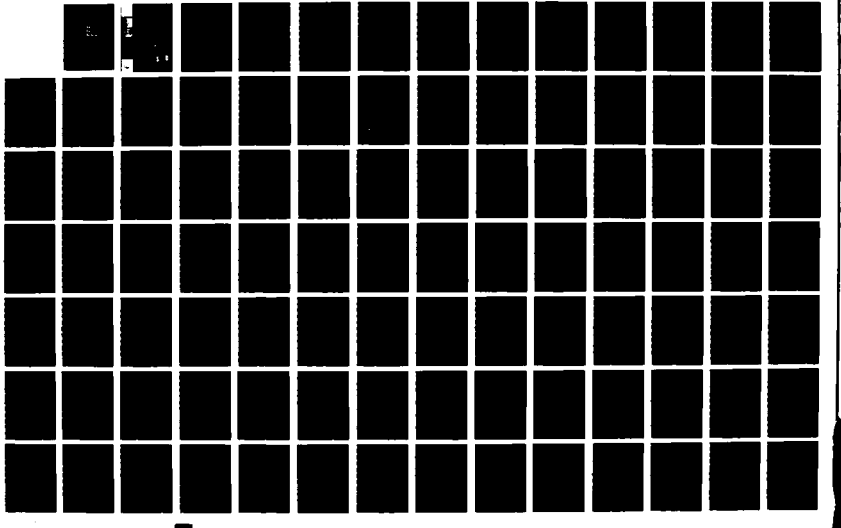

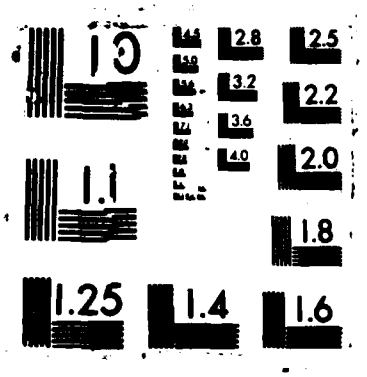
2.8
2.5
3.2
2.2
3.6
4.0
2.0
1.1
1.8
1.25
1.4
1.6

MISCELLANEOUS PAPER CERC-87-9

A NUMERICAL MODEL FOR SHOALING AND REFRACTION OF SECOND-ORDER CNOIDAL WAVES OVER AN IRREGULAR BOTTOM

by

Thomas A. Hardy, Nicholas C. Kraus

Coastal Engineering Research Center

DEPARTMENT OF THE ARMY
Waterways Experiment Station, Corps of Engineers
PO Box 631, Vicksburg, Mississippi 39180-0631

May 1987
Final Report

Prepared for DEPARTMENT OF THE ARMY
US Army Corps of Engineers
Washington, DC 20314-1000

US Army Corps of Engineers

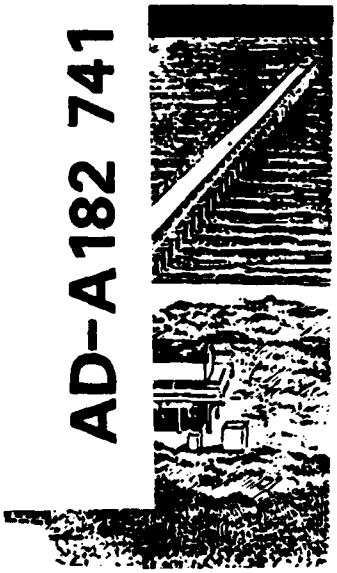

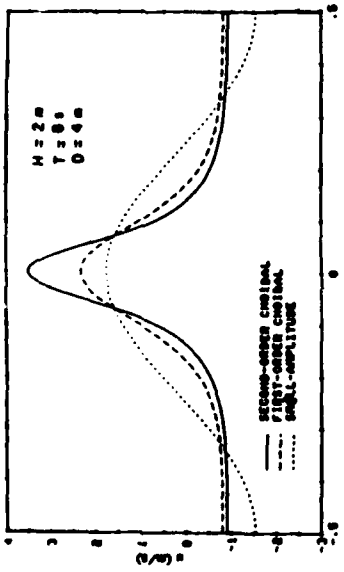

COASTAL ENGINEERING RESEARCH CENTER

Destroy this report when no longer needed. Do not return it to the originator.

The findings in this report are not to be construed as an official Department of the Army position unless so designated by other authorized documents.

The contents of this report are not to be used for advertising, publication, or promotional purposes. Citation of trade names does not constitute an official endorsement or approval of the use of such commercial products.

Unclassified
SECURITY CLASSIFICATION OF THIS PAGE

ADA182741

REPORT DOCUMENTATION PAGE

Form Approved
OMB No 0704-0188
Exp. Date Jun 30, 1986

1a. REPORT SECURITY CLASSIFICATION Unclassified	1b. RESTRICTIVE MARKINGS
2a. SECURITY CLASSIFICATION AUTHORITY	3. DISTRIBUTION/AVAILABILITY OF REPORT Approved for public release; distribution unlimited.
2b. DECLASSIFICATION/DOWNGRADING SCHEDULE	
4. PERFORMING ORGANIZATION REPORT NUMBER(S) Miscellaneous Paper CERC-87-9	5. MONITORING ORGANIZATION REPORT NUMBER(S)
6a. NAME OF PERFORMING ORGANIZATION USAEWES, Coastal Engineering Research Center 6b. OFFICE SYMBOL (If applicable)	7a. NAME OF MONITORING ORGANIZATION
6c. ADDRESS (City, State, and ZIP Code) PO Box 631 Vicksburg, MS 39180-0631	7b. ADDRESS (City, State, and ZIP Code)
8a. NAME OF FUNDING/SPONSORING ORGANIZATION US Army Corps of Engineers 8b. OFFICE SYMBOL (If applicable)	9. PROCUREMENT INSTRUMENT IDENTIFICATION NUMBER
8c. ADDRESS (City, State, and ZIP Code) Washington, DC 20314-1000	10. SOURCE OF FUNDING NUMBERS PROGRAM ELEMENT NO. / PROJECT NO. / TASK NO. / WORK UNIT ACCESSION NO

11. TITLE (Include Security Classification)
A Numerical Model for Shoaling and Refraction of Second-Order Cnoidal Waves over an Irregular Bottom

12. PERSONAL AUTHOR(S)
Hardy, Thomas A., Kraus, Nicholas C.

13a. TYPE OF REPORT	13b. TIME COVERED	14. DATE OF REPORT (Year, Month, Day)	15. PAGE COUNT
Final Report	FROM Jan 85 TO Apr 86	May 1986	200

16. SUPPLEMENTARY NOTATION
Available from National Technical Information Service, 5285 Port Royal Road, Springfield, VA 22161.

17. COSATI CODES			18. SUBJECT TERMS (Continue on reverse if necessary and identify by block number)
FIELD	GROUP	SUB-GROUP	Mathematical models (LC) Shoaling (WES) Water waves (LC)

19. ABSTRACT (Continue on reverse if necessary and identify by block number)

A numerical model for calculating shoaling and refraction of finite-amplitude waves in shallow water is presented. The model is designed to employ second-order cnoidal wave theory, but first-order cnoidal theory can be used also. A brief review of water-wave theory is given, followed by an outline of a second-order cnoidal wave theory derivation. A description is provided of the basic similarities and differences between cnoidal wave theory and the more commonly used small-amplitude wave theory. Methods for the efficient calculation of cnoidal wave theory are derived and used in the model. The model calculates wave height and direction directly at numerical grid points, resulting in a greater ease in calculation over models using the ray tracing method. A derivation is given of an expression for the energy flux of second-order cnoidal waves which is used in the calculation of wave height. The irrotationality wave number equation, adapted

(Continued)

20. DISTRIBUTION/AVAILABILITY OF ABSTRACT	21. ABSTRACT SECURITY CLASSIFICATION
☒ UNCLASSIFIED/UNLIMITED ☐ SAME AS RPT. ☐ DTIC USERS	Unclassified
22a. NAME OF RESPONSIBLE INDIVIDUAL	22b. TELEPHONE (Include Area Code) / 22c. OFFICE SYMBOL

DD FORM 1473, 84 MAR — 83 APR edition may be used until exhausted. All other editions are obsolete.

SECURITY CLASSIFICATION OF THIS PAGE
Unclassified

19. ABSTRACT (CONTINUED).

for cnoidal wave theory, was used to calculate the wave angle. Model results for shoaling and refraction over a plane bottom showed that second-order cnoidal waves shoaled more than small-amplitude waves but less than first-order cnoidal waves and refracted less than small-amplitude waves but more than first-order cnoidal waves. Second-order cnoidal waves were found to match experimental shoaling data more accurately than either small-amplitude or first-order cnoidal waves. Simulations for waves traveling over nonplane bathymetries consisting of a trench and a shoal proved that the model could perform excellently over a nonplanar bottom with reasonably smooth contours.

PREFACE

The investigation described herein was authorized as a part of the Civil Works Research and Development Program by the Office, Chief of Engineers (OCE), US Army Corps of Engineers. Work was performed under the Surf Zone Sediment Transport Processes work unit which is part of the Shore Protection and Restoration Program at the Coastal Engineering Research Center (CERC) of the US Army Engineer Waterways Experiment Station (WES). Messrs. J. H. Lockhart, Jr., and John G. Housley were OCE Technical Monitors.

The study was conducted from 1 January 1985 through 30 April 1986 by Mr. Thomas A. Hardy, Hydraulic Engineer, and Dr. Nicholas C. Kraus, Research Physical Scientist and Principal Investigator, Surf Zone Sediment Transport Processes work unit, Research Division (CR), CERC. This report is substantially the same as the thesis submitted to Mississippi State University by Mr. Hardy in partial fulfillment of the requirements for an M.S. degree in Civil Engineering. Dr. Kraus was thesis advisor. This study was performed under general supervision of Dr. James R. Houston, Chief, CERC; Mr. Charles C. Calhoun, Jr., Assistant Chief, CERC; and Dr. Charles L. Vincent, Program Manager, Shore Protection and Restoration Program, CERC; and under direct supervision of Mr. H. Lee Butler, Chief, CR, CERC.

COL Dwayne G. Lee, CE, was Commander and Director of WES during publication of this report. Dr. Robert W. Whalin was Technical Director.

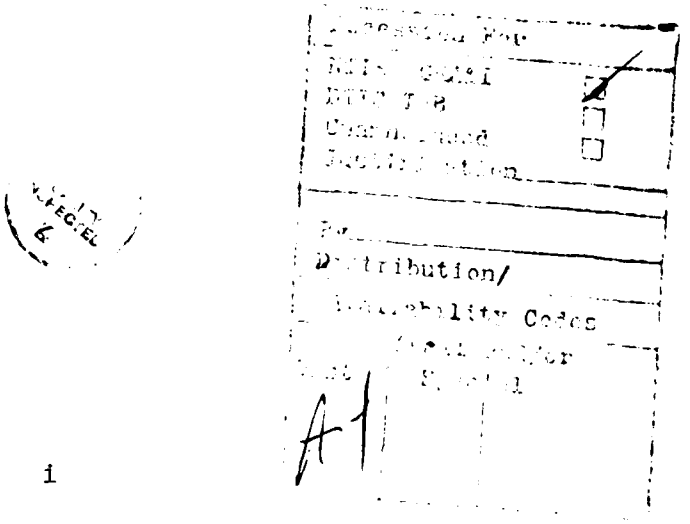

CONTENTS

CONTENTS (Concluded)

LIST OF TABLES

LIST OF FIGURES

LIST OF FIGURES (Continued)

LIST OF FIGURES (Continued)

CHAPTER I

INTRODUCTION

Coastal regions are a limited resource that must be shared among sometimes conflicting environmental, commercial, industrial, residential, and recreational needs. These competing interests make it difficult and expensive to design, build, and repair coastal projects. In order to more efficiently utilize our coastal areas, it is imperative to develop the best possible methods of engineering analysis. Accurate and efficient shallow water wave transformation models are one category of tool needed for coastal engineering analysis. These computer models predict changes in the height and the direction of waves propagating through water of varying depth. The purpose of this report is to develop a numerical model of the transformation of finite-amplitude waves, which will fill a gap in the engineering analysis of shallow water waves.

The unique features of this numerical model include the following items: a) A second approximation to cnoidal wave theory, a finite-amplitude theory valid for intermediate and shallow water, is used. (The first approximation to cnoidal wave theory can also be used.) b) Expressions for the efficient calculation of cnoidal waves (Isobe, 1985) are rederived and applied in the numerical model. c) Wave heights and angles of propagation resulting from the shoaling and refraction of finite-amplitude waves are calculated directly on a numerical grid (as opposed to the more cumbersome classical wave ray method).

The foundation of any wave transformation model is the wave theory

upon which it is based. The two main families of perturbation wave theory are Stokes theory (Stokes, 1847) and cnoidal theory (Korteweg and de Vries, 1895). Both are based on perturbation solutions to the non-linear equations of the water-wave boundary value problem. (A discussion of water-wave theory is given in Chapter II.) Stokes theory, valid for intermediate and deep water, is based on trigonometric functions. Cnoidal theory, valid for intermediate and shallow water, is based on the Jacobian elliptic functions.

The first approximation to Stokes theory, also called Airy, linear, or small-amplitude theory, is the basis for almost all wave transformation models presently in engineering use. Small-amplitude theory performs well in a wide variety of engineering applications. However, the infinitesimal wave height assumption used in the derivation of small-amplitude wave theory becomes increasing invalid in shallow water. In shallow water, where the wave height becomes large and can significantly affect wave properties, cnoidal theory offers an improvement over small-amplitude theory, since cnoidal wave theory, even at the first approximation, describes waves of finite height.

For the numerical model developed in this report, a second approximation to cnoidal wave theory (Isobe and Kraus, 1983b) is used. (Chapter II contains an outline of the derivation of this theory.) The second approximation was included to increase the accuracy of the calculation of shallow water waves. In particular, the second approximation more realistically predicts the horizontal water particle velocity. (The first approximation to cnoidal theory calculates velocities which do not vary with depth.) Including the second approximation

produces more realistic predictions of the depth dependence of the horizontal water particle velocities.

Although cnoidal wave theory has been available for over 90 years, its use in engineering analysis has been minimal. This is because of the complexity and unfamiliarity of the mathematics of cnoidal wave theory, and also the difficulty encountered in its computer calculation. A goal of this report is to promote cnoidal wave theory as a viable engineering design tool. This will be done by providing a discussion of the mathematical basis of cnoidal theory (Chapter III), and by deriving methods (Appendix A) for the efficient calculation of cnoidal wave theory, based on the work of Isobe (1985).

Many of the small-amplitude wave models and all of the known finite-amplitude wave models calculate refractive effects using ray theory (Munk and Authur, 1952). However, ray theory is difficult to use, and complicated interpolation is needed in order to specify model results on a numerical grid. A method of calculating results directly at grid locations (introduced for small-amplitude theory by Noda et al., 1974) is adapted here.

Shoaling and refraction are the traditional first steps in the calculation of wave transformation. (Wave transformation is discussed in Chapter IV.) The model presented in this report will calculate the effects of shoaling and refraction for the region from just seaward of the surf zone out to water of intermediate depth. Before the computer became an indispensable engineering analysis tool, shoaling and refraction were predicted using hand and graphical calculations. Usually, simplifications were made to the bathymetry by assuming a

locally plane bottom with straight and parallel depth contours. To use a more realistic bathymetry tedius computations were often necessary. The Shore Protection Manual (SPM) (SPM, 1984) provides tables for shoaling calculations and a template which speeds the hand calculation of refraction. With the advent of the computer, numerous numerical transformation models for irregular bathymetry were developed. The SPM (SPM, 1984, pp. 2-71) lists numerous sources. These models are all based on small-amplitude wave theory and most use ray theory for the calculation of refraction.

Recently, there has been much research and development of wave transformation numerical models. Theoretical developments for combined refraction and diffraction for small-amplitude waves were pioneered by Berkhoff (1972) and Radder (1979). Ebersole (1985) and Lozano and Liu (1980) are among those who have presented models using combined wave refraction and diffraction. These models improve accuracy in wave height and direction calculations, especially for simulations over complex bathymetry where ignoring the effect of diffraction can result in the calculation of inaccurate wave heights or the "blow up" of the computer run due to the convergence of wave rays (caustics). Models which incorporate wave-current interaction (Liu, 1985) and bottom friction (Liu and Tsay, 1985) with combined refraction and diffraction have further advanced the state of the art of the modeling of shallow water wave transformation.

The modeling of waves using a spectral approach also has been an area of active research. Directional spectral models (see Vincent, 1982 for a review) represent the random nature of the sea by spreading wave

energy over a two dimensional array of frequencies and directions. These spectral models have been used extensively by the offshore oil industry.

All of the efforts mentioned above, while contributing to the ability to model wave transformation, use small-amplitude wave theory. As will be dicussed in Chapter II, small amplitude wave theory is based on the assumption that the wave height is infinitesimally small. This assumption is clearly violated for real sea waves in the coastal zone. However, because of the increased complexity of finite-amplitude theory, only a few finite-amplitude numerical models that calculate wave transformation over an irregular bottom have been developed. Chu (1975) was a pioneer, developing a model which combined Stokes wave theory at a third approximation, cnoidal wave theory at a first approximation, and hyperbolic wave theory. Headland and Chu (1985) attempted to couple small-amplitude theory in deep and intermediate water with cnoidal theory in shallow water. Problems with connecting the two components forced them to present separate results for the deep and shallow water models. A model for the shoaling and refraction of finite-amplitude waves, using Stokes theory at the third approximation and incorporating bottom friction, was presented by Oh and Grosch (1985). However, the model was advocated for application in shallow water up to the breaking point, which is outside the region of validity of Stokes theory (Kraus, Cialone, and Hardy, 1987). No known finite-amplitude transformation model calculates directly at grid points. For the calculation of refraction, all three of the aforementioned finite-amplitude models

employed ray theory, which requires interpolation to specify information at grid locations.

The numerical model presented in this report is a first step in the development of a nearshore finite-amplitude wave transformation model. This model will couple a model employing Stokes theory at the third approximation (Cialone and Kraus, 1987) for use in deeper water with the cnoidal model described in this report for use in shallower water. The final form of this combined model will include additional wave transformations and may employ more sophisticated numerical techniques such as a boundary fitted numerical grid. This report will concentrate on the efficient and accurate computer calculation of both cnoidal wave theory up to a second approximation and the basic wave transformation mechanisms, shoaling and refraction. The numerical schemes presented at this first step will emphasize simplicity and economy of calculation.

The remainder of this report is structured as follows. Chapter II contains a brief discussion of water-wave theories used in engineering analysis, and an outline of a derivation of second-order cnoidal wave theory. In Chapter III, the role of Jacobian elliptic functions in cnoidal wave theory is described, and expressions for their efficient calculation are presented. The derivations of the governing equations used in the model for the calculation of shoaling and refraction are included in Chapter IV. Chapter V discusses the numerical model. Results from numerical simulations are presented and discussed in Part VI. And, Chapter VII contains the conclusions of this study, and some suggestions for future work. Appendix A contains a derivation of

the expressions for the efficient calculation of cnoidal wave theory and a short table of properties of Jacobian elliptic functions. Derivations of equations for wave energy, energy flux, and velocity of energy propagation for cnoidal waves at a second approximation are presented in Appendix B. Appendix C is a computer listing of the numerical model. Appendix D contains plots from the results of the refraction of second-order cnoidal waves. A list of symbols used throughout this report is contained in Appendix E.

CHAPTER II

SURVEY OF WATER WAVE THEORY

The fundamental element of any wave transformation model is the wave theory upon which the calculations are based. Before outlining a derivation of the second-order cnoidal wave theory used in this report, the basic water-wave boundary value problem will be presented and some of the major water-wave theories currently in engineering use will be briefly discussed. The motivation for presenting this brief survey of wave theory is to delineate the relationship of cnoidal theory to the commonly applied engineering wave theories. For a more detailed presentation of basic wave theory, Ippen (1966, Chapters 1 and 2), Sarpkaya and Isaacson (1981, Chapter 4), and Dean and Dalrymple (1984, Chapter 3) are recommended.

2.1 The Boundary Value Problem for Water Waves

The various water-wave theories are, in essence, composed of different sets of assumptions and techniques which attempt to describe the dynamics and kinematics of real waves. Real water waves have several properties which make their mathematical specification very difficult. Water is a viscous fluid and real waves travel over sea bottoms or lake beds which are in general neither impermeable nor flat. Because of these difficulties most of the wave theories used for engineering purposes begin with a series of identical assumptions. The problem is formulated as a boundary value problem in which a governing differential equation is solved over the region of interest and satisfies the appropriate boundary conditions.

Figure 2.1 is the definition sketch of the boundary value problem, where the following symbols* are used:

x,z - Coordinate axis with the origin at the still-water level, z positive upward, and the wave moving in the positive x direction.

D - Water depth, defined as the distance from the still-water level to the bottom.

η - Distance from the still-water level to the free surface.

H - Wave height, defined as the vertical distance from the crest to the trough.

L - Wavelength, defined as the distance between successive crests or any two points af equal phase.

$\vec{u}$ - Water particle velocity.

u - Horizontal component of the water particle velocity.

w - Vertical component of the water particle velocity.

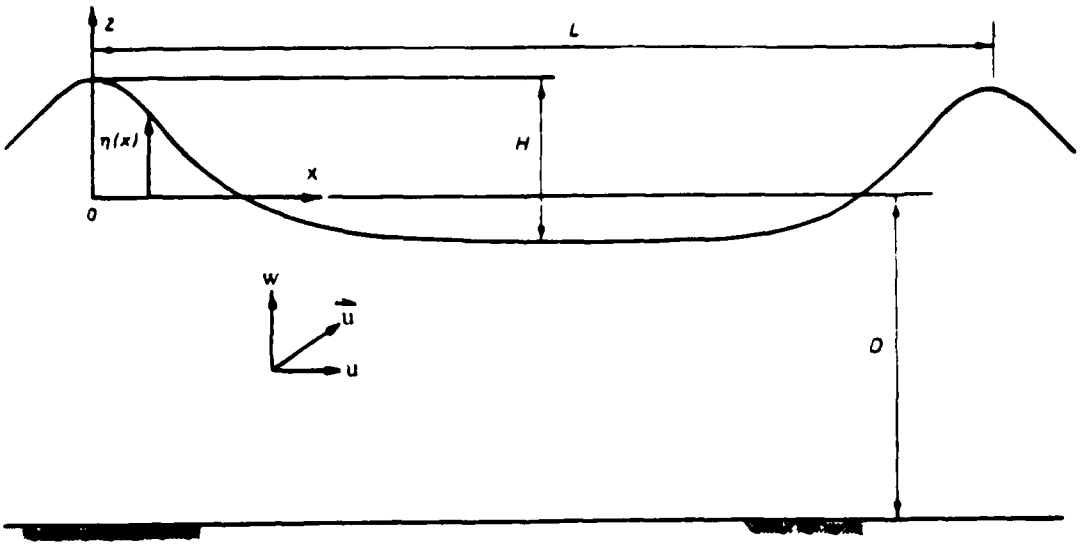

Figure 2.1 Definition sketch for the water wave boundary value problem

* Symbols used in this report are listed in Appendix E.

The assumption that the flow is two-dimensional is inherent in Figure 2.1. The wave is moving in the positive x - direction, and there is no component of the motion in the y - direction.

The assumption that water is incompressible is common to all surface wave theories. This assumption is justifiable given that water's bulk modulus of elasticity is very large relative to the small changes in pressures common to surface waves. Starting with this assumption, the governing equation is derived from the continuity equation for an incompressible fluid (Equation 2.1).

$$\nabla \cdot \vec{u} = 0 \tag{2.1}$$

The second major assumption is that the fluid motion is irrotational. Clearly, the fluid would be rotational in the boundary layers which exist at the bottom and at the water-air surface. Fortunately, these boundary layers are thin and the major portion of the water column can be considered as irrotational for engineering purposes. With the assumption of irrotationality, a velocity potential exists and the water particle velocity can be specified in terms of the velocity potential, ϕ (Equation 2.2). Equation 2.2 is substituted into Equation 2.1, resulting in Equation 2.3. Rewriting Equation 2.3 results in the Laplace equation (Equation 2.4), which is used as the governing equation in the water-wave boundary value problem.

$$\vec{u} = \nabla\phi \tag{2.2}$$

$$\nabla \cdot \nabla\phi = 0 \tag{2.3}$$

$$\nabla^2\phi = 0 \tag{2.4}$$

With the governing equation established, specification of boundary conditions is necessary before a solution can be determined. Boundary conditions are needed at the free surface, the bottom, and lateral sides of the region of interest.

Kinematic boundary conditions are specified at the bottom and at the free surface. These boundary conditions force the fluid to remain in contact with the boundaries. If contact were not maintained, either there would be gaps between the fluid and the boundary or the fluid would pass through the boundary (such as during wave breaking or at a permeable bottom). Thus the kinematic free surface boundary condition, KFSBC (Equation 2.5), and the kinematic bottom boundary condition, KBBC (Equation 2.6), have the inherent assumptions of non-breaking waves and an impermeable bottom, respectively.

The KBBC is further simplified by the assumptions of a horizontal bottom that does not change with time (no scour or deposition), resulting in Equation 2.7.

$$w = \eta_t + u\eta_x \qquad \text{on } z = \eta \tag{2.5}$$

$$w = D_t - uD_x \qquad \text{on } z = -D \tag{2.6}$$

$$w = 0 \qquad \text{on } z = -D \tag{2.7}$$

where subscripts denote partial differentiation.

The water-air surface requires an additional boundary condition. Rigid boundaries can support a pressure differential across the boundary surface. However, the water-air surface responds to pressure changes by adjusting in elevation to maintain a zero pressure differential across the boundary. (Here the assumption is made that surface tension can be ignored.) This extra boundary condition is needed because the location of the free surface is not known a priori, but is itself part of the solution. The unsteady Bernoulli equation evaluated at the free surface is used as the the dynamic free surface boundary condition, DFSBC (Equation 2.8) with the pressure, p, assumed to be zero or gage pressure. Here g is the acceleration of gravity and p_B is the Bernoulli constant.

$$-\phi_t + \frac{1}{2}(u^2 + w^2) + gz = \frac{p_B}{\rho} \qquad \text{on } z = \eta \qquad (2.8)$$

The lateral boundary conditions are expressed as the requirement that the wave is of permanent form and is periodic in both space and time. These periodic lateral boundary conditions, PLBC, are given in Equations 2.9 and 2.10. Here t is the independent variable for time and T is the period of the wave form.

$$\phi(x,t) = \phi(x+L,t) \qquad (2.9)$$

$$\phi(x,t) = \phi(x,t+T) \qquad (2.10)$$

The boundary value problem has been fully specified by the above governing equation and boundary conditions. The most common wave

theories used in engineering analysis can be derived by making further assumptions and alterations to this basic formulation. In conclusion, the basic assumptions can be summarized as follows:

1. Water is incompressible.
2. Water is inviscid and, therefore, is irrotational.
3. The bottom is horizontal and does not change with time.
4. Both the bottom and the free surface are impermeable.
5. Surface tension on the free surface is negligible.
6. The wave is periodic in space and time, i.e., is of permanent form.

The set of equations specifying the boundary value problem is summarized as

$$\nabla^2\phi = 0 \tag{2.11}$$

$$w = \eta_t + u\eta_x \qquad \text{on } z = \eta \tag{2.12}$$

$$-\phi_t + \frac{1}{2}(u^2 + w^2) + gZ = \frac{p_B}{\rho} \qquad \text{on } z = \eta \tag{2.13}$$

$$w = 0 \qquad \text{on } z = -D \tag{2.14}$$

$$\phi(x,t) = \phi(x+L,t) \tag{2.15}$$

$$\phi(x,t) = \phi(x,t+T) \tag{2.16}$$

In the next four sections the additional assumptions and modifications necessary for the development of small-amplitude, Stokes, cnoidal,

solitary, and numerical wave theories will be presented.

2.2 Small-Amplitude Wave Theory

A closed form solution of the wave boundary value problem specified by Equations 2.11 to 2.16 is extremely difficult to find. This difficulty results from the two free surface boundary conditions which contain the nonlinear terms, $u\eta_x$ and $1/2(u^2 + w^2)$. These nonlinear terms can be shown to be much smaller than the other terms in these two equations using the assumption that the wave height is infinitesimal. This process demands that both $H/D << 1$ and $H/L << 1$. Neglecting the nonlinear terms, the KFSBC and DFSBC can be written as Equations 2.17 and 2.18, respectively.

$$w = \eta_t \qquad \text{on } z = 0 \tag{2.17}$$

$$-\phi_t + gZ = \frac{p_B}{\rho} \qquad \text{on } z = 0 \tag{2.18}$$

The system of linear equations (2.11, 2.17, 2.18, 2.14, 2.15, 2.16) can be solved using the technique of separation of variables. The resulting equation for η is

$$\eta = \frac{H}{2} \cos 2\pi \left(\frac{x}{L} + \frac{t}{T}\right) \tag{2.19}$$

Small-amplitude theory is also called either linear wave theory because of the linearizing assumptions, or Airy wave theory after the man who first presented it (Airy, 1845). Small-amplitude wave theory has been

and continues to be the predominant water wave theory. This is because small-amplitude theory is easy to calculate, and is sufficiently accurate for many engineering and scientific applications.

2.3 Finite-Amplitude Wave Theory

Although small-amplitude wave theory performs adequately for many engineering applications, certain important phenomena are inherently nonlinear. For example, the last two decades have brought a boom in offshore engineering, particularly in the oil exploration industry. Here the emphasis is placed on large wave heights, which negates a basic assumption upon which linear theory is based. Specifically, H/L is not very much smaller than one. In relatively shallow water, where H/D is not very much smaller than one, finite wave height affects both wave refraction and wave shoaling, and thus the angle of wave attack on a beach and the location of the breaker line. For these and any other problems for which finite wave height is important, the boundary value problem must be solved using the set of nonlinear equations (Equations 2.11 to 2.16).

In the treatment of finite-amplitude waves, specification of a moving coordinate system usually precedes the solution of the nonlinear equations. Use of a coordinate system with a motion equal to the wave celerity removes the unsteady terms from the equations and greatly simplifies the solution procedure. However, since the final goal is a solution in a fixed coordinate system, the wave celerity must be specified externally of the solution of the nonlinear problem, i.e., it turns out that the wave celerity is not unique. Specification of the

celerity is usually done through a physical consideration. Stokes (1847) offered the two most commonly used definitions, called the first and second definitions of wave celerity. The first definition states that the wave celerity is specified so that the horizontal velocity averaged over a wave period is zero if evaluated at a point which is always in the fluid. The first definition of wave celerity can be expressed as

$$0 = \frac{1}{L} \int_0^L u \, dx \tag{2.20}$$

The second definition requires that the celerity be specified so that the mass flux is zero when averaged over a wave period. The second definition of wave celerity can be expressed as

$$0 = \frac{1}{L} \int_0^L \int_{-D}^{\eta} u \, dz \, dx \tag{2.21}$$

In this report, the second definition of wave celerity is used. It is often stated in the literature that finite-amplitude waves cause a mass flux in the direction of wave propagation. While this may be true at some locations in the nearshore wave field, it is not true for an average over the wave field in the steady state condition. For the steady state condition, it does not seem proper to account for the forward movement of mass without accounting for the return current which this forward flux must cause. Imagine the consequences for coastal regions if waves always caused a net forward mass flux! Often the second definition of celerity is proposed for matching theoretical

results with wave flume experimental data. The closed system of the wave flume demands that a no-flux condition exist after the steady state is reached. Granted that the natural environment can be far more complex than a wave flume; however, a steady state condition in nature requires the same balance of inflows and outflows as does the wave flume. Therefore, the zero mass flux of the second definition would seem to give the best overall representation. The second definition of celerity has another, more practical benefit. For the derivation of an expression to calculate energy flux (Appendix B), the second derivation allows a substantial simplification (see Equations B.9 and B.10). To keep this matter in perspective, it is important to note that the choice of one of these two definitions is a relatively academic decision. The choice does not effect the first two approximations to the wave celerity and only results in a small difference at higher order approximations.

The perturbation method is used to solve the set of nonlinear equations (2.11 to 2.16). In this technique, the dependent variables in the boundary value problem are assumed to be functions of an auxiliary parameter, δ , and are expanded in a power series of a perturbation parameter, ε , which is assumed to be small. For example, Equation 2.22 is a power series representation for η .

$$\eta = \varepsilon\eta_1 + \varepsilon^2\eta_2 + \varepsilon^3\eta_3 + \ldots \qquad (2.22)$$

Waves of permanent form can be described by three independent variables, H, L, and D. Two independent nondimensional quantities can be formed from these three variables. The most commonly used are H/L

and H/D. One of these quantities is usually chosen as ϵ . For a derivation of Stokes wave theory, H/L is often chosen as the perturbation parameter; whereas, for a derivation of cnoidal wave theory, H/D is often chosen.

The power series representations of the variables are inserted into the system of equations. Then the terms with an equal power of ϵ in each equation are grouped together and solved separately. For example, the equations of first-order involve only those terms multiplied by ϵ^1 , the equations of second-order involve only those terms multiplied by ϵ^2 , and the equations of nth-order involve only those terms multiplied by ϵ^n . The terminology, the nth-order solution or the nth-order theory, implies the solution of the equations up to and including nth-order. The solution of the equations of each successive order adds a correction to the (n-1)th-order solution. Unfortunately, the higher order solutions are gained at considerable algebraic expense.

2.4 Stokes Wave Theory

Sir George Stokes originated the family of wave theories bearing his name (Stokes, 1847) when he developed a second-order theory. This derivation showed that the first approximation was identical to Airy wave theory; consequently, first-order Stokes theory and small-amplitude theory are identical. There have been several derivations of higher order Stokes wave theories. Skjelbreia and Hendrickson (1960) obtained a fifth-order solution. Their derivation used the same expansion parameter as Stokes, ak, where $a = H/2$ is the wave amplitude at first order and the wave number, $k = 2\pi/L$. (Nishimura, Isobe and Horikawa

(1977) found a minor error in this solution.) Derivations using $\epsilon = kH/2$, include Isobe and Kraus (1983a) to third-order and Fenton (1985) to fifth-order.

Stokes wave theories are not valid over the whole range of relative depths, D/L. Isobe, Nishimura and Horikawa (1982) showed that their perturbation solution of Stokes theory is valid only if the Ursell parameter (Equation 2.23) has a value less than 25. (For other perturbation solutions this limit may vary slightly.) This implies validity only in intermediate to deep water. If Stokes theory is applied outside its range of validity, abnormalities such as secondary peaks of the wave free surface profile occur soon after the limiting value of U is exceeded. Naturally, the numerical values of certain physical quantities will also be inaccurate outside the range of validity.

$$U = \frac{HL^2}{D^3} \tag{2.23}$$

Goda (1983) presented an empirical parameter, $\Pi = \frac{H}{L_{SA}} \coth^3 k_{SA}D$, where the subscript SA denotes a quantity calculated from small-amplitude theory. This parameter smoothly connects a multiple of the Ursell parameter, which is used as a measure of nonlinearity in shallow water with the deepwater wave steepness, H/L, which serves as a measure of nonlinearity in deep water. Goda found that Stokes theory was valid below $\Pi \approx 0.2$. This parameter has not been thoroughly studied, but further research might prove it to be a valuable descriptor of finite amplitude waves.

2.5 Cnoidal Wave Theory

The Dutch mathematicians, Korteweg and de Vries (1895), during an investigation of the change in form of propagating long waves, developed a type of long wave surface profile which can be specified in terms of the Jacobian elliptic function, cn. Using an analogy with waves described by sinusoidal functions, they coined the term "cnoidal" for this wave type.

Keulegan and Patterson (1940), as part of treatise on irrotational waves, developed a well-known first-order cnoidal solution. Friedrichs (1948) introduced a systematic method for deriving shallow water wave theories by using a coordinate stretching nondimensionalization. This technique is the basis for many of the succeeding derivations of cnoidal theory. The most commonly cited derivations of cnoidal theory include Keller (1948), Laitone (1960), and Chappelear (1962). Svendsen (1974), in a report which gives a thorough discussion of first-order cnoidal wave theory, provides tabulated values of the parameters necessary for the engineering calculation of first-order cnoidal waves.

The region of applicability of cnoidal theory is in intermediate to shallow water, up to but perhaps not including the wave breaking point. Svendsen (1974) derived a deepwater limit for cnoidal theory. This limit varies between $D/L_o = 0.12$ for waves of infinitely small wave height to $D/L_o = 0.14$ for waves that are steep enough to break at the deepwater limit. L_o is the small-amplitude theory deepwater wavelength, $L_o = gT^2/(2\pi)$. Isobe, Nishimura and Horikawa (1982) investigated the error in the DFSBC for cnoidal solutions of several different orders. Their findings indicate a deepwater limit close to $D/L = 0.2$. (Note

that the actual wavelength is used.) These values of relative water depth indicate that Stokes and cnoidal theories have an overlapping range of Ursell numbers in which both theories are valid, approximately $25 > U > 10$. Cnoidal theory is valid at higher Ursell numbers and Stokes theory is valid at lower Ursell numbers. Because of the complexity of cnoidal theory, Isobe, Nishimura, and Horikawa (1982) suggest that Stokes theory be used in the region of overlap in validity with cnoidal theory. However, calculation techniques introduced by Isobe (1985) increase the ease of cnoidal wave calculations and diminish the difference in the difficulty of calculation between the two theories. These expressions are introduced in Chapter III, derived in Appendix A, and used in the numerical model developed in this thesis.

2.6 Solitary Wave Theory

Scott Russell, while serving as an engineering consultant to an English river barge company, first studied solitary waves in the 1830's. His historic report (Russell, 1844) describing these waves of translation served as a catalyst which helped stimulate much of the early theoretical work in water wave theory. Boussinesq (1872), Rayleigh (1876), and McCowan (1891) are the commonly cited classical references for the mathematical development of solitary wave theory.

The solitary wave is related to cnoidal waves, as the same assumptions and equations are used to specify the boundary value problem. The solitary wave results as a limiting case of the cnoidal wave as the wavelength, and therefore, the wave period approaches infinity. For a solitary wave, the wave form exists totally above the

still water surface, and the water particle velocities have only a forward motion. The periodic motion which characterizes the other wave theories is replaced by a wave of translation in solitary wave theory. Since waves in the surf zone often take on the appearance of solitary waves, these waves have been suggested for engineering use in very shallow water (Munk, 1949).

2.7 Numerical Wave Theories

Increasing the order of a perturbation-type analytical wave theory is done only with great effort. Also, two analytical theories are needed to cover the full range of water depths. Therefore, methods were sought which would accurately solve the boundary value problem without the need for the derivation of a high-order analytical theory. Dean (1965) presented such a method which he called the Stream Function Wave Theory. The KFSBC is automatically satisfied if the stream function is used instead of the velocity potential. The only boundary condition not exactly satisfied is the DFSBC. (The use of the stream function is not unique to this theory, but is also commonly used in both Stokes and cnoidal theory derivations.) The coefficients of a Stokes-like expansion are determined for a given H, T, and D, so that the least-square error of the DFSBC is reduced to a very small value. The theory has been shown to very accurately match experimental data (Dean, 1974).

Cokelet (1977) presented a computer-generated solution of a very high order Stokes-like expansion. He used a specially developed perturbation parameter and Pade approximates, a mathematical tool for summing series. This solution is considered an exact solution to the

nonlinear water wave boundary value problem for waves of permanent form. Results obtained using Cokelet's theory are often used for comparison with the results from other theories. Nishimura, Isobe and Horikawa (1977) provide very high order solutions to both cnoidal and Stokes waves using computer solved recurrence formulae. They used these solutions to study the accuracy with which the higher order theories matched the free surface boundary conditions.

These and other computer-dependent solution techniques are important for the theoretical study of such problems as determining regions of validity, and for engineering studies where the problem is highly nonlinear, such as calculating the forces from the highest possible wave. However, a major disadvantage results from these computer generated solutions. There are no explicit formulae for engineering quantities, so every combination of H, T, and D requires a separate solution. Tabulated values have been provided of the important engineering quantities for various values of H, T, and D (Dean, 1974). However, use of either the tables or the numerical techniques would be difficult and expensive in a wave transformation model where thousands of different combinations of the basic parameters would result for each simulation.

2.8 Brief Outline of a Derivation Second-Order Cnoidal Wave Theory

The finite-amplitude wave transformation described in this report is intended for use in intermediate and shallow water, seaward of the breaker line. Stokes wave theory is not applicable to this region. Solitary wave theory does not adequately describe the periodic nature of

the waves in the region outside of the surf zone. Numerical theories are not computationally efficient. Therefore, cnoidal theory was chosen. Second-order theory was selected to increase the accuracy with which the theory would predict the needed engineering quantities. In particular, second-order theory more realistically predicts the vertical variation of the horizontal water particle velocity, since first-order theory predicts a uniform velocity from the water surface to the sea bottom.

The derivation of second-order cnoidal theory (Isobe and Kraus, 1983b) was chosen for two reasons. First, this derivation is rigorous, systematic, and easy to use. Second, a companion derivation for third-order Stokes theory (Isobe and Kraus, 1983a) provides the foundation for a numerical model which will serve as a companion refraction model, providing seaward boundary conditions for the model developed in this report.

It is not the purpose of this report to fully document the second-order cnoidal solution. A brief outline of the derivation will be presented in order to provide some background for the reader.

Using the relationship between the velocity potential and stream function (Equation 2.24), and assuming a coordinate system which moves with the speed of the wave form, the governing equation and boundary conditions for the nonlinear wave boundary value problem (Equations 2.11 to 2.16) are replaced by Equations 2.25 to 2.30.

$$\psi_z = \phi_x = u \qquad ; \qquad -\psi_x = \phi_z = w \tag{2.24}$$

$$\nabla^2\psi = 0 \tag{2.25}$$

$$\psi = q \qquad \text{on} \quad z = \eta \tag{2.26}$$

$$\frac{1}{2}\left[(\psi_x)^2 + (\psi_z)^2\right] + g\eta = \frac{p_B}{\rho} \qquad \text{on} \quad z = \eta \tag{2.27}$$

$$\psi = 0 \qquad \text{on} \quad z = -D \tag{2.28}$$

$$\overline{\eta} = 0 \tag{2.29}$$

where the over bar denotes the quantity is averaged over wavelength, and

$$\eta(0) - \eta(L/2) = H \tag{2.30}$$

Note that the use of the stream function simplifies the KFSBC (Equation 2.26), as was mentioned in discussing Dean's Stream Function Wave Theory. Also the PLBC (Equations 2.15, 2.17) are replaced by Equations 2.29 and 2.30. Equations 2.25 to 2.30 can be nondimensionalized using

$$X = \frac{x}{L} \tag{2.31}$$

$$Z = \frac{z}{D} \tag{2.32}$$

$$N = \frac{\eta}{D} \tag{2.33}$$

$$\Psi = \frac{\psi}{D\sqrt{gD}} \tag{2.34}$$

$$Q = \frac{q}{D\sqrt{gD}} \tag{2.35}$$

$$P = \frac{p}{\rho g D} \tag{2.36}$$

$$P_B = \frac{p_B}{\rho g D} \tag{2.37}$$

Substituting Equations 2.31 to 2.37 into Equations 2.25 to 2.30 results in

$$\Psi_{ZZ} + \frac{D^2}{L^2}\Psi_{XX} = 0 \tag{2.38}$$

$$\Psi = Q \qquad \text{on } Z = N \tag{2.39}$$

$$\frac{1}{2}\left[(\Psi_z)^2 + \frac{D^2}{L^2}(\Psi_x)^2\right] + N = P_B \qquad \text{on } Z = N \tag{2.40}$$

$$\Psi = 0 \qquad \text{on } Z = -1 \tag{2.41}$$

$$\bar{N} = 0 \tag{2.42}$$

$$N(0) - N(1/2) = \frac{H}{D} \tag{2.43}$$

The term, D^2/L^2, which appears in Equations 2.38 and 2.40, as will be seen more clearly below, causes a difference in order between the x and z derivatives. It is this feature which determines that these equations

will produce a shallow water wave solution.

After the equations are readied, the next step in setting up the perturbation method of solution is to select an ordering parameter. For this derivation the ordering or perturbation parameter is

$$\varepsilon \equiv \frac{H}{D} \tag{2.44}$$

Next, all the variables in the Equations 2.38 to 2.43 are expressed as functions of the auxliliary parameter, δ , and expanded as a power series about ε . In cnoidal theory, the modulus of the elliptic integral, κ , is usually selected as the auxiliary parameter. These expansions are given in Equations 2.45 to 2.49.

$$\Psi(X,Z,\kappa,\varepsilon) = \Psi_0 + \varepsilon\Psi_1 + \varepsilon^2\Psi_2 + \varepsilon^3\Psi_3 + \ldots \tag{2.45}$$

$$N(X;\kappa,\varepsilon) = \varepsilon N_1 + \varepsilon^2 N_2 + \varepsilon^3 N_3 + \ldots \tag{2.46}$$

$$Q(\kappa,\varepsilon) = Q_0 + \varepsilon Q_1 + \varepsilon^2 Q_2 + \varepsilon^3 Q_3 + \ldots \tag{2.47}$$

$$P_B(\kappa,\varepsilon) = P_0 + \varepsilon P_1 + \varepsilon^2 P_2 + \varepsilon^3 P_3 + \ldots \tag{2.48}$$

$$\left(\frac{D}{L}\right)^2(\kappa,\varepsilon) = \varepsilon d_1 + \varepsilon^2 d_2 + \varepsilon^3 d_3 + \ldots \tag{2.49}$$

Note that all the series in Equations 2.45 to 2.49 begin with a zeroth-order quantity except the expansions of N and D^2/L^2, which start with the first order. N is always smaller than ε ; therefore, N will not

have a zeroth-order term. Some other derivations of cnoidal theory, including Keller (1948), Laitone (1960), and Chappelear (1962), have used D^2/L^2 as the perturbation parameter. These two choices of perturbation parameter, H/D and D^2/L^2 are related by the Ursell parameter (Equation 2.23) as shown in Equation 2.50. Since cnoidal theory is valid for Ursell numbers greater than approximately ten (as was discussed in Section 2.5), D^2/L^2 is smaller than ε , and D^2/L^2 cannot have a zeroth-order term when expanded in a power series about ε .

$$U = \frac{HL^2}{D^3} = \frac{H}{D}\frac{L^2}{D^2} = \frac{\varepsilon}{D^2/L^2} \tag{2.50}$$

The expanded form of the variables are inserted into the Equations 2.38 to 2.43. For example, if Equation 2.45 is substituted into the Equation 2.38 the results are

$$\left(\Psi_{0ZZ} + \varepsilon\Psi_{1ZZ} + \varepsilon^2\Psi_{2ZZ} + \varepsilon^3\Psi_{3ZZ} + \ldots\right) + \left(\varepsilon d_1 + \varepsilon^2 d_2 + \varepsilon^3 d_3 + \ldots\right) \times \left(\Psi_{0XX} + \varepsilon\Psi_{1XX} + \varepsilon^2\Psi_{2XX} + \ldots\right) = 0 \tag{2.51}$$

If the wave height were zero, the only motion would be the uniform horizontal flow resulting from the moving coordinate system. Therefore, the zeroth-order contribution to the stream function can be expressed as Equation 2.52, where b_{00} is a constant to be determined. Equation 2.53 follows directly from Equation 2.52.

$$\Psi_0 = b_{00}Z \tag{2.52}$$

$$\Psi_{0XX} = \Psi_{0ZZ} = 0 \tag{2.53}$$

According to the perturbation method, terms are grouped in equal powers of ϵ . The terms of each order on the right side of an equation must equal the terms of like order on the left side of the equation. With this grouping, Equation 2.51 becomes

$$\Psi_{1ZZ} = 0 \tag{2.54}$$

$$\Psi_{2ZZ} + d_1\Psi_{1XX} = 0 \tag{2.55}$$

$$\Psi_{3ZZ} + d_1\Psi_{2XX} + d_2\psi_{1XX} = 0 \tag{2.56}$$

The boundary conditions (Equations 2.39 to 2.43) are treated in a similar manner. However, special treatment is needed for the two free surface boundary conditions. Since the location of the free surface is, a priori, unknown, variables evaluated at the free surface are expanded using a Taylor series expanded about z = 0. For example, the expansion for $\psi(x,\eta)$ is

$$\Psi(X,N) = \Psi(X,0) + N\,\Psi_Z(X,0) + \frac{N^2}{2}\,\Psi_{ZZ}\,(X,0) + \ldots \tag{2.57}$$

After the expanded variables are inserted into the governing equation and all five boundary conditions and the coefficients of each power of ϵ are separated, a set of equations for each order results. For illustration, the equations of second-order (coefficients of ϵ^2) are

$$\Psi_{2ZZ} + d_1 \Psi_{1XX} = 0 \tag{2.58}$$

$$\Psi_2 + b_{00} N_2 + N_1 \Psi_{1Z} = Q_2 \qquad \text{on } Z = N \tag{2.59}$$

$$N_2 + b_{00} \left(\Psi_{2Z} + N_1 \Psi_{1ZZ} \right) + \frac{1}{2} (\Psi_{1z})^2 = P_2 \qquad \text{on } Z = N \tag{2.60}$$

$$\Psi_2 = 0 \qquad \text{on } Z = -1 \tag{2.61}$$

$$\bar{N}_2 = 0 \tag{2.62}$$

$$N_2(0) - N_2(1/2) = 0 \tag{2.63}$$

It is not possible to obtain the solution of the nth-order equations without using the equations of (n+1)th-order. The solution is not closed at the level of each order, but instead spirals upward to include information from the next order. The solution procedure can be summarized as follows. The equations of zeroth-order will determine P_0 and Q_0, once b_{00} is determined. The equations of first-order determine b_{00} so that a nontrivial solution for η_1 and Ψ_1 will exist. Then, if a nontrivial solution for η_2 and Ψ_2 exists, η_1 and Ψ_1 can be determined from the equations of second order. Likewise the equations of third order are used to determine η_2 and Ψ_2 .

As was mentioned in Section 2.4, the artifact of a moving coordinate system requires that the wave celerity be specified from considerations other than the governing equations and boundary conditions. The derivation used in this report employed the second

definition of Stokes. With the mass flux equal to zero, the celerity becomes

$$C = -\frac{q}{D} \tag{2.64}$$

With Equation 2.64 and after re-dimensionalizing the variables, the solution of second-order cnoidal theory in a fixed coordinate system gives

$$C = \sqrt{gD}\left(C_0 + \varepsilon C_1 + \varepsilon^2 C_2\right)$$

$$= \sqrt{gD}\left[1 + \varepsilon\left(\frac{1 + 2\lambda - 3\mu}{2}\right)\right.$$

$$\left. + \varepsilon^2\left(\frac{-6 - 16\lambda + 5\mu - 16\lambda^2 + 10\lambda\mu + 15\mu^2}{40}\right)\right] \tag{2.65}$$

$$\eta = D\left(A_0 + A_1 c_1 + A_2 c_2\right) \tag{2.66}$$

$$u = \sqrt{gD}\left[\left(B_{00} + B_{10} c_1 + B_{20} c_2\right)\right.$$

$$\left. - \frac{1}{2}\left(\frac{z + D}{D}\right)^2\left(B_{01} + B_{11} c_1 + B_{21} c_2\right)\right] \tag{2.67}$$

$$w = \sqrt{gD}\,\frac{4KD}{L}\,\mathrm{csd}\left[\left(\frac{z + D}{D}\right)\left(B_{10} + 2B_{20} c_1\right)\right.$$

$$\left. - \frac{1}{6}\left(\frac{z + D}{D}\right)^3\left(B_{11} + 2B_{21} c_1\right)\right] \tag{2.68}$$

and the dispersion relation

$$\frac{16\kappa^2 K^2}{3} = \frac{HL^2}{D^3}\left[1 + \varepsilon\left(\frac{-5 - 10\lambda + 12\mu}{4}\right)\right] \tag{2.69}$$

where from Appendix A (Equations A.76 and A.84)

$$\lambda = \frac{(1 - \kappa^2)}{\kappa^2} \tag{2.70}$$

$$\mu = \frac{E_e}{\kappa^2 K} \tag{2.71}$$

and K (Equation A.2) and E_e (Equation A.4) are the complete elliptic integrals of the first and second kind, respectively,

and

$$A_0 = \varepsilon(\lambda - \mu) + \varepsilon^2\left(\frac{-2\lambda + \mu - 2\lambda^2 + 2\lambda\mu}{4}\right) \tag{2.72}$$

$$A_1 = \varepsilon + \varepsilon^2\left(-\frac{3}{4}\right) \tag{2.73}$$

$$A_2 = \varepsilon^2\left(\frac{3}{4}\right) \tag{2.74}$$

$$B_{00} = \varepsilon(\lambda - \mu) + \varepsilon^2\left(\frac{\lambda - \mu - 2\lambda^2 + 2\mu^2}{4}\right) \tag{2.75}$$

$$B_{10} = \varepsilon + \varepsilon^2\left(\frac{1 - 6\lambda + 2\mu}{4}\right) \tag{2.76}$$

$$B_{20} = \varepsilon^2\,(-1) \tag{2.77}$$

$$B_{01} = \varepsilon^2\left(\frac{3\lambda}{2}\right) \tag{2.78}$$

$$B_{11} = \varepsilon^2\,(3 - 3\lambda) \tag{2.79}$$

$$B_{21} = \varepsilon^2 \left(- \frac{9}{2} \right) \tag{2.80}$$

$$\varepsilon = \frac{H}{D} \tag{2.81}$$

$$c_1 = cn^2 \left[2K \left(\frac{x}{L} - \frac{t}{T} \right) \right] \tag{2.82}$$

$$c_2 = cn^4 \left[2K \left(\frac{x}{L} - \frac{t}{T} \right) \right] \tag{2.83}$$

$$csd = cn \left[2K \left(\frac{x}{L} - \frac{t}{T} \right) \right] sn \left[2K \left(\frac{x}{L} - \frac{t}{T} \right) \right] dn \left[2K \left(\frac{x}{L} - \frac{t}{T} \right) \right] \tag{2.84}$$

and cn, sn, and dn are Jacobian elliptic functions with modulus κ .

Equation 2.69, the dispersion relationship for second-order cnoidal wave theory, can be more conveniently expressed if it is put in terms of T rather than L. From the relation C = L/T and using Equation 2.65, Equation 2.69 can be rewritten as

$$\frac{16\kappa^2 K^2}{3} = \frac{gHT^2}{D^2} \left[1 + \varepsilon \left(\frac{- 1 - 2\lambda}{4} \right) \right] \tag{2.85}$$

These results are compared to the results of first- and second-order cnoidal theories and linear theory for H = 2 m, T = 8 s, and D = 4 m (U = 81) in Figures 2.2 to 2.4. As seen in Figure 2.2, the free-surface profiles of the two cnoidal theories are very similar, and differ significantly from that of linear theory. The asymmetry of the surface profiles also appears in the plots of the horizontal water particle velocities at the surface and bottom, Figures 2.3 and 2.4, respectively. (This asymmetry of water particle velocities is very

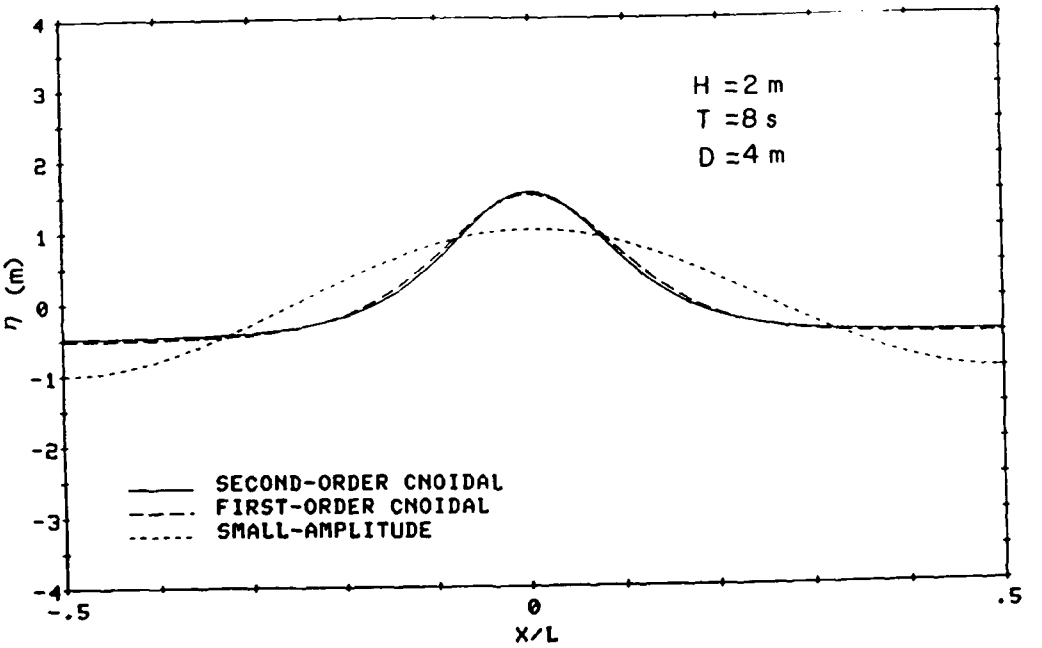

Figure 2.2. Free surface profiles of small-amplitude, first-order cnoidal, and second-order cnoidal waves.

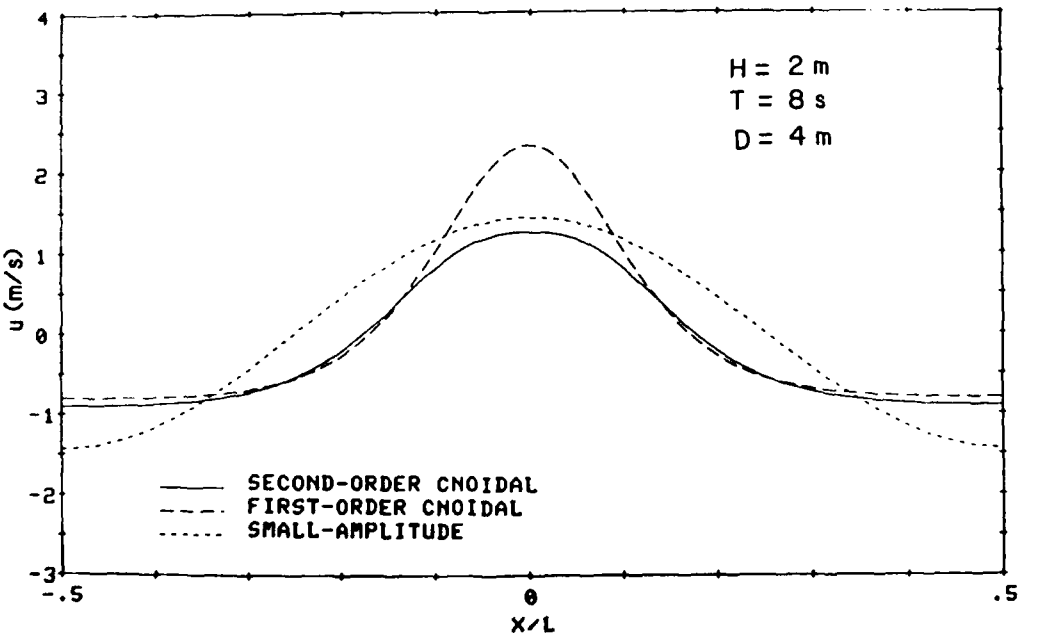

Figure 2.3. Horizontal water particle velocity at z = -D for small-amplitude, first-order cnoidal, and second-order cnoidal waves.

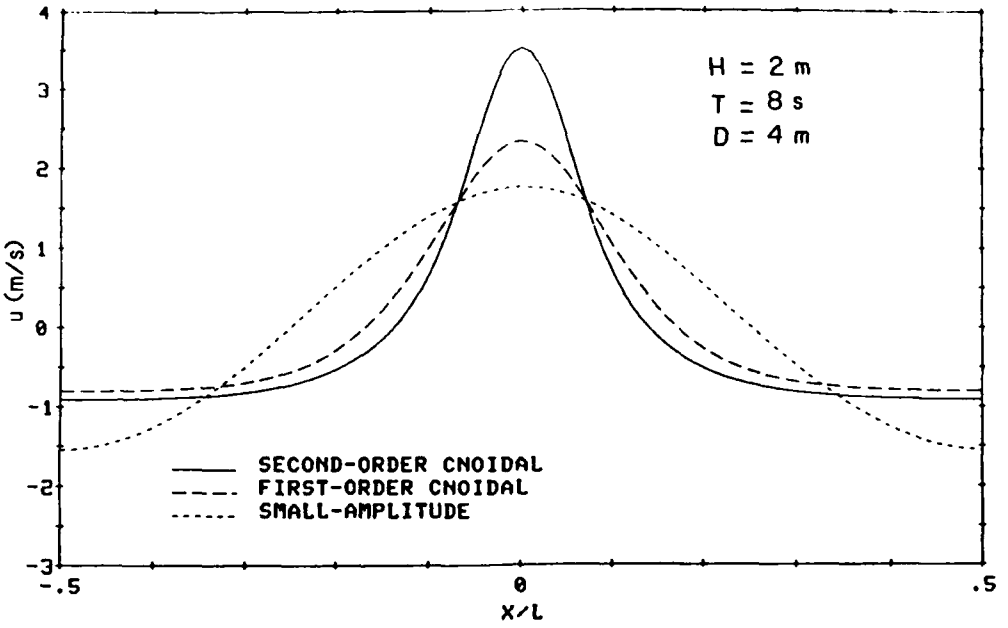

Figure 2.4. Horizontal water particle velocity at z = η for small amplitude, first-order cnoidal, and second-order cnoidal waves.

important for an accurate description of sediment transport.) It is interesting to note that, in this example, although the surface profiles of the first and second-order cnoidal waves are almost identical, the horizontal velocities differ significantly. As in small-amplitude theory applied to shallow water, first-order cnoidal theory predicts no vertical variation in horizontal velocity, whereas second-order cnoidal theory predicts a greater velocity at the surface than at the bottom.

As can be seen from the above results, the use of cnoidal theory depends upon the capability to calculate Jacobian elliptic functions. Chapter III will attempt to provide understanding of the role these functions have in cnoidal theory, as well as present expressions for their efficient calculation.

CHAPTER III

USE OF ELLIPTIC FUNCTIONS IN CNOIDAL WAVE THEORY

3.1 An Illustration of the Role of the cn Function in Cnoidal Wave Theory

Most coastal engineers and coastal scientists have little or no experience with elliptic integrals or Jacobian elliptic functions. This lack of familiarity with the mathematical basis of cnoidal wave theory is a hinderance to its dissemination and use as an analysis tool. Some insight can be gained into the role of Jacobian elliptic functions in cnoidal wave theory by comparing the surface profiles of cnoidal and small-amplitude waves. The following is not intended to be a rigorous discussion of elliptic functions, but it will serve as an introduction to the mathematical basis of cnoidal wave theory. For a more complete treatment of elliptic functions, Byrd and Freidman (1954), Milne-Thomson (1950), and Neville (1951) are recommended.

Figure 3.1 compares the free surface profiles of small-amplitude and first-order cnoidal waves. The two profiles have obvious differences. The small-amplitude wave is symmetric about the still-water level, whereas the cnoidal wave is not. The crest of the cnoidal wave is more peaked and reaches a higher elevation, and the trough is longer, flatter, and at a higher elevation than the corresponding parts of a small-amplitude wave. Assymmetry of the cnoidal wave profile is expected, since waves in the nearshore zone (shallow water) typically have sharp peaks and long shallow troughs.

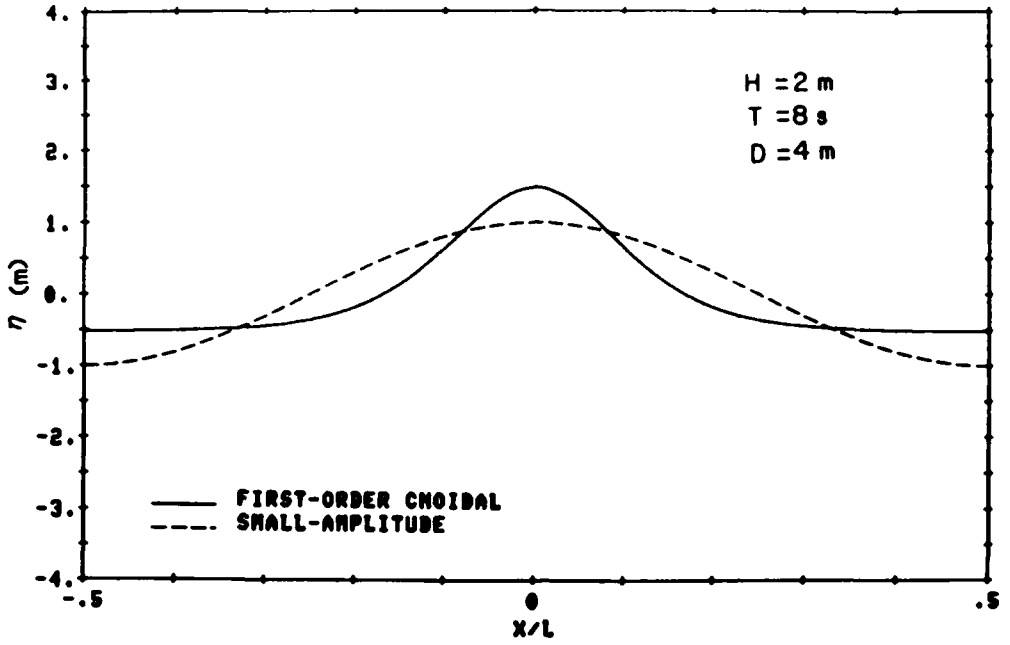

Figure 3.1. Cnoidal wave and small-amplitude wave profiles

Although Figure 3.1 shows that there are distinct differences between small-amplitude and cnoidal waves, an examination of the equations for the wave profiles will illustrate some important similarities. Equations 3.1 and 3.2, the equations for the small amplitude and first-orden cnoidal wave profiles, respectively, are almost directly analogous:

$$\eta_{SA} = \frac{H}{2} \cos\left[2\pi\left(\frac{x}{L} - \frac{t}{T}\right)\right] = \frac{H}{2} \cos \theta_{SA} \tag{3.1}$$

$$\eta = H\left\{cn^2\left[2K\left(\frac{x}{L} - \frac{t}{T}\right)\right] - \overline{cn^2}\right\} = H\left(cn^2\,\theta - \overline{cn^2}\right) \tag{3.2}$$

a. Wave height is used in the amplitude portion of both equations.

b. Periodic functions, cosine and cn^2 , are the foundation of both equations.

c. The phase functions are similar. The only difference is that cosine is periodic with 2π , whereas cn^2 is periodic with $2K$. (The quantity, K , Equation A.2, is the complete elliptic integral of the first kind.)

d. There are differences in structure between the two equations, the $\overline{cn^2}$, the value of $cn^2\theta$ averaged over wavelength (see Equation A.77), and the absence of the factor of 1/2 in the equation for the cnoidal wave profile. These differences result because the range of cosine varies from -1 to 1, whereas the range of cn^2 (as will be illustrated below) varies from 0 to 1. Since the range of cosine is twice that of cn^2 , the "missing" 1/2 in Equation 3.2 maintains the same wave height for both profiles. The values of $cn^2\theta$ are always positive; therefore, the $\overline{cn^2}$ term is needed to position the cnoidal profile at the still-water level.

e. The periodic functions, cosine for the small-amplitude waves and cn for cnoidal waves, are the most fundamental differences between Equations 3.1 and 3.2. However, even in this most basic difference there is a direct connection between the equations for the two wave profiles. The cn function is defined in terms of the cosine, as

$$cn\ \xi = \cos\ \phi \tag{3.3}$$

The elliptic integral, ξ, is defined as

$$\xi = \int_0^{\phi} \frac{d\theta}{\left(1 - \kappa^2 \sin^2 \theta\right)^{1/2}} \tag{3.4}$$

The creation of $cn\ \xi$ from $\cos \phi$ will be explained in the following discussion and illustration, which are modified from Isobe and Kraus (1983b, Appendix B). Each phase, ξ, of the cn function (Figure 3.2) corresponds to a value of the elliptic integral (step 1). This value of ξ uniquely determines a phase, ϕ, of the cosine function (step 2). The value of $\cos \phi$ (step 3) defines the value of $cn\ \xi$ as in Equation 3.3 (step 4). Note that $cn\ \xi$ is periodic with $4K$ and has values ranging from -1 to 1. By squaring $cn\xi$, the quantity $cn^2\xi$ (the shallow water wave shape) is created with a period of $2K$ and a range of values from 0 to 1. In essence, the elliptic integral is used as a mapping function that "stretches" the symmetrical cosine shape into the elongated trough and sharper peak of the cn^2 shape. Thus it can be seen that mathematics of cnoidal wave theory is not as radical a departure from the more familiar mathematics of small-amplitude wave theory as might first appear.

An interesting feature of Jacobian elliptic functions is that they are periodic with a multiple of K, which is not a constant. Unlike the cosine which is periodic with the multiple of a constant, π, the K of the Jacobian elliptic functions varies with the modulus, κ. Figure 3.3 (adapted from Isobe and Kraus 1983b) shows the effect of changes in κ on the values of K. Since κ (from Equation 2.69)

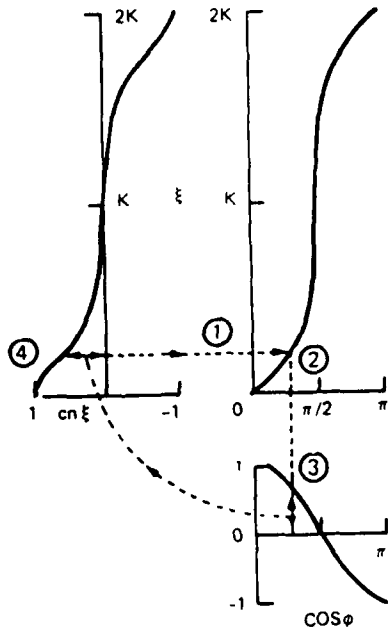

Figure 3.2. The creation of cn ξ from cos ϕ .

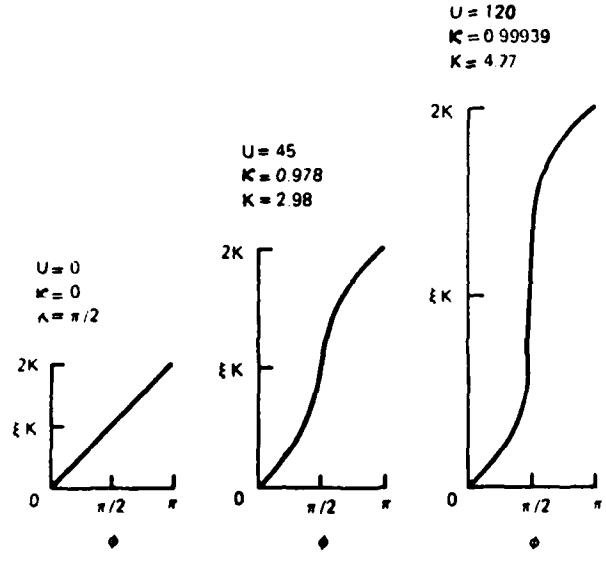

Figure 3.3. The effect on K from changes in κ .

varies with the value of the Ursell number (Equation 2.23), the shape of the wave profile is altered as the Ursell number changes value. For Ursell numbers 10 and 500, K is approximately 1.88 and 9.68, respectively. At large Ursell numbers, the wave profile approaches a solitary wave form. At small Ursell numbers, the profile tends more toward the shape of a small-amplitude wave. Thus cnoidal wave theory encompasses the major wave forms observed in shallow water.

3.2 Efficient Calculation of Elliptic Quantities

Methods of calculating elliptic integrals and Jacobian elliptic functions are neither as readily available nor as easy to execute as are the methods of calculating the trigonometric functions of small-amplitude wave theory. This has been a major drawback to the use of cnoidal wave theory.

At an Ursell number of 25 the value of κ is approximately 0.92. As the Ursell number increases, κ approaches 1.0. Subroutines in computer mathematics libraries and formulae found in mathematics handbooks for the calculation of elliptic functions are not conveniently adapted to this very small range of κ values. Consequently, use of these routines or formulae can result in more expensive computer calculations and perhaps inaccuracies in the quantities calculated. Isobe (1985) introduced expressions for the efficient calculation of cnoidal waves. (Since the derivation of these expressions does not appear to have been published in English, their development (Isobe, private communication, 1985) is included in Appendix A.) These formulae are given as power series of the complementary nome of the theta

function, q' . The definition of q' is repeated here from Equation A.7 as

$$q' = e^{-\pi\frac{K}{K'}} \tag{3.5}$$

The maximum value of q' applicable to cnoidal theory ($U \approx 10$) is $q' \approx 0.04$. Therefore, as can be seen in the following equations, the power series converge very rapidly, and only the first two or three terms are needed to ensure accuracy. These efficient expressions are the bases of the cnoidal wave calculations in the numerical model which is developed in this thesis.

The results of the derivation of second-order cnoidal theory presented in the previous chapter show that expressions are needed for the following seven quantities (Equations 3.6 to 3.12). This presentation of equations follows from Isobe (1985).

$$\kappa = \left(\frac{T_{02}}{T_{03}}\right)^2 \tag{3.6}$$

$$\kappa' \equiv \left(1 - \kappa^2\right)^{1/2} = 4\, q'^{1/2} \left(\frac{T_{04}}{T_{03}}\right)^2 \tag{3.7}$$

$$K = (T_{03})^2 \left(\frac{-\ln q'}{2}\right) \tag{3.8}$$

$$E_e = \frac{1}{(T_{03})^2} \left\{ 1 - \left[S - (T_{03})^4 \right] \left(\frac{-\ln q'}{2} \right) \right\} \tag{3.9}$$

$$cn(\theta;k) = \left(\frac{T_{04}}{T_{02}} \right) \left[\frac{T_2(\beta')}{T_4(\beta')} \right] \qquad (|\theta| \leq K) \tag{3.10}$$

$$sn(\theta;\kappa) = \left(\frac{T_{03}}{T_{02}} \right) \left[\frac{T_1(\beta')}{T_4(\beta')} \right] \qquad (|\theta| \leq K) \tag{3.11}$$

$$dn(\theta;k) = \left(\frac{T_{04}}{T_{03}} \right) \left[\frac{T_3(\beta')}{T_4(\beta')} \right] \qquad (|\theta| \leq K) \tag{3.12}$$

where

$$\beta' = \frac{\theta}{(T_{03})^2} \tag{3.13}$$

$$T_1(\beta') = \sinh \beta' - q'^2 \sinh 3\beta' + q'^6 \sinh 5\beta' - \ldots \tag{3.14}$$

$$T_2(\beta') = 1 - 2q' \cosh 2\beta' + 2q'^4 \cosh 4\beta' - \ldots \quad . \tag{3.15}$$

$$T_3(\beta') = 1 + 2q' \cosh 2\beta' + 2q'^4 \cosh 4\beta' + \ldots \tag{3.16}$$

$$T_4(\beta') = \cosh \beta' + q'^2 \cosh 3\beta' + q'^6 \cosh 5\beta' + \ldots \quad (3.17)$$

$$T_{02} \equiv T_2(0) = 1 - 2q' + 2q'^4 - \ldots \quad (3.18)$$

$$T_{03} \equiv T_3(0) = 1 + 2q' + 2q'^4 + \ldots \quad (3.19)$$

$$T_{04} \equiv T_4(0) = 1 + q'^2 + q'^6 + \ldots \quad (3.20)$$

$$S = 1 + 8q'^2 - 8q'^4 + \ldots \quad (3.21)$$

If $|\theta| > K$, the elliptic functions can be calculated from the expressions for $|\theta| < K$ through the following relations:

$$cn(\theta + 2nK;\kappa) = (-1)^n cn(\theta;\kappa) \quad (3.22)$$

$$sn(\theta + 2nK;\kappa) = (-1)^n sn(\theta;\kappa) \quad (3.23)$$

$$dn(\theta + 2nK;\kappa) = dn(\theta;\kappa) \quad (3.24)$$

where $n = 1,2,3\ldots$

The development and presentation of the expressions for the calculation of second-order cnoidal waves has been completed (Chapters II, III, and Appendix A). The next chapter will discuss the shoaling and refraction of second-order cnoidal waves which propagate over an irregular bottom.

CHAPTER IV

SHOALING AND REFRACTION OVER AN IRREGULAR SEA BOTTOM

Once the wave height, H, wave period, T, and water depth, D, are specified at a given location, equations presented in Chapters II and III, and in Appendices A and B can be used to calculate the surface profile, length, celerity, water particle velocities, energy, energy flux, and group velocity for both first-order and second-order cnoidal waves (provided that $U > 10$). The direction of wave propagation, α , is a fourth important variable. The value of α enters into the calculation of H, as well as other important engineering quantities such as wave-induced currents and the location of wave breaking. The values of the four variables, H, T, D, and α , are necessary at every location where wave and wave-induced current calculations are needed.

The quantities T and D are determined or specified externally to the model. Depths are specified at each grid node prior to simulation. For monochromatic wave modeling, the wave period is conserved as the wave transforms over the irregular bottom. Therefore, the period specified for each steady-state simulation is the period used for calculation at each grid node. Consequently, of the four main variables, only H and α remain to be determined. Their calculation is the primary function of the numerical model.

Refraction and shoaling (discussed later in this chapter) are the transformation mechanisms which will alter H and α as the wave propagates over the irregular bathymetry. Energy sources and sinks are not included in the model. The action of wind at the water-air surface is therefore ignored. The model "assumes" that the waves are formed

outside the modeled area, and the local winds do not add appreciable energy. The effect of friction at the bottom is also omitted, so the model will give best results if used for coasts that have sandy rather than muddy bottoms. (Muddy bottoms can cause significant dampening effects.) Dissipation through bottom friction could be straightforwardly included in the model, and might be considered in future developments. The model is not intended for use in the surf zone, so losses from wave breaking are not considered. Diffraction caused either by structures or from spatial variation of bathymetry is not included. Therefore, the model is an "open coast model" and cannot be used to determine wave heights in the lee of structures, or in locations where the geometry of the bottom appreciably focuses or scatters wave energy. The addition of any such transformations will demand research beyond the scope of this report.

The capability to calculate heights and angles of cnoidal waves directly on a numerical grid is an important feature of the numerical model developed in this report. No other known finite-amplitude wave transformation model has this capability. All other known finite-amplitude models and many of the small-amplitude wave transformation models use ray theory, a classical method for calculating the effects of wave refraction over an irregular bottom (Munk and Authur, 1952). Defining a wave front as a line of constant wave phase (such as the crest), a wave ray is a line which is normal to the wave front. In the ray tracing method, a ray equation is used to trace rays from a location where wave properties are known across a region where wave information is desired. A second equation called the ray separation equation

determines the wave height resulting from refraction by assuming constant energy flux between adjacent wave rays.

The ray tracing technique does not calculate directly on a numerical grid. In order for depth information to be available at the ray location and for the calculated heights and angles to be given at grid nodes, interpolation is necessary. Therefore, a technique first applied by Noda et al. (1974) was adopted in this study. This method calculates, directly on a numerical grid, the wave angles and heights resulting from the shoaling and refraction of waves over an irregular bottom. Two equations are used to predict the effects of shoaling and refraction: an equation for the calculation of the angle of wave propagation, and a conservation of energy flux equation, which is used to determine wave height.

In the next two sections, refraction is discussed, and the wave angle equation is derived. Next, the mechanism of shoaling is discussed, and the energy conservation equation used to predict wave height will be derived. Finally, expressions for energy flux and average wave energy per unit surface area of second-order cnoidal waves will be presented.

4.1 Wave Refraction

As can be seen from Equation 2.65, at a first approximation, the wave celerity varies as the square root of the depth. Therefore, if the depth is not constant along the wave front, the local wave celerity will also vary along the wave front. With different portions of the wave front traveling at different speeds, the wave begins to align parallel

to the bottom contours. This transformation, called refraction in a direct analogy with optics, can significantly affect the wave height by causing the convergence or divergence of wave energy.

Refraction is especially important for the calculation of sediment transport. The magnitude of wave-induced longshore current, the principal cause of longshore sediment transport and beach change, is a function of the angle of wave propagation at wave breaking (SPM, 1984, p. 4-54). Also, since the position of wave breaking is a function of wave height and water depth, the location of the wave breaking point is controlled in part by wave refraction. The location of wave breaking determines the width of the area over which the longshore current and intense sediment transport occur.

Traditionally, coastal engineers and scientists have broadened the usage of the terminology "wave refraction" to include wave shoaling in addition to pure refraction. Thus, a numerical model of wave refraction usually implies that both shoaling and refraction have been considered. All three of the finite-amplitude refraction models for an irregular bathymetry discussed in the introduction (Chu, 1975; Headland and Chu, 1984; and Oh and Grosch, 1985), predicted that finite-amplitude waves refract less than do small-amplitude waves. Skovgaard and Petersen (1977) calculated the refraction of first-order cnoidal waves for straight and parallel bottom contours with the same result.

Wang and Le Méhauté (1980) found that the prediction of less refraction for finite-amplitude waves did not match well to one set of laboratory experiment observations. They developed a "hybrid" model, which uses the assumption of a plane bottom. The hybrid model employs

cnoidal wave theory for shoaling calculations and small-amplitude theory for refraction calculations. This combination matched the experimental data for waves of relatively high deep-water steepness. The results showed that both the data and the hybrid model indicated less refraction than small-amplitude theory, but more refraction than predicted by finite-amplitude theory. However, the differences in wave refraction which motivated the hybrid model were observed in the laboratory experiment and calculated in the numerical model at wave breaking, where the numerical model must estimate the breaking point, as well as calculate refraction. Therefore, it is difficult to determine if the differences between calculated and observed wave angle were due to errors in the physical model observations, under-prediction in the numerical modeling of refraction by finite-amplitude theory, difference between the breaking criterion used in the numerical model and the breaking position observed in the physical modeling, or some combination of the three. The question of whether finite-amplitude theory under-predicts refraction cannot be answered without more experimental results. The hybrid model seems to be too drastic a step based on the observations of one experiment. Additional well-controlled laboratory experiments are required to resolve this point.

4.2 Derivation of the Wave Angle Equation

The equation and procedure for calculating the wave angle as introduced by Noda et al. (1974) was derived for small-amplitude wave theory. It is based on the irrotationality of wave number. The wave number in small-amplitude theory is defined as the gradient of the phase

function of the surface profile. Since the phase functions of cnoidal and small-amplitude waves are different, the wave angle equation must be rederived for use with cnoidal wave theory. The following development of the wave angle equation is patterned after a derivation for small-amplitude theory found in Dean and Dalrymple (1984, Chapter 4).

The surface profile of a second-order cnoidal wave (Equation 2.66) is repeated in Equation 4.1 for easy reference.

$$\eta = D\left(A_0 + A_1\, cn^2\,\theta + A_2\, cn^4\,\theta\right) \tag{4.1}$$

For a wave which is traveling in an arbitary direction in the x-y plane, θ is given as

$$\theta = 2K\left(\frac{x}{L}\cos\alpha + \frac{y}{L}\sin\alpha - \frac{t}{T}\right) \tag{4.2}$$

where $L/\cos\alpha$ and $L/\sin\alpha$, the projections of the wave crest on the x and y axis, respectively; and α, the direction of wave propagation, are shown in Fiqure 4.1.

The phase function can be written as

$$\theta = 2K\Omega \tag{4.3}$$

where from Equation 4.2

$$\Omega = \frac{x}{L}\cos\alpha + \frac{y}{L}\sin\alpha - \frac{t}{T} \tag{4.4}$$

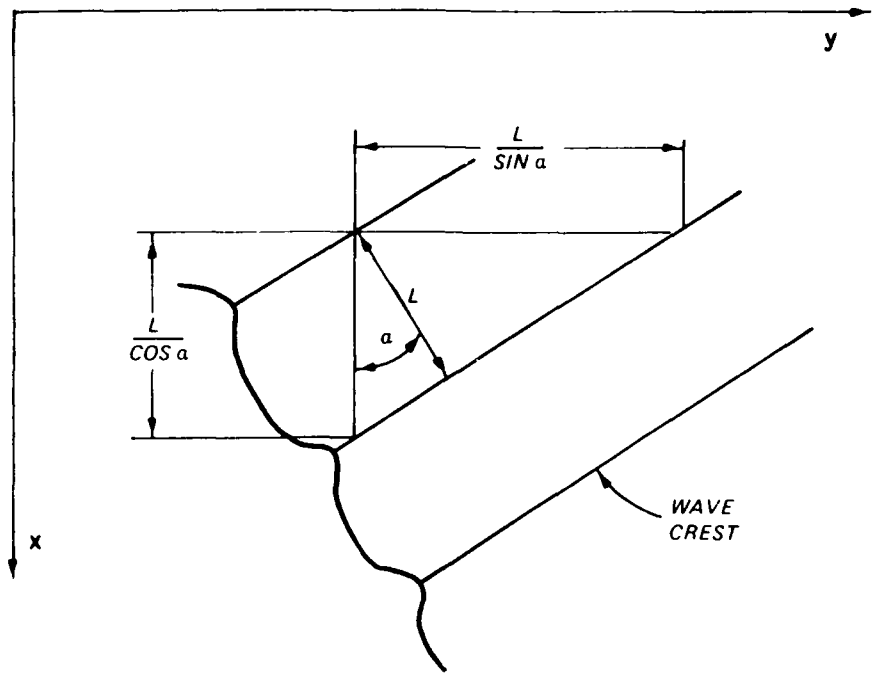

Fiqure 4.1. Definition sketch for α , L/cos α , and L/sin α .

As illustrated in Appendix A, the periodic functions $cn^2\ \theta$ and $cn^4\ \theta$ of Equation 4.1 have a non-constant period, 2K. However, the crest of the wave of Equation 4.1 occurs for Ω = n; n = 0,1,2,.... , regardless of the value of K. Therefore, the normal vector to the crest (and thus the direction of wave propagation) can be determined by taking the gradient of Ω , as in

$$\nabla\Omega = \left(\frac{\cos\alpha}{L}\right)\hat{i} + \left(\frac{\sin\alpha}{L}\right)\hat{j} \qquad (4.5)$$

where $\hat{i}$ and $\hat{j}$ are the unit vectors in the x and y directions.

From a vector identity that states that the curl of the gradient of a scaler is equal to zero,

$$\nabla \times \nabla\Omega \equiv 0 \tag{4.6}$$

which can be rewritten as

$$\frac{\partial}{\partial x}\left(\frac{\sin \alpha}{L}\right) - \frac{\partial}{\partial y}\left(\frac{\cos \alpha}{L}\right) = 0 \tag{4.7}$$

This is the governing equation used in the numerical model to calculate α on a fixed grid. The finite difference representation of Equation 4.7 will be presented in Chapter V. It is important to note that wavelength, L, is a function of wave height, H, in a finite-amplitude wave theory. This can be shown using the basic relationship, $L = CT$, and from Equation 2.65, where it is seen that wave celerity, C, (from $\varepsilon = H/D$) is a function of H. This has important implications for the calculation of refraction based on a finite-amplitude wave theory. First, refraction causes changes in wave height, which will in turn affect the calculation of wave angle in Equation 4.7. Shoaling also causes changes in wave height, as will be discussed below. Therefore, the dependence of refraction on wave height couples shoaling and refraction.

The equation derived for the calculation of the angle of wave propagation (Equation 4.7) reduces to a simpler form often used for refraction studies. Snell's law (Equation 4.8) is used to study refraction in analytical and theoretical studies. It is also commonly used if the assumption of straight and parallel bottom contours is justified or used locally over short distances for a more complicated bathymetry.

$$\frac{\sin \alpha}{C} = \text{constant} \tag{4.8}$$

Establishing a coordinate system so that the x-axis is normal to shore and the y-axis is along the shore, the y-derivatives vanish for the case of straight and parallel bottom contours. Equation 4.7 becomes

$$\frac{\partial}{\partial x}\left(\frac{\sin \alpha}{L}\right) = 0 \qquad (4.9)$$

This equation can be converted to Snell's law (Equation 4.8) by multiplying by T, using the relationship, C = L/T, and integrating in the x direction. The constant in Equation 4.8 is usually evaluated as $\sin \alpha_o / L_o$ in which the subscript "o" denotes known quantities at a reference depth, usually in deep water.

4.3 Wave Shoaling

Changes in water depth can also cause changes in wave height due to the mechanism known as wave shoaling. As a wave "shoals," the wave height adjusts to compensate for variations in the velocity of wave energy propagation caused by changes in depth. In general, as a wave first begins to shoal there is a region where the wave height will decrease slightly. Then, as the wave enters progressively shallower water, the wave height will increase. Observations of waves just before the breaking point show that a rapid increase in height can occur. The investigation of the equations governing energy propagation of second-order cnoidal waves will exhibit the effect of depth on shoaling.

The average rate of wave energy propagation through a vertical cross section normal to the direction of wave propagation, called the energy flux, F, is defined in Equation 4.10 (Phillips, 1977, p. 25). (An

equation for the calculation of energy flux for second-order cnoidal waves is derived in Appendix B and is presented and discussed at the end of this chapter.) The quantity E is the average energy per unit surface area of the wave, and the group velocity, C_g, is the velocity of wave energy propagation.

$$\vec{F} = E \vec{C}_g \tag{4.10}$$

Both group velocity and energy flux are vector quantities, but the vector notation will be omitted for convenience, except if the directionality of the two quantities is emphasized. The customary term, group "velocity," will be used instead of the term, group "speed," when referring to C_g. Equations 4.11 and 4.12, for C_g and E, are derived in Appendix B (Equations B.88 and B.83). E_0, E_1, and F_1, functions of λ and μ, are defined in Equations B.83 and B.46.

$$C_g = \sqrt{gD}\left[1 + \varepsilon\left(\frac{F_1 - E_1}{E_0}\right)\right] \tag{4.11}$$

$$E = \rho g H^2 (E_0 + \varepsilon E_1) \tag{4.12}$$

At a first approximation, Equation 4.11 indicates that C_g varies with the square root of depth. As will be discussed below, it is assumed that F is conserved as the wave shoals. Therefore, from Equation 4.10, if C_g decreases with decreasing depth, then E, in order to conserve F, must compensate by increasing. Since E is proportional to H^2, changes in E cause corresponding changes in H.

There have been numerous investigations devoted to the subject of shoaling of finite-amplitude waves. All the researchers have found that predictions of wave shoaling using small-amplitude theory underestimate shoaling rates predicted by either finite-amplitude theories or exhibited in experimental data. Le Méhauté and Webb (1964) used the conservation of energy flux to study the shoaling of third-order Stokes waves. Koh and Le Méhauté (1966) found that fifth-order Stokes waves have a slightly lower shoaling coefficient than do third-order Stokes waves. An equation to calculate shoaling for first-order cnoidal waves was derived by Svendsen and Brink-Kjaer (1972). They supplied tables which can be used to predict wave height and wave length in shallow water using deepwater inputs. Shuto (1974) derived a law of shoaling from basic hydrodynamic equations, and presented expressions for the engineering calculation of shoaling in three different regions defined by the Ursell number. The expression given for the region $U > 30$ corresponds to first-order cnoidal theory. Sakai and Battjes (1980) calculated shoaling based on Cokelet's high-order and essentially mathematically exact wave theory, and compared the results with those of the above researchers. They found that Cokelet's numerical theory predicted slightly higher shoaling than the above-mentioned studies. Walker and Headland (1982) compared several of the above theoretical shoaling calculations with empirically based wave breaking indices. They found that the theoretical results predicted greater shoaling rates than indicated by the empirical breaking indices. However, they concluded that the wave flume data on which the empirical curves are based may be contaminated by unwanted harmonics resulting from sinusoidal motion of

the wave generator. Isobe (1985) used small-amplitude theory (for deeper water) and first-order cnoidal theory (for shallower water) to compute shoaling, and compared results to experimental data. The comparison was favorable for waves of small to intermediate deepwater wave steepness.

4.4 Derivation of the Conservation of Energy Flux Equation

The conservation of energy principle applied in a control volume approach shows that

$$\nabla \cdot \vec{F} = 0 \tag{4.13}$$

under the following assumptions:

a. The bottom slope is sufficiently mild so that reflection is negligible.

b. There are no energy sources or sinks.

c. The solution is for the steady state.

Equation 4.13 is the basis for the calculation of wave height in the numerical model. The technique and the finite difference equations will be presented in Chapter V. Use of this equation in the numerical model requires an expression for the energy flux of second-order cnoidal waves. The development of this expression was a nontrivial task and is a major accomplishment of this study. The derivation of an expression for the energy flux of second-order cnoidal waves is included in Appendix B, and the resulting equation for F (Equation B.46), is repeated as

$$F = \rho g H^2 \sqrt{gD}\,(F_0 + \varepsilon F_1)$$

$$= \rho g H^2 \sqrt{gD}\left[(-\lambda + 2\mu + 4\lambda\mu - \lambda^2 - 3\mu^2)\,\frac{1}{3}\right.$$

$$+ \varepsilon\,(-4\lambda + 8\mu + 53\lambda\mu - 12\lambda^2 - 60\mu^2$$

$$\left. + 53\lambda^2\mu - 120\lambda\mu^2 - 8\lambda^3 + 75\mu^3)\,\frac{1}{30}\right] \quad (4.14)$$

For comparison, only one other source could be found which gave expressions for F and E for second-order cnoidal waves. The equation for F (Sarpkaya and Isaacson, 1981, Chapter 4), derived from the second-order cnoidal theory presented by Laitone (1960) is

$$F_{S\&I} = \rho g D^2 \sqrt{gD}\,\varepsilon^2\left(\left[-\frac{E_e}{K}\left(3\,\frac{E_e}{K} + 2\kappa^2 - 4\right) - \kappa'^2\right]\frac{1}{3\kappa^4}\right.$$

$$+ \varepsilon\left\{\frac{E_e}{K}\left[75\,\frac{E_e^2}{K^2} + 60\,\frac{E_e}{K}\,(\kappa^2 - 2) + 8\kappa^4 + 53\kappa'^2\right]\right.$$

$$\left.\left. + 4\kappa'^2\,(\kappa^2 - 2)\right\}\,\frac{1}{30\kappa^6}\right) \quad (4.15)$$

From $\lambda = \kappa'/\kappa$ (Equation 2.70), and from $\mu = E_e/\kappa^2 K$ (Equation 2.71) Equation 4.14 can be shown to be equivient to Equation 4.15. This result is expected since both Laitone's derivation of second-order cnoidal wave theory and the derivation used in this thesis (Isobe and Kraus, 1983b) use Stokes' second definition of wave celerity (Equation 2.21). The expression for E (Equation B.83) was also found to be equivalent to that given by Sarpkaya and Isaacson (1981, Chapter 4). A

similar check for C_g Equation B.88 is not possible since no other expression for the group velocity of second-order cnoidal waves is known.

The basis has been established for the calculation of the shoaling and refraction of second-order cnoidal waves over an irregular bathymetry. The next chapter describes the numerical model designed to execute this task.

CHAPTER V

DESCRIPTION OF THE NUMERICAL MODEL

5.1 Overview of Technique

As was discussed in Chapter IV, shoaling and refraction result from changes in group velocity, C_g and wave celerity, C, respectively, as waves propagate over varying water depth. For small-amplitude wave theory, C and C_g are functions of wave period and water depth only. Since neither the wave period nor water depth are affected by shoaling or refraction, shoaling and refraction can be directly and independently calculated in a model based on small-amplitude wave theory. For instance, the wave height at any location can be calculated by determining a shoaling coefficient, K_s, and a refraction coefficient, K_r, each calculated independently of the other. With the deep water wave height signified by H_o, the wave height from a small-amplitude model is given as $H = K_r K_s H_o$.

For finite-amplitude wave theory (in this report, both first and second-order cnoidal theory), both C_g (Equation B.88) and C (Equation 2.65), are functions of wave height, as well as wave period and water depth. Therefore, since both shoaling and refraction cause changes in wave height, there is an interdependence between the two transformations. Consequently, the calculation of wave height caused by shoaling and refraction using a finite-amplitude theory is not as direct as with small-amplitude theory. In the numerical model developed in this study, an iterative technique is used to account for the interdependence of shoaling and refraction. First an estimate for the angle of wave propagation is calculated, followed by the calculation of an

estimate for the wave height. The process is repeated until the change in wave height from one iteration to the next is below a specified tolerance. The number of iterations varies from two to six for convergence to a tolerance that is about 0.1% of the wave height. In general, more iterations are necessary near to the wave breaking point, where the wave height is changing rapidly, than are needed near to the seaward boundary of the model.

Figure 5.1 shows the arrangement of the numerical grid. The grid is aligned so that the y-axis (j=1,n) lies in the alongshore direction and the x-axis (i=1,m) lies normal to the shoreline. With the origin of the grid located on dry land it is easier to adjust the position of the seaward boundary of the area to be modeled. The x-axis is placed so that all the area to be modeled has positive y-coordinates. For ease of

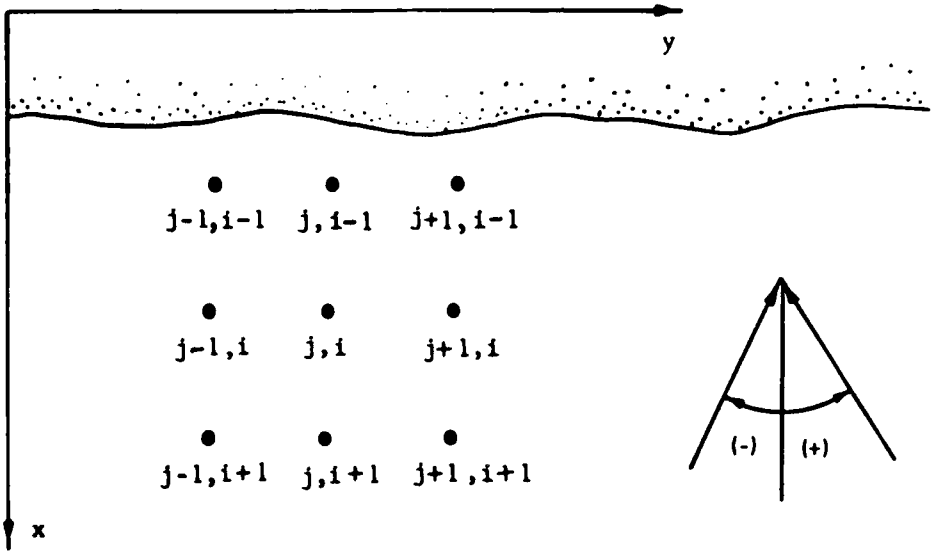

Figure 5.1. The numerical grid.

description in the remainder of this chapter, the term "row" is used to mean a line of constant x (roughly parallel to the shoreline), where the nodes of the numerical grid are designated (j,i); j=1,n ; i=constant. (The order of all field arrays in the computer code is (j,i) to allow for more efficient use of computer memory.)

Figure 5.1 also contains a definition sketch for the wave angle. Both input and output wave angles are measured counterclockwise (direction from which the waves are incident) from a line parallel to the x-axis. For internal model calculations 180° is added to these defined angles so that calculations can use a definition of angle which matches the sign of the trigonometric functions and the coordinate system of the numerical grid. For the internal calculations wave angle is measured counterclockwise (direction which the wave is traveling) from a line parallel to the x-axis.

The wave parameters of height (H), period (T), and angle (α) are the basic inputs to the model. The numerical model calculates for a steady state condition, so each wave condition requires a separate simulation. Each simulation assumes that wave conditions are constant for the time that it would take a wave to travel from the seaward boundary to the breaking point. The wave period is specified as a constant for all grid nodes during each simulation. Wave height and wave angle can be specified as constant along the whole seaward boundary or they can vary for each grid node on the seaward boundary, resulting from the calculations of a companion model used for deeper water. (Methods of connection with a companion model will not be investigated in this thesis.) The boundary conditions on the lateral sides of the

grid are the simplest possible. The lateral boundary values of H, α, and the energy flux, F, take the values of the node next to the boundary. Tests showed that the model is insensitive to the lateral boundary conditions. As long as the lateral boundaries are not close to areas of interest, the model results are negligibly affected by the lateral boundary conditions. In the present version of the model the lateral boundaries are assumed to be in water; therefore, the model is configured for simulations on a relatively straight coastline with no significant embayments.

Since the computational scheme marches toward the shoreline, a boundary condition along the shoreline is not essential from a numerical standpoint. However, since the model is not intended for use shoreward of the wave breaking point, the computations are halted before the marching scheme reaches the shoreline. For operation in a plane beach mode, the wave heights will be identical along each row. In this case a standard breaking criterion, $H_b = 0.8D$, is used. The simulation is halted if the breaking criterion is exceeded. For the case of irregular bathymetry, wave heights will vary along each row, and the onset wave breaking will not occur at the same row throughout the modeled area. If the calculated wave height exceeds the breaking criterion at a node, the wave height is truncated so that $H = 0.8D$. This technique allows the location of wave breaking to be determined for the entire modeled area. The simulation halts if the breaking criterion has been exceeded at all nodes on a row.

Judgement must be exercised in applying model results near the breaking point. The perturbation solution for the second-order cnoidal

wave theory used in this report is based on the assumption that the ratio of wave height to water depth is small; therefore, model results as H/D approaches 1.0 are suspect. Futhermore, as a wave nears breaking, the assumption of permanent form, which is fundamental to the derivation of cnoidal wave theory, is violated. This difficulty is not unique to this numerical model; it occurs in all shallow water wave transformation models currently available for engineering use.

A flow chart of the numerical model is presented in Figure 5.2. One of chief assets of this model is its simplicity. The difficult work has been the development of the equations for the calculation of shoaling and refraction directly at grid points (Chapter IV and Appendix B), and the development of expressions for the efficient calculation of elliptic integrals and Jacobian elliptic functions (Appendix A). This is the advantage of using an analytical wave theory instead of a numerical wave theory. The model, written in FORTRAN V, is divided into three main segments, an input segment, the main calculation segment, and an output segment.

5.2 Model Output and Input

The primary results of the model are wave height and wave angle at each node on the numerical grid. Depth, wave length, wave celerity, group velocity, and Ursell number can also be included in the output by specifying a keyed number in the model input file. The output file consists of one grid for each of the chosen quantities with the values of the particular quantity given at each node.

The input file read into the model at the beginning of each

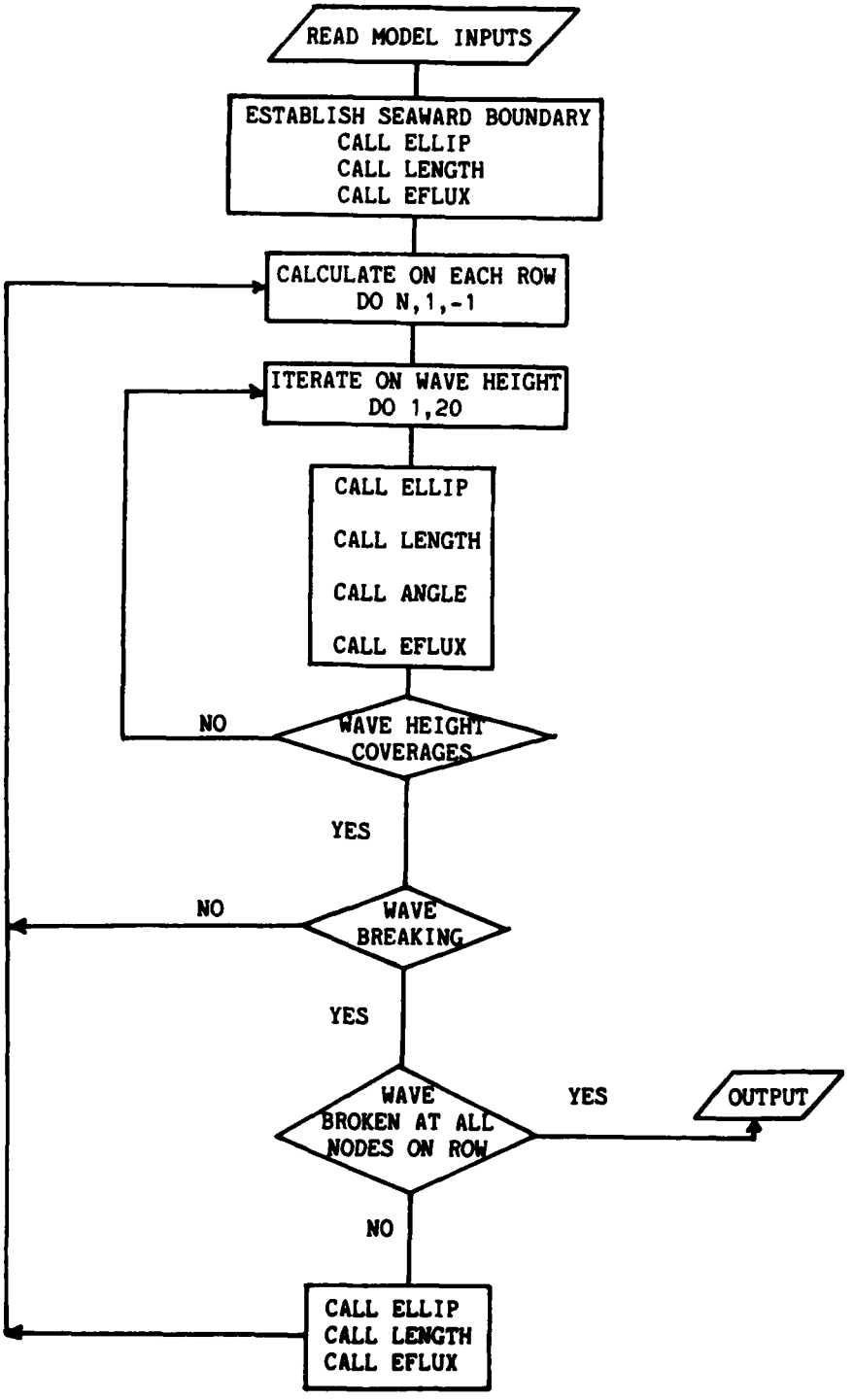

Figure 5.2. Flow chart of numerical model.

simulation contains values of the acceleration of gravity, the density of water, the desired convergence criterion, a correction to the water depths to account for changes in water depth due to tide or storm surge, the output specifier, a flag which triggers the input or calculation of the depth grid, and constants for use in calculating an idealized bathymetry. Also read in from the input file are the grid spacing in the both the x and y directions. The numerical grid is a fixed rectangular grid, and the values of the grid spacing, Δx and Δy, do not have to be equal. Also read from the input file is a flag, through which the user can specify that either first or second-order cnoidal wave theory be used.

The depths at each grid node are read from the input file for the case of prototype bathymetry or can be calculated for the case of idealized bathymetry using

$$D_{j,i} = a + bx - (d)(i/m) \cos [2\pi(j/n)] + (d)(i/m) \qquad (5.1)$$

This equation is composed of a plane beach component and a longshore rythmic component. Such a topography is an idealization of periodic rip channels superimposed on a uniformly sloping bottom, as is frequently seen along sandy coasts. The symbols for the plane bottom component, "a" and b, are the depth at i=0 and the bottom slope, respectively. The rythmic component varies the depth in the longshore direction with a sinosoidal pattern which has a phase determined by the normalized alongshore position. The sinisoidal pattern has an maximum amplitude of 2d at the seaward boundary and decays towards the shoreline depending

upon the value of the normalized onshore-offshore position. If d is positive, a trench is created. If d is negative, a shoal is created.

5.3 Calculating Wave Height and Wave Angle

Four subroutines are used for the main computational scheme, ELLIP, LENGTH, ANGLE, and EFLUX. Before calculations can begin for the interior of the grid, wave celerity (C), wave length (L), and energy flux (F) must be calculated on the seaward boundary. Since C, L, and F are all functions of λ and μ (Equations 2.65, L = CT, and 4.14), ELLIP is used to calculate λ and μ. Then C and L are calculated in LENGTH. Finally the calculation of F in EFLUX completes the specification of the seaward boundary conditions. (The wave angle, α is read from the input file.) Once the above quantities are calculated on the seaward boundary the computational scheme marches toward shore (in the negative x direction) one row at a time. The numerical scheme is explicit, with information from from i^{th} row used to calculate values at the $(i-1)^{th}$ row. Calculations are repeated until H converges to within the specified tolerance at each node on the row before preceeding to the next row. Before the first iteration on each row, as an initial guess, the wave height at each node is set equal to the wave height of the node from the previous row in the same column, $(H^0)_{j,i-1} = (H^k)_{j,i}$; j = 1,n, where the superscript, k, denotes iteration level. The four subroutines used in the calculations are described in the following sections.

5.3.1 Subroutine ELLIP

Since the first and second-order cnoidal wave quantities have been

expressed in terms of λ and μ, evaluation of λ and μ is necessary. An equation for the evaluation of λ derived from Equations 2.70, 3.6, and 3.7 is

$$\lambda = 16q' \left(\frac{T_{04}}{T_{02}}\right)^4 \tag{5.2}$$

An equation for the evaluation of μ derived from Equations 2.71, 3.6, 3.8, and 3.9 is

$$\mu = \frac{1}{(T_{02})^4} \left[\frac{2}{(-\ln q')} - S + (T_{03})^4\right] \tag{5.3}$$

The complementary nome, q' is the basic quantity used in the calculation of these two quantities, as well as all other cnoidal wave quantities. An equation for the calculation of q' can be derived from Equation 2.85, the dispersion relation for second-order cnoidal waves repeated here as

$$\frac{16}{3} \kappa^2 K^2 = \frac{gHT^2}{D^2} \left[1 + \epsilon \left(\frac{-1 - 2\lambda}{4}\right)\right] \tag{5.4}$$

If the second term in the brackets of the above equation is neglected, the dispersion relation for first-order cnoidal waves results. From κ and K (Equations 3.5 and 3.7), Equation 5.4 can be rewritten as

$$\frac{4}{3} (T_{02})^4 (-\ln q')^2 = \frac{gHT^2}{D^2} \left[1 + \epsilon \left(\frac{-1 - 2\lambda}{4}\right)\right] \tag{5.5}$$

Solving this equation for q' gives

$$q' = \exp\left(-\frac{1}{(T_{02})^2}\left\{\frac{3}{4}\frac{gHT^2}{D^2}\left[1 + \varepsilon\left(\frac{-1 - 2\lambda}{4}\right)\right]\right\}^{1/2}\right) \qquad (5.6)$$

For a simulation employing first-order cnoidal wave theory, the higher order contribution to q' (the coefficient of ε in Equation 5.6) is set equal to zero.

Note that both T_{02} (Equation 3.18) and λ (Equation 2.70) are functions of q'. Therefore, an iterative solution is used to solve for q'. Since the iteration for q' is inside the iteration loop for H, a technique using under-relaxation was developed to converge on q' in as few iterations as possible. Without the relaxation technique it can take up to 13 iterations to converge to $(q'^{k} - q'^{k-1})/q'^{k-1} < 0.001$ for U = 10. This would increase computer time since q' must be calculated at each node. The relaxation equation is

$$q'^{k} = q'^{*} - (q'^{*} - q'^{k-1})\,R \qquad (5.7)$$

where R is the relaxation parameter and q'^{*} is the value of q' at the k^{th} iteration before relaxation. Initial tests showed that a constant value for R does not produce acceptable results for the full range of Ursell numbers applicable to cnoidal wave theory (U > 10). Difficulties with convergence occur at smaller Ursell numbers so the optimum value of R was determined for a series of Ursell numbers between 10 and 100. Since the optimum value varies not only with the Ursell number but also with the value of the perturbation parameter, representative values of ε

were used, and an exponential curve was fit through the optimum R values for U = 10 (ϵ = 0.1) and U = 30 (ϵ = 0.2), giving

$$R(U) = e^{(-0.61-0.054U)} \tag{5.8}$$

The calculation for q' converges to $(q'^{k} - q'^{k-1})/q'^{k-1} < 0.001$ after only three iterations for U > 10, using Equation 5.8 to determine the relaxation parameter. For the interior of the grid, since calculations are repeated at least twice because of the iteration for wave height, only two iterations for q' are needed during each iteration for wave height. For calculations on the seaward boundary six iterations are used to ensure very accurate determinations of q' for the boundary conditions. (This row is not included inside the iteration for H.) The model determines the least accurate convergence for each row and those values are printed at the end of the simulation. The method of using a fixed number of iterations has the advantage of not having to check a convergence criterion with FORTRAN "IF" statements.

5.3.2. Subroutine LENGTH

Once λ and μ are calculated, the wave celerity is calculated from Equation 2.65. The zeroth-order contribution to C, i.e., C_0, is also calculated for use in the calculation of C_g and F in Subroutine EFLUX. The wave length, L, is then calculated using the relation L = CT.

For a simulation employing first-order cnoidal wave theory, the second-order contribution to C, i.e., C_2, is set equal to zero.

5.3.3 Subroutine ANGLE

Equation 4.7, the governing equation for the calculation of the angle of wave propagation is repeated here as

$$\frac{\partial}{\partial x}\left(\frac{\sin \alpha}{L}\right) - \frac{\partial}{\partial y}\left(\frac{\cos \alpha}{L}\right) = 0 \tag{5.9}$$

The FTCS (forward time, central space, where the x is considered "time") explicit finite difference scheme used in the model is given as

$$\frac{1}{\Delta x}\left[\left(\frac{\sin \alpha}{L}\right)_{j,i} - \left(\frac{\sin \alpha}{L}\right)_{j,i-1}\right] - \frac{1}{2\Delta y}\left[\left(\frac{\cos \alpha}{L}\right)_{j+1,i} - \left(\frac{\cos \alpha}{L}\right)_{j-1,i}\right] = 0 \tag{5.10}$$

This equation is solved for $\alpha_{j,i-1}$; j = 1,n, (The scheme marches in the minus x-direction.) which gives

$$\alpha_{j,i-1} = \sin^{-1}\left(L_{j,i-1}\left\{\left(\frac{\sin \alpha}{L}\right)_{j,i} - \frac{\Delta x}{2\Delta y}\left[\left(\frac{\cos \alpha}{L}\right)_{j+1,i} - \left(\frac{\cos \alpha}{L}\right)_{j-1,i}\right]\right\}\right) \tag{5.11}$$

In their numerical model of small-amplitude wave refraction, Perlin and Dean (1983) found that an implicit version of this finite difference scheme can cause oscillations with a wavelength equal to $2\Delta y$. They added a "dissipative interface" to the finite difference scheme to control these spurious oscillations. This problem has not yet been encountered in the model developed in this report. Equation 5.11 has been well-behaved, possibly, because only smoothly varying idealized bathymetries

have been used in the simulations. Future testing of the model will involve optimizing the finite difference technique.

5.3.4 Subroutine EFFLUX

The governing equation for the calculation of energy flux (Equation 4.13) is repeated here as

$$\nabla \cdot \vec{F} = 0 \tag{5.12}$$

Expanding this equation gives

$$\frac{\partial}{\partial x}(F \cos \alpha) + \frac{\partial}{\partial y}(F \sin \alpha) = 0 \tag{5.13}$$

Again as in the finite differencing of the wave equation an explicit FTCS finite difference algorithm is used. This results in

$$F_{j,i-1} = \frac{1}{(\cos \alpha)_{j,i-1}} \left\{ (F\cos \alpha)_{j,i} + \frac{\Delta x}{2\Delta y}\left[(F\sin \alpha)_{j+1,i} - (F\sin \alpha)_{j-1,i}\right] \right\} \tag{5.14}$$

From Equation 4.14, F can be rewritten as

$$F_{j,i} = H^2_{j,i} \, F^*_{j,i} \tag{5.15}$$

where F^* is given as

$$F^*_{j,i} = \rho g \sqrt{gD} \left[(F_0)_{j,i} + (\varepsilon F_1)_{j,i} \right] \tag{5.16}$$

The wave height is calculated using

$$H_{j,i} = \left(\frac{F_{j,i}}{F^*_{j,i}} \right)^{1/2} \tag{5.17}$$

where F_0 and F_1 are defined in Equation B.46.

Finally, C_g is calculated from Equation B.88, after a value for E_0 is determined using Equation B.83.

If first-order cnoidal wave theory is selected in the input file, the values of F_1 and E_1 are set equal to zero.

The next chapter will present results from simulations of the shoaling and refraction of both first and second-order cnoidal waves.

CHAPTER VI

NUMERICAL MODEL RESULTS

Results from numerical simulations of the shoaling and refraction of shallow water waves will be presented in this chapter. Section A.1 and Section A.2 contain results for shoaling and refraction, respectively, over a plane bottom. In these sections, a comparison is made among the results produced by small-amplitude, first-order cnoidal, and second-order cnoidal wave theories. In Section A.3, results from small-amplitude and second-order cnoidal wave theories for a spherical shoal and an idealized trench are compared. A discussion of the computer time required for second-order cnoidal vs. small-amplitude wave modeling is given in Section 6.4.

For simulations using either first-order or second-order cnoidal wave theory, the numerical model developed in this report was used. For simulations using small-amplitude wave theory, a model employing numerical methods similar to the cnoidal model was developed. The wave angle was determined from the irrotionality of wave number, $\nabla \times k = 0$, and wave height was determined by using conservation of energy flux, $\nabla \cdot F = 0$. Equations 6.1 and 6.2 were used to calculate k and F for small-amplitude wave theory. (The subscript SA denotes small amplitude.)

$$\left(\frac{2\pi}{T}\right)^2 = gk \tanh kD \tag{6.1}$$

$$F_{SA} = \frac{1}{8} \rho g H^2 \left(\frac{L}{T}\right) \frac{1}{2} \left[1 + \left(\frac{2kD}{\sinh 2kD}\right)\right] \tag{6.2}$$

It is customary to identify waves by the deepwater values of L_o and H_o, as determined by small-amplitude wave theory. Since cnoidal wave theory is not valid in deep water, boundary conditions are needed on the seaward boundary of the cnoidal wave model if the simulations are to be characterized by deepwater wave parameters. In Chapter I it was mentioned that a future version of the second-order cnoidal wave model would be coupled with a model using third-order Stokes wave theory for use in deeper water. The coupling of these two models will require further research. For the results presented in this chapter, the small-amplitude wave model described above was used to transform the deepwater wave inputs (H_o and α_o) to the seaward boundary of the cnoidal wave model. The seaward boundary of the cnoidal model was placed at the depth where the value of the Ursell parameter ($U = HL^2/D^3$) was equal to 15, as calculated from small-amplitude theory. Thus, wave heights and wave angles were identical at the "connection point" for all three theories (small-amplitude, first-order cnoidal, and second-order cnoidal) if the same deepwater wave condition is simulated.

In all the simulations conducted in this chapter, a square grid spacing of 5 m was used. The acceleration of gravity was set equal to 9.806 m/s^2, and the density of sea water was set at 1026 kg/m^3.

6.1 Shoaling Over a Plane Bottom

In Section 6.1.1 the shoaling of small-amplitude, first-order cnoidal, and second-order cnoidal waves is compared. Numerical results from the three wave theories are compared to laboratory wave flume results in Section 6.1.2. Plots for multiple combinations of wave period

and deepwater wave steepness comparing second-order cnoidal wave theory to small-amplitude wave theory are presented in Section 6.1.3.

6.1.1 Comparison of wave shoaling among small-amplitude, first-order cnoidal, and second-order cnoidal waves

Small-amplitude, first-order cnoidal, and second-order cnoidal wave theories are compared for the calculation of shoaling in Figures 6.1 and 6.2. Results are presented for two deepwater wave steepnesses (H_o/L_o equal to 0.005 and 0.020) at each of two wave periods (8 and 12 s). The ordinate of these plots is nondimensional wave height (H/H_o), and the abscissa is depth in meters. The curves stop where the breaking criterion H/D = 0.8 is reached.

Several features can be seen in Figures 6.1 and 6.2. Second-order cnoidal wave theory (cn II) always produces a shoaling rate intermediate between the rates predicted by the two other theories. This was found to be true in all cases simulated. The highest shoaling rate is always given by first-order cnoidal wave theory (cn I), and the lowest rate by small-amplitude wave theory (SA). For a given wave period, the cn II curve is closest to the cn I curve at the smaller deepwater wave steepness (Figures 6.1a and 6.2a) and closest to the SA curve at the greater deepwater wave steepness (Figures 6.1b and 6.2b).

As described in Chapter V, there are three steps in the calculation of wave height using cnoidal wave theory:

a. The energy flux, F, is calculated for the seaward boundary based on the primary variables H, T, and D (Equations 5.15 and 5.16). Equations 5.15 and 5.16 are repeated as

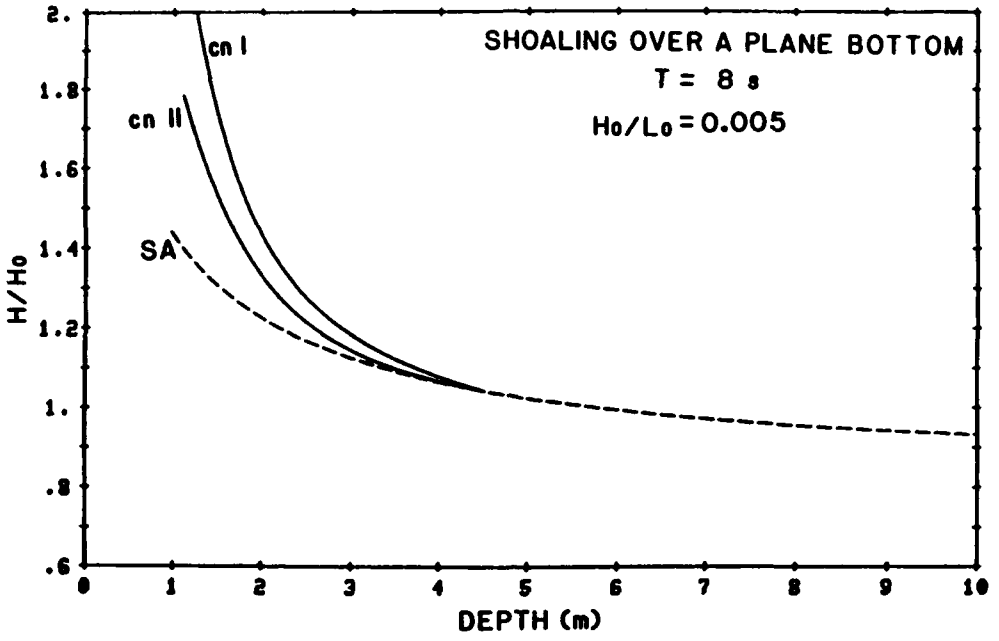

a. H_o/L_o = 0.005

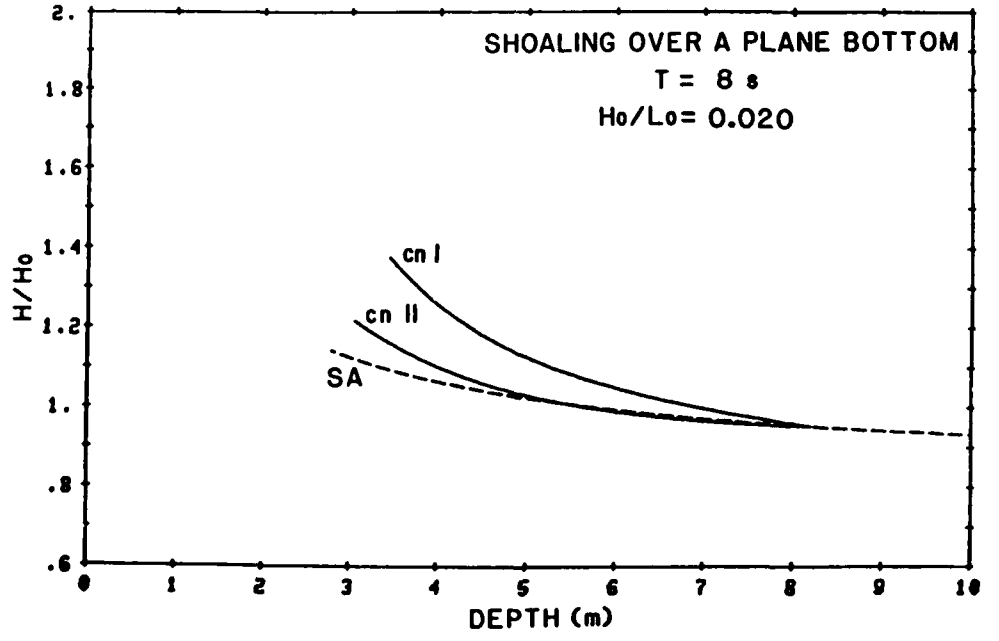

b. H_o/L_o = 0.020

Figure 6.1 Comparison of wave shoaling: SA, cn I, and cn II waves, T = 8 s.

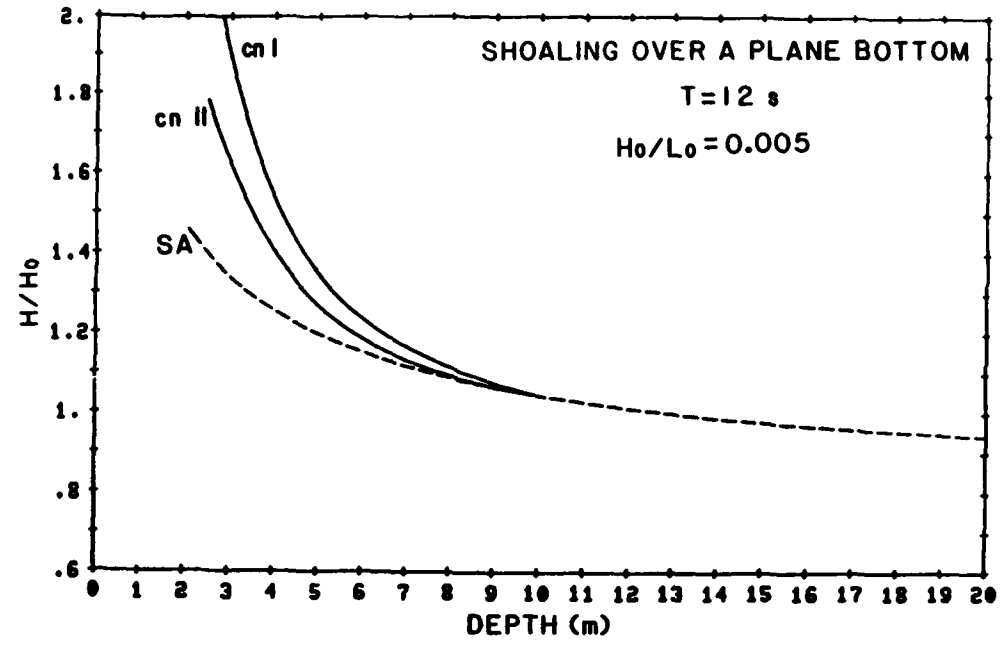

a. H_o/L_o = 0.005

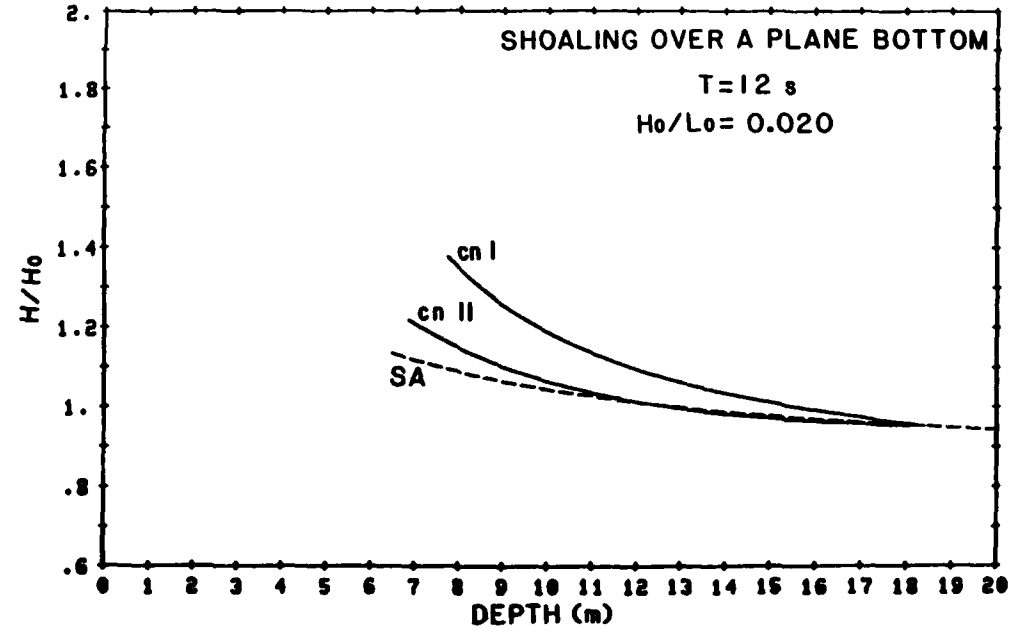

b. H_o/L_o = 0.020

Figure 6.2 Comparison of wave shoaling: SA, cn I, and cn II waves, T = 12 s.

$$F = H^2 F^*$$

$$= H^2 \rho g \sqrt{gD} \left(F_0 + \varepsilon F_1 \right) \tag{6.3}$$

Recall that F for first-order cnoidal wave theory is calculated from Equation 6.3 if εF_1 is set equal to zero.

b. For the case of pure shoaling, i.e., $\alpha_o = 0$, the value of the energy flux remains constant at each grid node as the wave propagates towards the point of wave breaking.

c. The energy flux has two components, H^2 and F^*. As F^* which is a function of Ursell parameter and depth, changes value, the wave height is calculated by imposing the conservation of energy flux (Equation 5.17). Equation 5.17 is repeated as

$$H = \left(\frac{F}{F^*} \right)^{1/2} \tag{6.4}$$

Three terms ($\sqrt{gD}$, F_0, and εF_0) in the equation for F^* (Equation 6.3) change in value as the wave shoals. The terms $\sqrt{gD}$ and F_0 decrease during shoaling, exerting a tendency to produce larger wave heights. However, the third term, εF_1, which occurs in the calculation of second-order energy flux, increases as the wave shoals, negating some of the effect of the first two terms. The value of ε is directly affected by the value of the deepwater wave steepness. The greater the

value of H_o/L_o, the greater the value of ϵ throughout the domain of the simulation, and the greater the effect of the ϵF_1 term in the calculation of F^*. Thus, the shoaling curve for cn II is "pushed downward," away from the cn I shoaling curve, with the difference between the two cnoidal theories increasing at larger deepwater wave steepnesses.

Multiple wave period and deepwater wave steepness combinations were simulated for the pure shoaling case ($\alpha_o = 0$) over a plane bottom slope of 1:50. For each of five wave periods (6, 8, 10, 12, and 14 s), six deepwater wave steepnesses (H_o/L_o = 0.005, 0.010, 0.015, 0.020, 0.025, 0.030) were simulated. The ensemble of simulations was repeated employing small-amplitude, first-order cnoidal, and second-order cnoidal wave theories. Table 6.1 contains the wave height at breaking (H_b) and the location of wave breaking relative to the shoreline (x_b) calculated by each of the three wave theories. Table 6.2 contains of the maximum and minimum percent differences among the three theories calculated from the results shown in Table 6.1. Also in Table 6.2 are the values of H_o/L_o corresponding to the maximum and minimum percent differences. The percent difference between any two wave theories is a function of deepwater wave steepness but is not a function of wave period for a given deepwater wave steepness.

In Table 6.2 the largest percent differences between SA and cn II occur at H_o/L_o = 0.005, with H_b and x_b, determined from cn II, 22% greater than the SA values. This difference diminishes to 3% at H_o/L_o = 0.030. The largest percent difference between cn I and SA is also at H_o/L_o = 0.005, with the cn I values approximately 37% higher

Table 6.1. Shoaling over a plane bottom (1:50): Height and position of waves at breaking (H_b = 0.8D) as determined by SA, cn I, and cn II

T (s)	Ho/Lo	Ho (m)	Hb (m) SA	Hb (m) cn I	Hb (m) cn II	xb (m) SA	xb (m) cn I	xb (m) cn II
	0.005	0.28	0.41	0.56	0.50	26	35	32
	0.010	0.56	0.72	0.92	0.82	45	58	52
6	0.015	0.84	1.01	1.25	1.11	63	78	69
	0.020	1.12	1.28	1.55	1.37	80	97	86
	0.025	1.40	1.54	1.84	1.62	96	115	101
	0.030	1.69	1.79	2.11	1.85	112	132	116
	0.005	0.50	0.73	1.00	0.89	46	63	56
	0.010	1.00	1.29	1.64	1.47	80	103	92
8	0.015	1.50	1.79	2.22	1.97	112	139	123
	0.020	2.00	2.27	2.75	2.43	142	172	152
	0.025	2.50	2.74	3.26	2.87	171	204	180
	0.030	3.00	3.19	3.75	3.29	199	234	206
	0.005	0.78	1.14	1.56	1.39	72	98	87
	0.010	1.56	2.01	2.57	2.29	126	161	143
10	0.015	2.34	2.80	3.46	3.08	175	217	192
	0.020	3.12	3.55	4.29	3.80	222	269	238
	0.025	3.90	4.28	5.09	4.49	267	318	281
	0.030	4.68	4.98	5.86	5.14	312	366	321
	0.005	1.12	1.65	2.25	2.00	103	140	125
	0.010	2.25	2.89	3.70	3.30	181	231	206
12	0.015	3.37	4.03	4.99	4.43	252	312	277
	0.020	4.49	5.11	6.19	5.48	320	387	342
	0.025	5.62	6.16	7.33	6.46	385	458	404
	0.030	6.74	7.18	8.43	7.40	449	527	463
	0.005	1.53	2.24	3.04	2.73	140	191	170
	0.010	3.06	3.94	5.04	4.49	246	315	281
14	0.015	4.59	5.49	6.79	6.03	343	424	377
	0.020	6.12	6.96	8.42	7.45	435	526	466
	0.025	7.65	8.38	9.97	8.80	524	623	550
	0.030	9.18	9.77	11.48	10.07	611	718	630

Table 6.2. Shoaling over a plane bottom (1:50): Maximum and minimum percent differences of wave height at breaking among SA, cn I, and cn II

	Breaking Height			
	MAX %DIFF	at Hb/Lo	MIN %DIFF	at Hb/Lo
cn I : SA	37	0.005	17	0.030
cn II : SA	22	0.005	3	0.030
cn I : cn II	14	0.030	12	0.010

than the corresponding SA values. This difference diminishes to 18% at H_o/L_o = 0.030. The difference between H_b as determined from cn I and cn II shows the opposite trend; the largest percent difference (as was noted in Figures 6.1 and 6.2) occurs at H_o/L_o = 0.030, with cn I values 14% higher than cn II values. This difference is relatively constant over the range of deepwater wave steepness considered, reducing only to 12% at H_o/L_o = 0.005.

6.1.2 Comparison of Theoretical and Experimental Shoaling Rates

Numerical model results for shoaling over a plane beach were compared to laboratory experimental data from Buhr Hansen and Svendsen (1979). In this set of experiments, shoaling on a plane bottom (1:34.26) for waves of various deepwater wave steepnesses was investigated. The experimenters suppressed the contaminating free second harmonic disturbance, which usually results from the difference between the motion of the wave generator and the water particle velocities of waves,

by driving the generator with a signal that contained a component designed to cancel the second harmonic. A profile view of the wave flume used in the experiment is shown in Figure 6.3.

The results of 17 tests were published. Four of these tests were chosen for comparison with theoretical shoaling predicted by the numerical model. The four tests (Table 6.3) were chosen to cover a range of deepwater wave steepnesses (0.004 to 0.025) for tests applicable to cnoidal wave theory (U >10). Numerical results were calculated starting at the beginning of the sloping bottom of the wave flume. The wave height for input to the numerical models was the wave height measured at this point. Note that the deepwater wave steepnesses shown in Table 6.3 differ from those reported by the experimenters. The deepwater wave steepnesses in Table 6.3 were calculated using

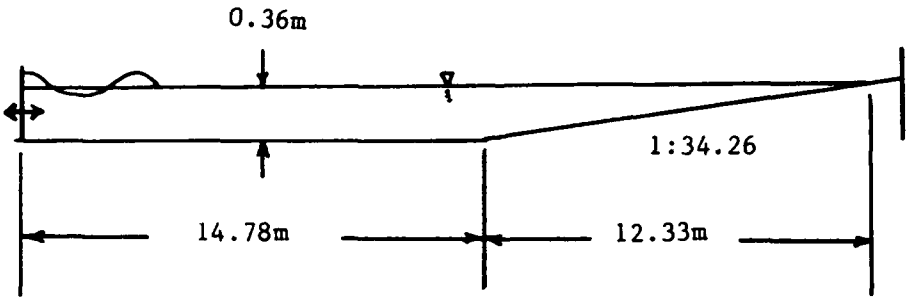

Figure 6.3. The wave flume used in the Buhr Hansen and Svendsen (1979) shoaling experiments

small-amplitude wave theory and the wave height measured at the beginning of the sloping portion of the wave flume.

Table 6.3. Experimental data of wave shoaling

Test*	H (at start of slope) (m)	H_o/L_o	H_b/D_b (data)
H	0.097	0.025	0.937
K	0.080	0.021	0.861
N	0.065	0.011	0.982
Q	0.039	0.004	1.001

* Letter identifying the test corresponds to the notation of Buhr Hansen and Svendsen (1979).

The results from the numerical simulations (SA, cn I, and cn II) are compared to the experimental results in Figures 6.4 to 6.7. The numerical simulations were continued until the wave height to depth ratio at breaking measured in the flume experiments (Table 6.3) was reached.

The same relation among the three theoretical shoaling curves that was noted in Figures 6.1 and 6.2 is seen in Figures 6.4 to 6.7 . The cn II curve is situated between the higher-lying cn I curve and the lower-lying SA curve. The cn II curve is closer to the cn I curve at smaller deepwater wave steepnesses and closer to the SA curve at larger steepnesses. For all four cases, the cn II curve more accurately describes the measurements than the SA curve. For the two larger deepwater wave steepnesses (Figures 6.4 and 6.5), the SA curve is a better match to the data than the cn I curve, except in the region just prior to wave breaking, where the SA curve grossly underpredicts the

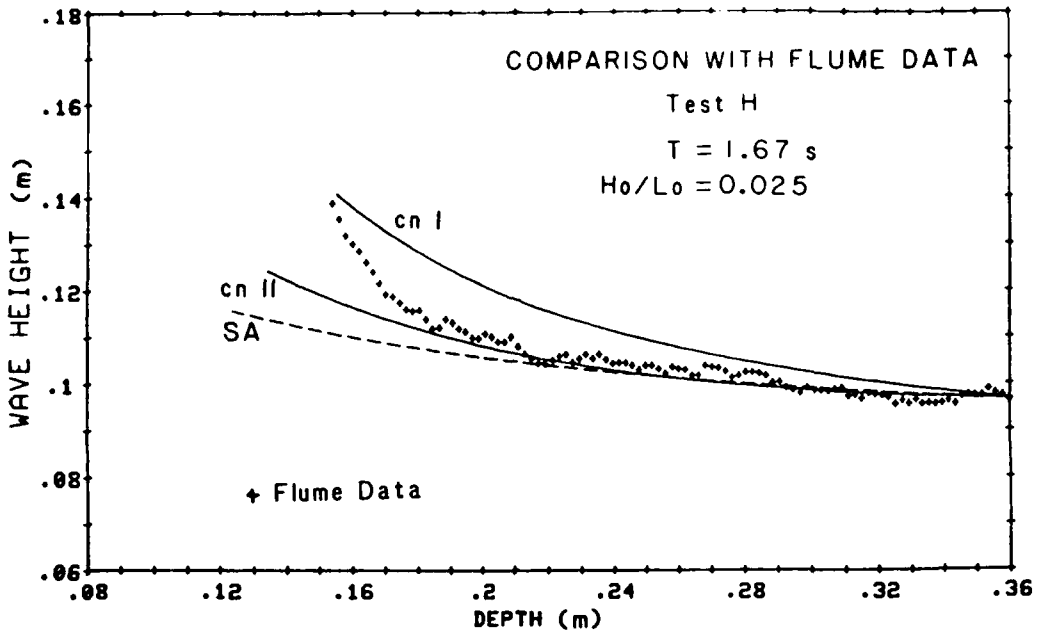

Figure 6.4 Comparison with flume data - Test H

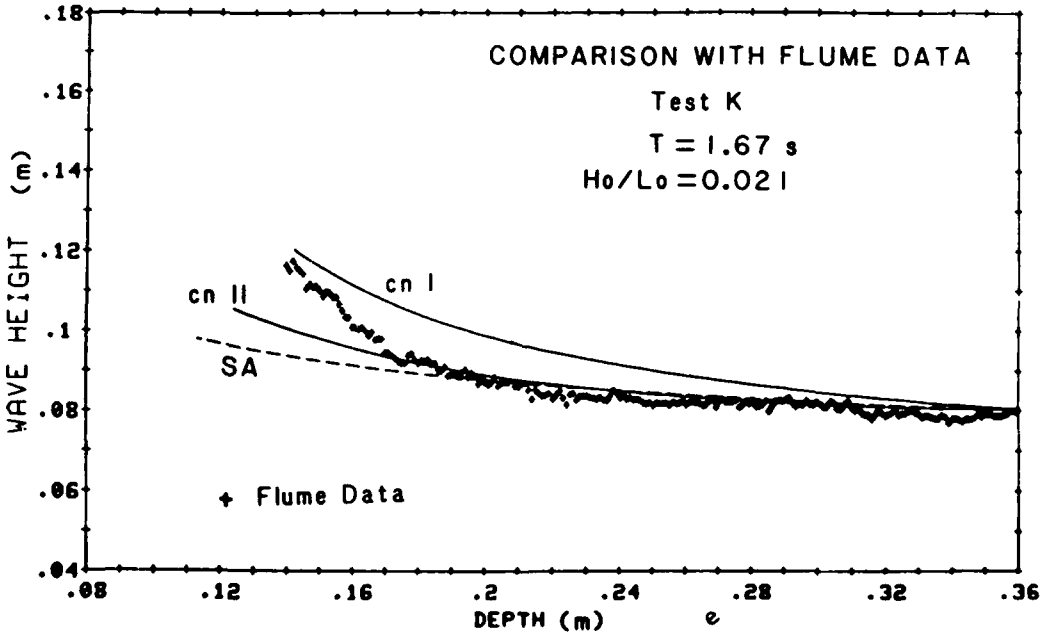

Figure 6.5 Comparison with flume data - Test K

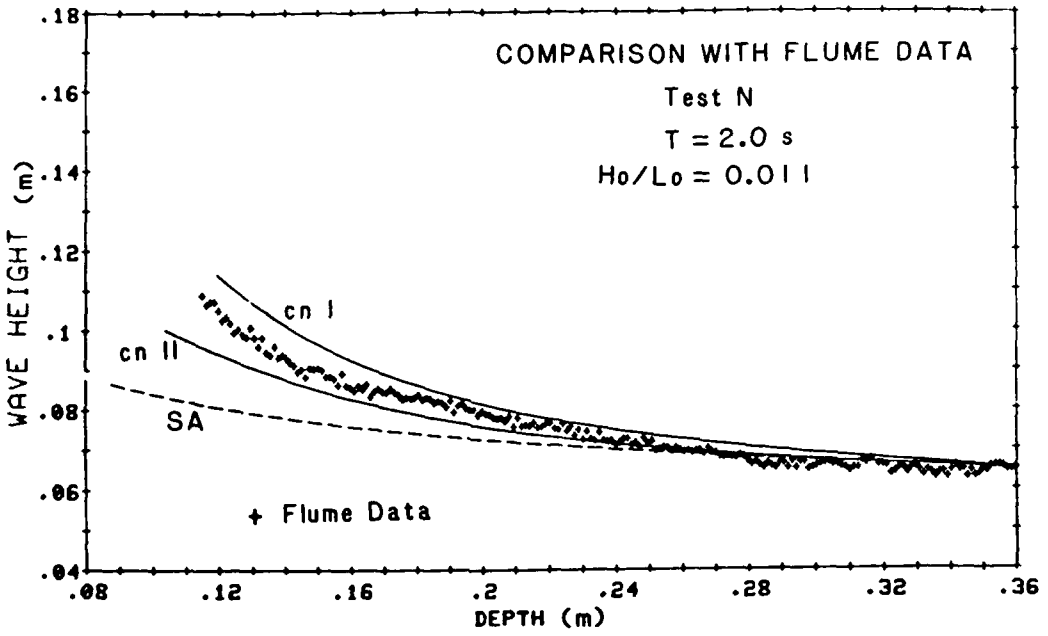

Figure 6.6 Comparison with flume data - Test N

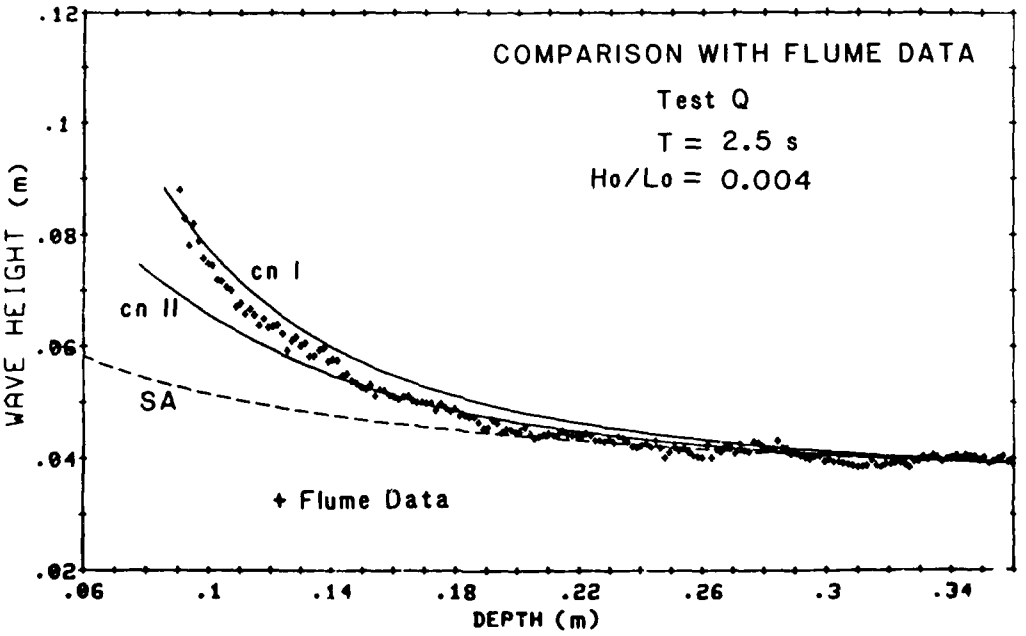

Figure 6.7 Comparison with flume data - Test Q

AD-A182 741 A NUMERICAL MODEL FOR SHOALING AND REFRACTION OF SECOND-ORDER CNOIDAL WAV (U) COASTAL ENGINEERING RESEARCH CENTER VICKSBURG MS T A HARDY ET AL MAY 86 2/3

UNCLASSIFIED CERC-MP-87-9 F/G 20/4 NL

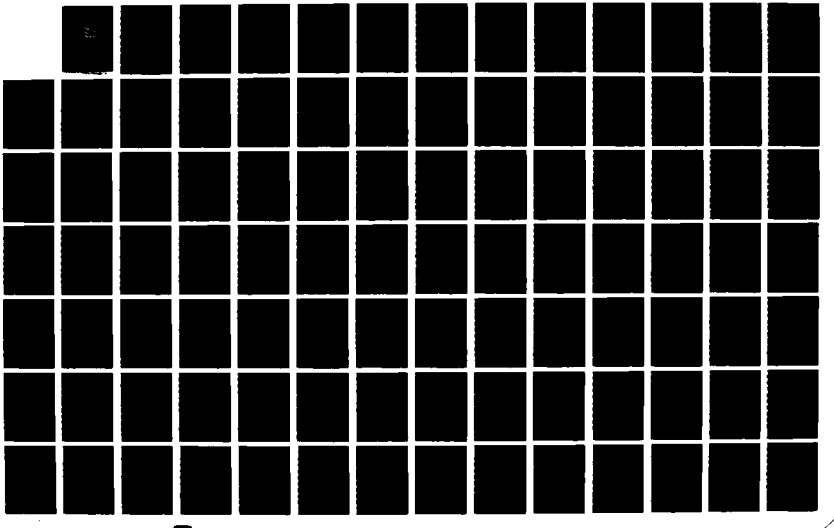

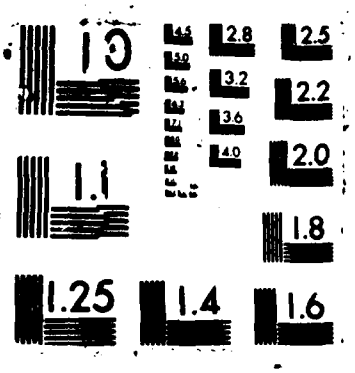
2.8
2.5
3.2
2.2
3.6
4.0
2.0
1.8
1.25
1.4
1.6

trend of the data. The shoaling rate is overpredicted by cn I in deeper water for the two larger deepwater wave steepnesses (Figures 6.4 and 6.5), and although the cn I curve approaches the experimental data at the breaking point in these two figures, the shape of the experimental curve is not duplicated. The cn II curve is an acceptable match to the experimental data in all four cases except near the breaking point, where the cn II curve underpredicts the trend of the data, especially for the larger deepwater wave steepnesses (Figures 6.4 and 6.5).

The failure of second-order cnoidal wave theory to accurately match experimental data near to wave breaking, although somewhat disappointing, should not be completely unexpected. As discussed in Section 6.1.1 the term εF_1 exerts a downward influence on the shoaling curve which increases as ε = H/D increases. A perturbation solution which assumes that ε is small can not be expected to perform well if the value of ε approaches 1.0. These results suggest that third-order cnoidal wave theory may provide better results near wave breaking and for steeper waves.

6.1.3 The shoaling of second-order cnoidal waves over a plane bottom

Shoaling calculated by second-order cnoidal wave theory is compared to shoaling calculated by small-amplitude wave theory in Figures 6.8 to 6.12. The bottom slope used for all cases was 1:50. Six deepwater wave steepnesses (H_o/L_o = 0.005, 0.010, 0.015, 0.020, 0.025, and 0.030) were simulated for each of five wave periods (T = 6, 8, 10, 12, and 14 s). The curve for H_o/L_o = 0.030 was not plotted since it was indistinguishable from the curve for H_o/L_o = 0.025 . The ordinate in

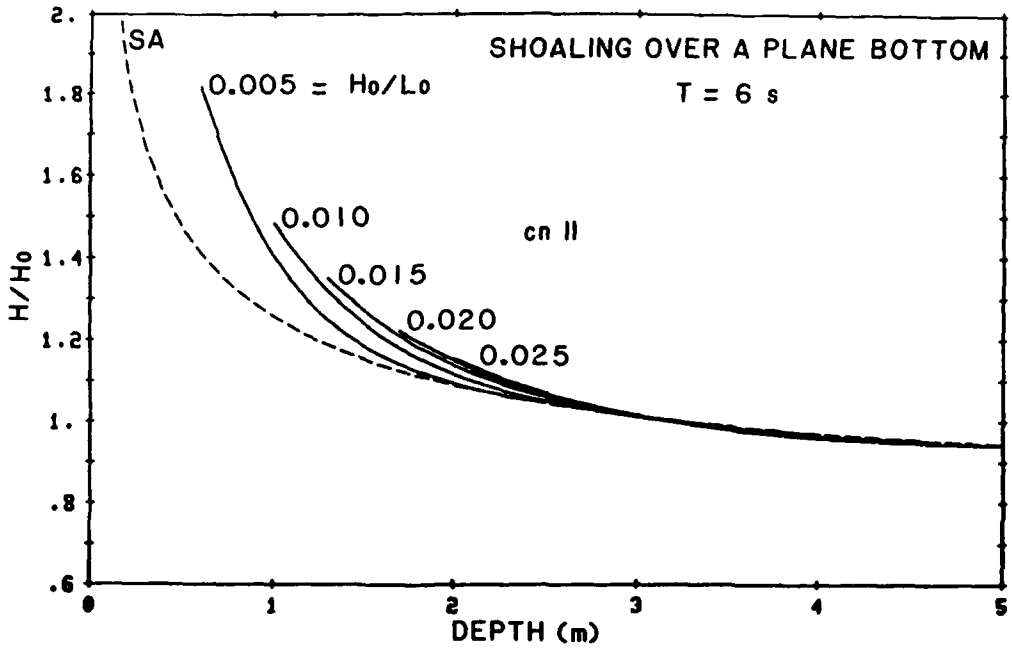

Figure 6.8 Shoaling of second-order cnoidal and small-amplitude waves over a plane bottom (1:50) T = 6 s.

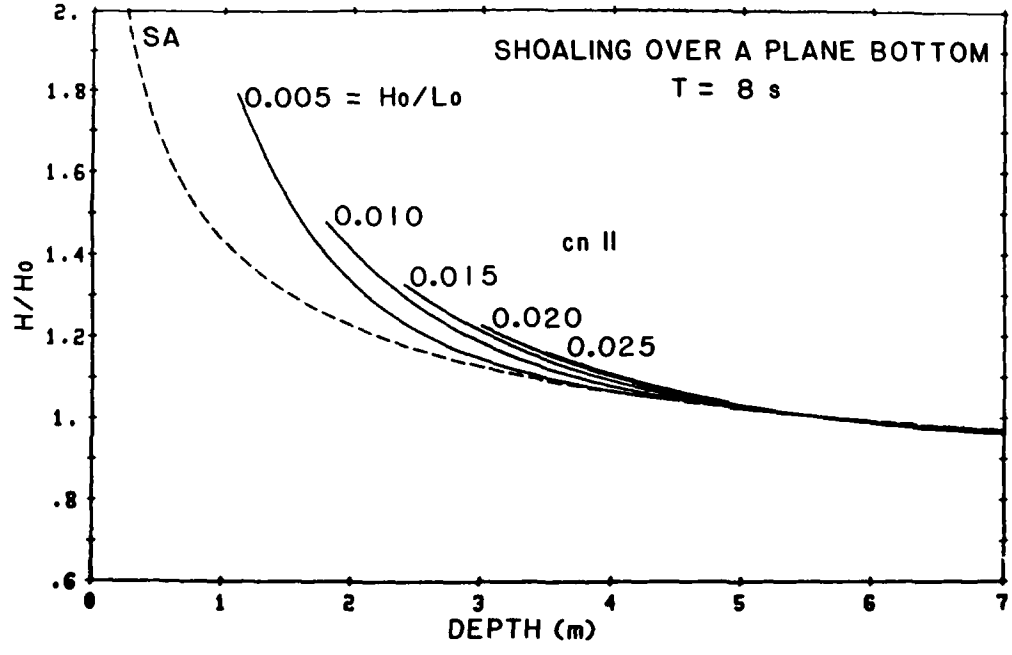

Figure 6.9. Shoaling of second-order cnoidal and small-amplitude waves over a plane bottom (1:50), T = 8 s.

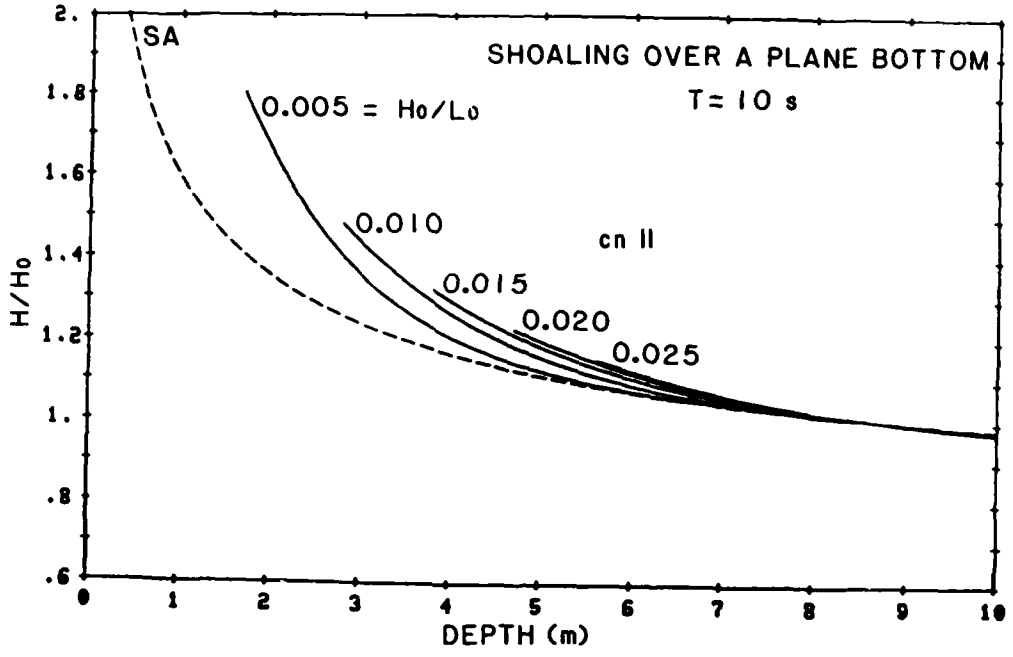

Figure 6.10. Shoaling of second-order cnoidal and small-amplitude waves over a plane bottom (1:50), T = 10 s.

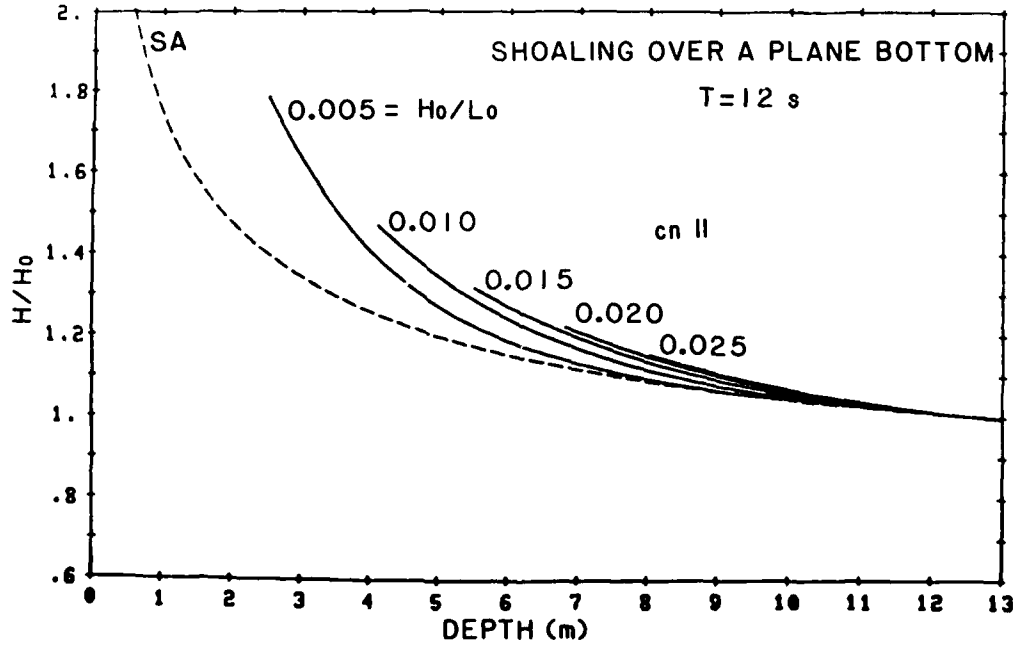

Figure 6.11. Shoaling of second-order cnoidal and small-amplitude waves over a plane bottom (1:50), T = 12 s.

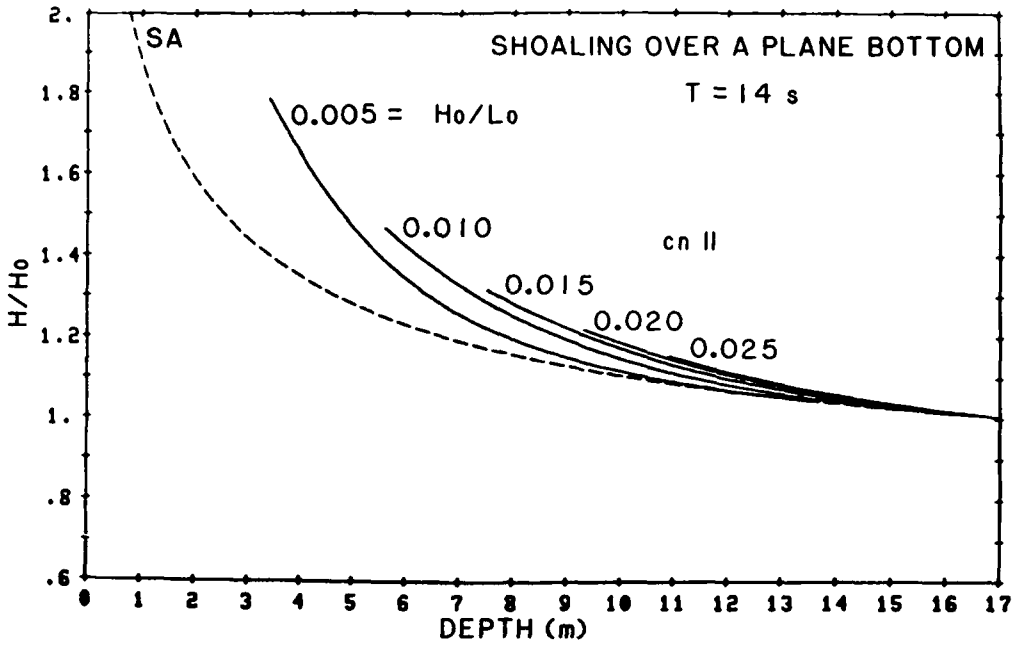

Figure 6.12. Shoaling of second-order cnoidal and small-amplitude waves over a plane bottom (1:50), T = 14 s.

these plots is nondimensional wave height (H/H_o). The abscissa is water depth in meters, and the scale of the abscissa varies from plot to plot. The curves for the five deepwater wave steepnesses on each plot are halted at reaching the breaking criterion of H/D = 0.8 . The small-amplitude curve shown in Figures 6.8 to 6.12 is not halted at a breaking point. Small-amplitude shoaling is not dependent on wave steepness, for a given period; therefore, only one SA curve need be presented. The SA curve is continued past all the cn II curves for ease in comparison.

6.2 Refraction Over a Plane Bottom

Refraction over a plane bottom of small-amplitude, first-order cnoidal, and second-order cnoidal waves is investigated in Section

6.2.1. Plots comparing small-amplitude and second-order cnoidal wave refraction are presented in Section 6.2.2 .

6.2.1 Comparison of wave refraction among small-amplitude, first-order cnoidal, and second-order cnoidal waves

The refraction of small-amplitude, first-order cnoidal, and second-order cnoidal waves is compared in Figures 6.13 and 6.14 for wave periods of 6 and 14 s, respectively. For each figure, the deepwater wave angle α_o = 60° and the bottom slope is 1:50. In Figures 6.13a and 6.14a, H_o/L_o = 0.005 and in Figures 6.13b and 6.14b, H_o/L_o = 0.020. Note that the curves plotted in these figures are not traces of the wave rays. The ordinate is nondimensional wave angle α/α_o, and the abscissa is water depth in meters. The two cnoidal simulations began with the wave height, wave angle, and depth where U = 15, as calculated using small-amplitude wave theory. The plots stop where the breaking criterion H/D = 0.8 is reached.

As in the shoaling results, the cn II curve lies between the cn I curve and the SA curve. Less refraction is predicted by cn I and greater refraction is predicted by SA.

The cn I curves show an interesting characteristic just seaward of the wave breaking point. The change in wave angle "stalls," and the angle increases very slightly with decreasing depth for the H_o/L_o = 0.005 cases. Referring to Snell's law (Equation 4.8), this behavior requires that, near to wave breaking, the wavelength remain constant with decreasing depth , and in the case of increasing angle with decreasing depth, the wavelength must increase with decreasing depth. Svendsen (1974) and Wang and Le Méhauté (1980) provide plots of

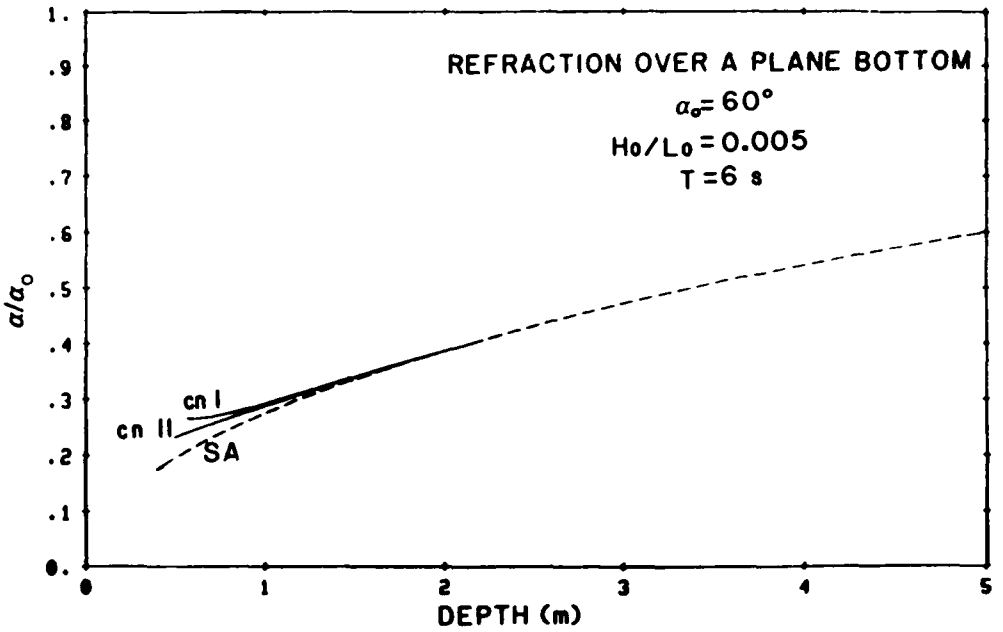

a. H_o/L_o = 0.005

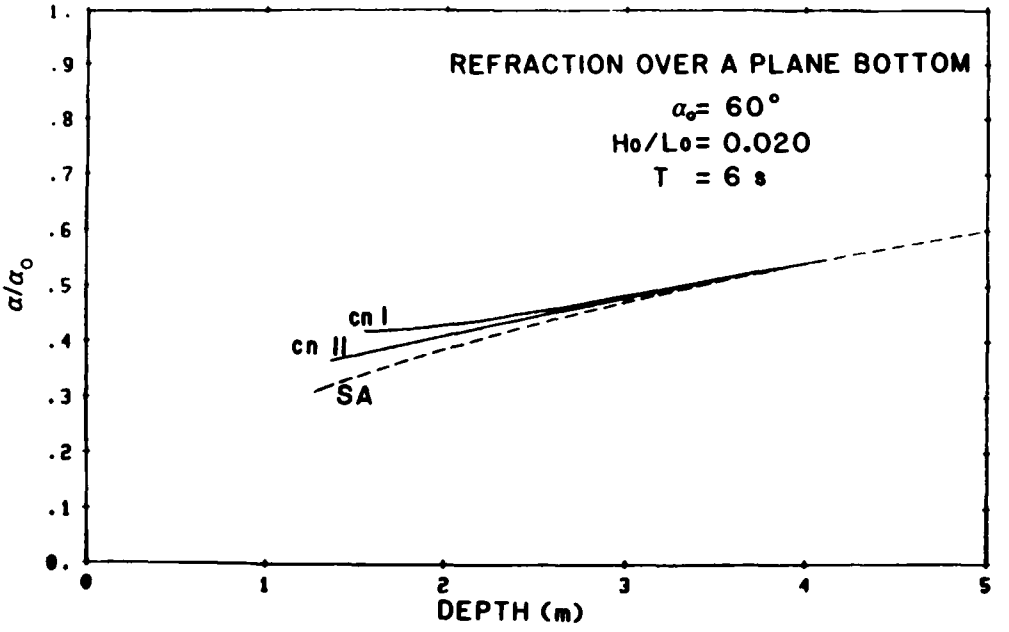

b. H_o/L_o = 0.020

Figure 6.13. Comparison of wave refraction: SA, cn I, and cn II waves, T = 6 s, α_o = 60°.

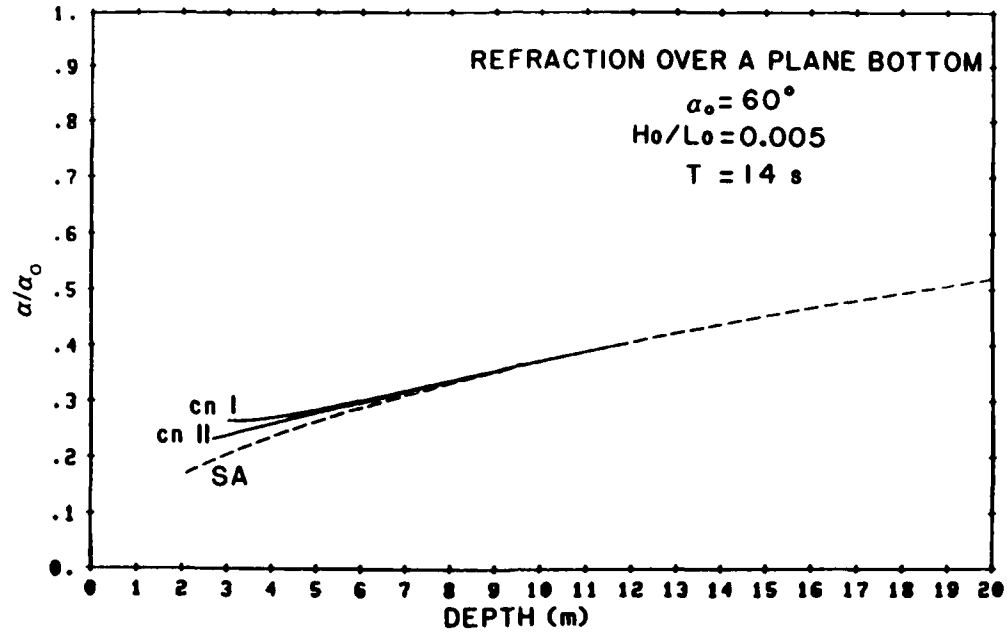

a. H_o/L_o = 0.005

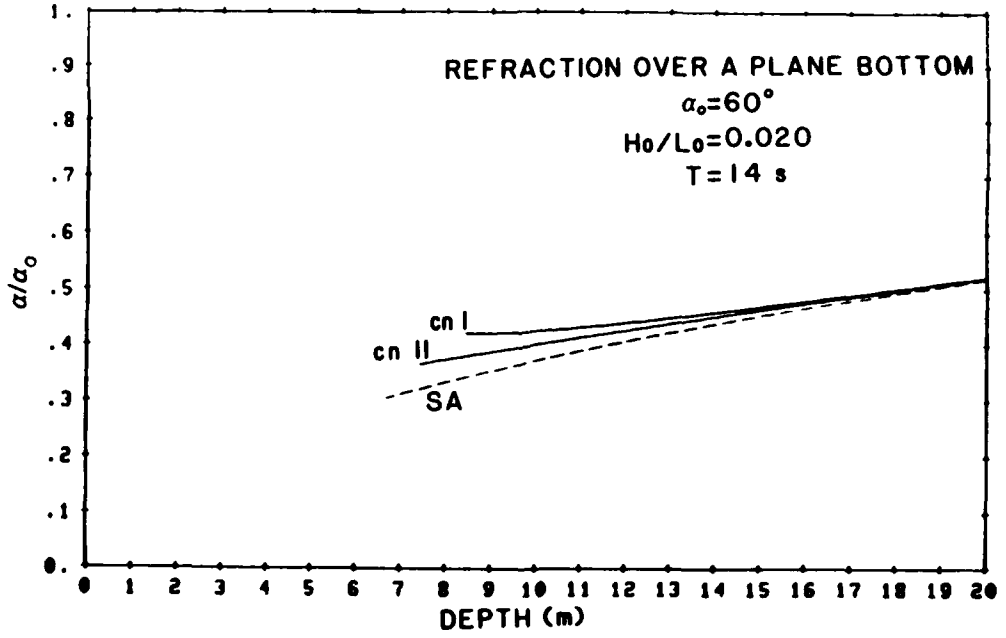

b. H_o/L_o = 0.020

Figure 6.14. Comparison of wave refraction: SA, cn I, and cn II waves, T = 14 s, α_o = 60°.

L/L_o vs D/L_o which show that the wavelength calculated using first-order cnoidal wave theory begins increasing shoreward of approximately H/D = 0.78 for a plane bottom. This tendency may indicate a limit of applicability for first-order cnoidal wave theory, since the increase of wavelength with decreasing depth is counter to intuition, and no known evidence exists to support this phenomenon.

As is discussed in Chapter IV, the calculation of the angle of wave propagation is important for the determination of the wave-induced longshore current and resulting wave-induced longshore sediment transport. Therefore, the unverified behavior of refraction calculations near the wave breaking point obtained by using first-order cnoidal wave theory is a strong incentive to use second-order rather than first-order cnoidal theory for refraction calculations.

The refraction of shallow water waves was investigated in a manner similar to the investigation of shoaling in Section 6.1.3 . A bottom slope of 1:50 was used in all the simulations. Five wave periods (6, 8, 10, 12, and 14 s) combined with each of six deepwater wave steepnesses (0.005, 0.010, 0.015, 0.020, 0.025, and 0.030) were simulated. This ensemble of thirty simulations was repeated for each of three deepwater wave angles (30°, 45°, and 60°). (See Figure 5.1 for a definition of wave angle.) The resulting ninety simulations were repeated using small-amptitude, first-order cnoidal, and second-order cnoidal wave theories, for a grand total of 270 numerical simulations. The seaward boundary conditions for the simulations employing either first or second-order cnoidal wave theory were obtained from the simulations using small-amplitude wave theory at U = 15. The results for deepwater

wave angles 30°, 45°, and 60° are presented in Tables 6.4, 6.5, and 6.6, respectively. These tables list the values of the wave height at breaking, the wave angle at breaking, and the location of the wave breaking point relative to the shoreline.

Table 6.7 lists the maximum and minimum percent differences among the three wave theories in the calculated quantities of H_b and α_b. The maximum percent differences for α_b occur at the smallest deepwater wave steepness and the minimum percent differences at the largest deepwater wave steepness in a comparison of SA against either cn I or cn II. The percent difference between cn I and cn II wave angles at breaking is almost constant with deepwater wave steepness. Recalling the results for shoaling presented in Table 6.2, Table 6.7 shows the same trends for differences in the calculation of H_b by the three wave theories.

It is interesting to compare the magnitudes in the differences in H_b recorded in Tables 6.2 and 6.7 . As discussed in Chapter V, the numerical calculation of refraction implicitly includes the effects of shoaling. The percent differences at α_o = 30° are very similar to the results for shoaling (α_o = 0°). The results at α_o = 45° and α_o = 60° show only a small increase in the percent differences among the three theories in the calculation of H_b. It must be concluded that the percent difference in wave height at breaking among the three wave theories is due primarily to differences in the calculation of shoaling.

6.2.2 The refraction of second-order cnoidal waves over a plane bottom

Figures 6.15 to 6.29 are plots (nondimensional wave angle vs depth) for the second-order cnoidal refraction simulations. In a

Table 6.4. Refraction over a plane bottom (1:50): Height, angle, and position of waves at breaking, $\alpha_o = 30°$

T (s)	Ho/Lo	Ho (m)	Hb (m)			α_b (deg)			xb (m)		
			SA	cn I	cn II	SA	cn I	cn II	SA	cn I	cn II
	0.005	0.28	0.39	0.53	0.48	6.7	9.9	8.7	25	34	30
	0.010	0.56	0.68	0.89	0.79	8.8	12.4	10.8	43	55	49
6	0.015	0.84	0.96	1.20	1.06	10.3	14.0	12.3	60	75	66
	0.020	1.12	1.21	1.49	1.31	11.6	15.3	13.5	76	93	82
	0.025	1.40	1.47	1.77	1.55	12.6	16.4	14.4	92	110	97
	0.030	1.69	1.71	2.03	1.78	13.6	17.3	15.2	107	127	111
	0.005	0.50	0.69	0.95	0.85	6.6	9.9	8.7	43	60	53
	0.010	1.00	1.22	1.57	1.40	8.8	12.3	10.8	76	99	88
8	0.015	1.50	1.70	2.13	1.88	10.3	14.0	12.3	106	133	118
	0.020	2.00	2.16	2.64	2.33	11.5	15.3	13.5	135	165	146
	0.025	2.50	2.60	3.13	2.75	12.6	16.3	14.4	163	196	172
	0.030	3.00	3.04	3.61	3.16	13.6	17.2	15.2	190	226	197
	0.005	0.78	1.08	1.49	1.33	6.6	9.9	8.7	68	93	83
	0.010	1.56	1.90	2.46	2.19	8.8	12.3	10.8	119	154	137
10	0.015	2.34	2.66	3.32	2.94	10.3	14.0	12.3	166	208	184
	0.020	3.12	3.37	4.13	3.64	11.5	15.3	13.5	211	258	228
	0.025	3.90	4.07	4.90	4.30	12.6	16.4	14.4	254	306	269
	0.030	4.68	4.75	5.64	4.93	13.6	17.3	15.2	297	353	308
	0.005	1.12	1.56	2.15	1.91	6.6	9.9	8.7	97	134	120
	0.010	2.25	2.74	3.54	3.15	8.8	12.3	10.8	171	222	197
12	0.015	3.37	3.83	4.79	4.24	10.3	14.0	12.3	239	299	265
	0.020	4.49	4.86	5.94	5.24	11.5	15.3	13.5	304	372	328
	0.025	5.62	5.86	7.05	6.19	12.6	16.4	14.4	366	441	387
	0.030	6.74	6.84	8.12	7.10	13.6	17.3	15.2	427	508	444
	0.005	1.53	2.12	2.92	2.60	6.6	9.9	8.7	133	183	163
	0.010	3.06	3.73	4.82	4.29	8.8	12.3	10.8	233	302	268
14	0.015	4.59	5.21	6.51	5.77	10.3	14.0	12.3	325	407	361
	0.020	6.12	6.61	8.09	7.14	11.5	15.3	13.5	413	506	446
	0.025	7.65	7.97	9.60	8.43	12.6	16.3	14.3	498	600	527
	0.030	9.18	9.31	11.06	9.67	13.6	17.3	15.2	582	691	604

Table 6.5. Refraction over a plane bottom (1:50): Height, angle, and position of waves at breaking, $\alpha_o = 45°$

T (s)	Ho/Lo	Ho (m)	Hb (m) SA	Hb (m) cn I	Hb (m) cn II	α_b (deg) SA	α_b (deg) cn I	α_b (deg) cn II	xb (m) SA	xb (m) cn I	xb (m) cn II
	0.005	0.28	0.36	0.50	0.45	9.1	13.7	12.0	23	32	28
	0.010	0.56	0.63	0.83	0.74	12.0	17.1	14.9	40	52	46
6	0.015	0.84	0.89	1.12	0.99	14.1	19.5	17.0	55	70	62
	0.020	1.12	1.13	1.40	1.23	15.9	21.4	18.7	70	88	77
	0.025	1.40	1.36	1.66	1.45	17.4	22.9	20.0	85	104	91
	0.030	1.69	1.59	1.91	1.67	18.7	24.2	21.2	99	120	104
	0.005	0.50	0.64	0.89	0.79	9.0	13.6	11.9	40	56	50
	0.010	1.00	1.13	1.48	1.31	12.0	17.1	15.0	70	92	82
8	0.015	1.50	1.57	1.99	1.76	14.1	19.4	17.0	98	125	110
	0.020	2.00	2.00	2.48	2.18	15.9	21.3	18.6	125	155	137
	0.025	2.50	2.42	2.95	2.58	17.4	22.9	20.0	151	184	161
	0.030	3.00	2.82	3.40	2.96	18.7	24.3	21.2	176	213	185
	0.005	0.78	1.00	1.39	1.24	9.0	13.6	11.9	63	87	78
	0.010	1.56	1.76	2.31	2.04	12.0	17.1	14.9	110	144	128
10	0.015	2.34	2.46	3.12	2.75	14.1	19.5	17.0	154	195	172
	0.020	3.12	3.13	3.88	3.41	15.8	21.4	18.7	195	242	213
	0.025	3.90	3.77	4.61	4.03	17.4	22.9	20.0	236	288	252
	0.030	4.68	4.41	5.31	4.63	18.7	24.3	21.2	276	332	289
	0.005	1.12	1.44	2.01	1.79	9.0	13.7	12.0	90	126	112
	0.010	2.25	2.53	3.32	2.94	12.0	17.1	14.9	158	208	184
12	0.015	3.37	3.54	4.49	3.97	14.1	19.5	17.0	221	281	248
	0.020	4.49	4.50	5.59	4.91	15.8	21.3	18.6	281	349	307
	0.025	5.62	5.43	6.63	5.81	17.4	22.9	20.0	340	415	363
	0.030	6.74	6.35	7.65	6.67	18.7	24.3	21.2	397	478	417
	0.005	1.53	1.96	2.73	2.43	9.0	13.7	12.0	122	171	152
	0.010	3.06	3.45	4.52	4.01	12.0	17.1	14.9	216	282	250
14	0.015	4.59	4.82	6.11	5.40	14.1	19.5	17.0	301	382	337
	0.020	6.12	6.13	7.60	6.68	15.8	21.3	18.6	383	475	418
	0.025	7.65	7.40	9.03	7.90	17.4	22.9	20.0	462	564	494
	0.030	9.18	8.64	10.41	9.07	18.7	24.3	21.2	540	651	567

Table 6.6. Refraction over a plane bottom (1:50): Height, angle, and position of waves at breaking, $\alpha_o = 60°$

T (s)	Ho/Lo	Ho (m)	Hb (m)			α_b (deg)			xb (m)		
			SA	cn I	cn II	SA	cn I	cn II	SA	cn I	cn II
	0.005	0.28	0.31	0.44	0.40	10.4	16.0	13.9	20	28	25
	0.010	0.56	0.55	0.74	0.65	13.7	20.0	17.5	35	46	41
6	0.015	0.84	0.77	1.00	0.88	16.2	22.9	19.9	48	63	55
	0.020	1.12	0.98	1.24	1.09	18.3	25.2	21.9	61	78	68
	0.025	1.40	1.18	1.47	1.29	20.0	27.0	23.5	74	92	81
	0.030	1.69	1.38	1.70	1.48	21.6	28.7	25.0	87	106	93
	0.005	0.50	0.56	0.79	0.70	10.4	15.9	13.9	35	50	44
	0.010	1.00	0.98	1.31	1.16	13.7	20.0	17.5	61	82	73
8	0.015	1.50	1.37	1.77	1.56	16.2	22.8	19.9	86	111	98
	0.020	2.00	1.74	2.21	1.94	18.3	25.2	21.9	109	138	121
	0.025	2.50	2.11	2.62	2.29	20.0	27.1	23.5	132	164	143
	0.030	3.00	2.46	3.03	2.63	21.6	28.8	25.0	154	189	164
	0.005	0.78	0.87	1.24	1.10	10.4	15.9	13.9	54	78	69
	0.010	1.56	1.53	2.05	1.81	13.7	20.0	17.4	96	128	113
10	0.015	2.34	2.14	2.77	2.44	16.2	22.8	19.9	134	173	153
	0.020	3.12	2.72	3.45	3.03	18.3	25.2	21.9	170	215	189
	0.025	3.90	3.29	4.10	3.58	20.0	27.1	23.6	206	256	224
	0.030	4.68	3.84	4.73	4.11	21.6	28.8	25.0	240	296	257
	0.005	1.12	1.25	1.78	1.58	10.4	15.9	13.9	78	112	99
	0.010	2.25	2.21	2.95	2.61	13.7	20.0	17.5	138	184	163
12	0.015	3.37	3.08	3.99	3.52	16.2	22.8	19.9	193	249	220
	0.020	4.49	3.92	4.96	4.36	18.3	25.2	21.9	245	310	272
	0.025	5.62	4.74	5.90	5.15	20.0	27.1	23.5	296	369	322
	0.030	6.74	5.54	6.81	5.92	21.6	28.8	25.0	346	426	370
	0.005	1.53	1.70	2.43	2.15	10.4	15.9	13.9	107	152	135
	0.010	3.06	3.00	4.01	3.55	13.7	20.0	17.4	188	251	222
14	0.015	4.59	4.20	5.43	4.79	16.2	22.8	19.9	262	339	299
	0.020	6.12	5.34	6.75	5.93	18.3	25.2	21.9	334	422	371
	0.025	7.65	6.45	8.03	7.01	20.0	27.1	23.6	403	502	438
	0.030	9.18	7.54	9.27	8.06	21.6	28.8	25.0	471	579	504

Table 6.7. Refraction over a plane bottom (1:50): Maximum and minimum percent differences of wave height and angle at breaking (H_b = 0.8D) among SA, cn I, and cn II

		Breaking Height				Breaking Angle			
	Models	MAX	at	MIN	at	MAX	at	MIN	at
(deg)	Compared	%DIFF	Ho/Lo	%DIFF	Ho/Lo	%DIFF	Ho/Lo	%DIFF	Ho/Lo
	cn I : SA	38	0.005	19	0.030	50	0.005	26	0.030
30	cn II : SA	23	0.005	4	0.030	32	0.005	12	0.030
	cn I : cn II	14	0.030	10	0.005	15	0.010	13	0.030
	cn I : SA	40	0.005	20	0.030	52	0.005	29	0.030
45	cn II : SA	25	0.005	5	0.030	33	0.005	13	0.030
	cn I : cn II	15	0.030	11	0.005	15	0.010	14	0.010
	cn I : SA	43	0.005	23	0.030	54	0.005	33	0.030
60	cn II : SA	29	0.005	7	0.030	34	0.005	16	0.030
	cn I : cn II	15	0.030	10	0.005	15	0.025	14	0.010

similar manner to the plots for wave shoaling, curves for five deepwater wave steepnesses (0.005, 0.010, 0.015, 0.020, 0.025) are plotted with a small-amplitude curve for each of five wave periods (6, 8, 10, 12, and 14 s). Figures 6.15 to 6.19 are the plots for T = 6 s to T = 14 s for a deepwater wave angle of 30°. Likewise, Figures 6.20 to 6.24 and Figures 6.25 to 6.29 are plots for α_o = 45° and 60°, respectively. The curves for the various deepwater wave steepnesses stop at the breaking criterion H/D = 0.8. As with shoaling, small-amplitude wave refraction does not depend on wave steepness, so only one small-amplitude curve is presented for each wave period, and that curve was allowed to continue beyond the breaking criterion. Companion plots to these wave angle plots (nondimensional wave height vs depth) are included in Appendix D.

From this series of figures it is seen that second-order cnoidal

waves refract less than do small-amplitude waves. The rate of refraction decreases with increasing deepwater wave steepness for a given wave period for second-order cnoidal waves.

6.3 Shoaling and refraction over non-plane bathymetry

The results presented in the beginning sections of this chapter demonstrate the properties of shoaling and refraction of shallow water waves as predicted by small-amplitude, first-order cnoidal, and second-order cnoidal wave theories. Even though the results corresponded to a plane bathymetry, the physical mechanisms which cause shoaling and refraction do not change if the bathymetry becomes non-planar. The differences in the prediction of shoaling and refraction among the three theories remain the same as for the non-planar case. This is true as long as the basic assumptions in the derivation of the wave theories, especically the assumption that the waves are of constant form, remain reasonably valid. Each location can be thought of as locally having a plane bottom, and the shoaling and refraction predicted by the three theories being determined by the local bottom slope. This argument, of course, holds only if the effects of shoaling and refraction alone are considered. As the bottom becomes increasingly complex, other transformation mechanisms neglected in the present model, notably diffraction, become increasingly important.

Therefore, given the arguments in the preceeding paragraph, the prediction of shoaling and refraction for a non-planar bottom is a problem in the numerical calculation, rather than a problem of different physics. The techniques used for wave angle and wave height

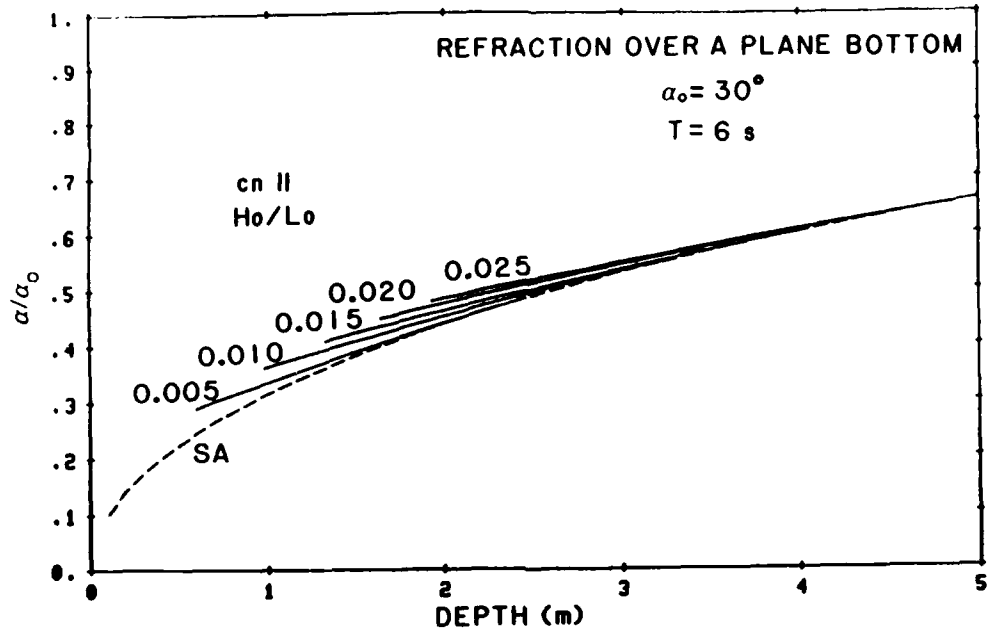

Figure 6.15. Refraction over a plane bottom (1:50), α_o = 30°, T = 6 s.

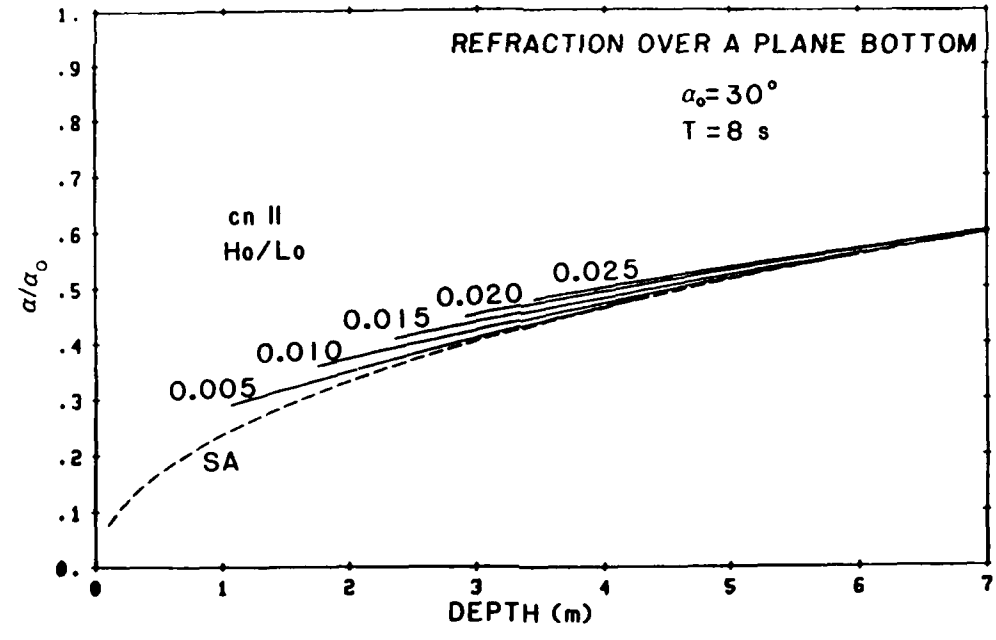

Figure 6.16. Refraction over a plane bottom (1:50), α_o = 30°, T = 8 s.

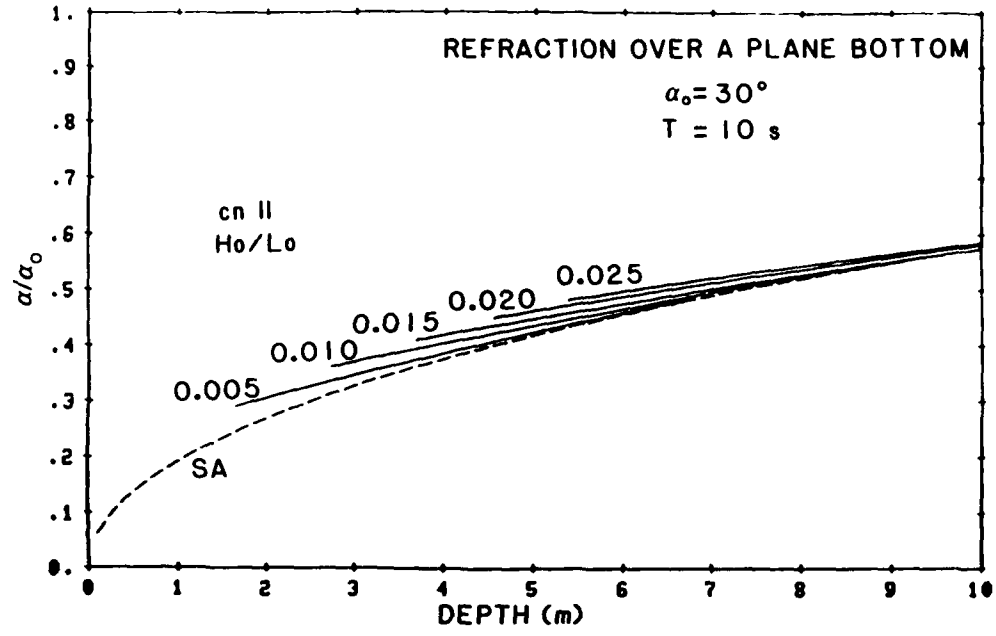

Figure 6.17. Refraction over a plane bottom (1:50), α_o = 30°, T = 10 s.

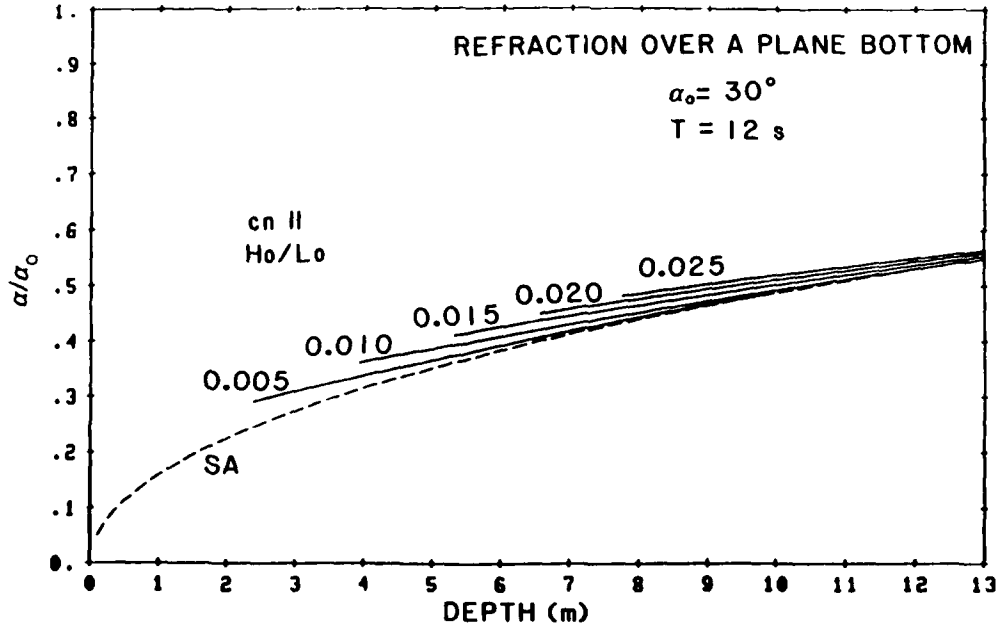

Figure 6.18. Refraction over a plane bottom (1:50), α_o = 30°, T = 12 s.

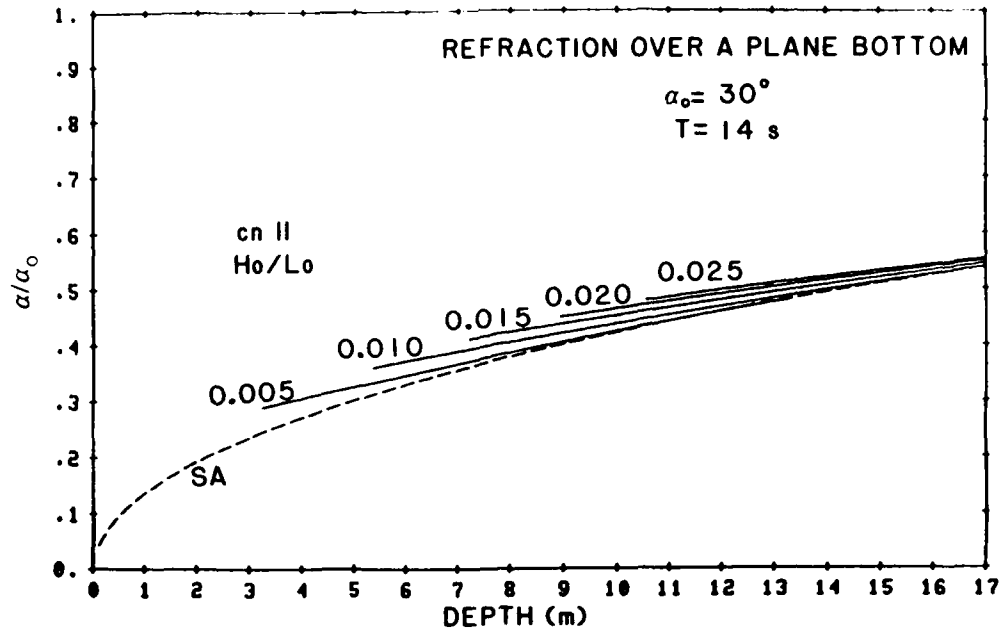

Figure 6.19. Refraction over a plane bottom (1:50), α_o = 30°, T = 14 s.

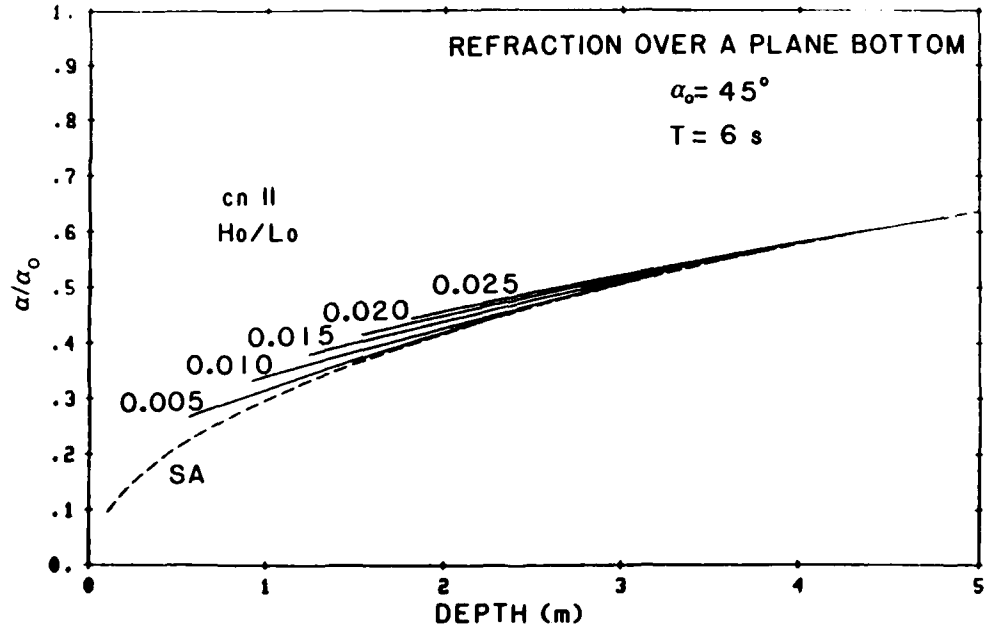

Figure 6.20. Refraction over a plane bottom (1:50), α_o = 45°, T = 6 s.

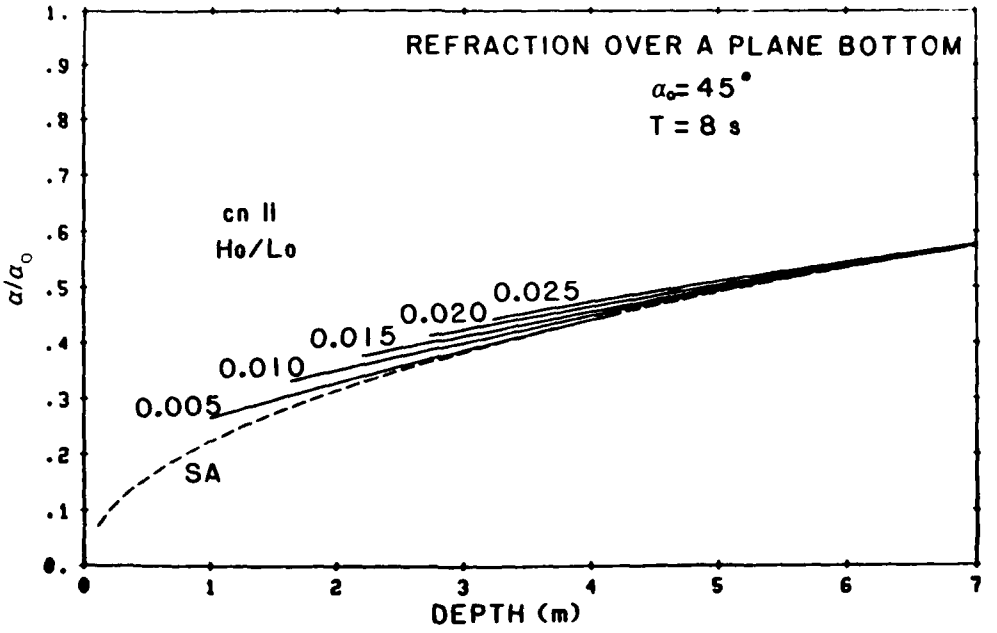

Figure 6.21. Refraction over a plane bottom (1:50), α_o = 45°, T = 8 s.

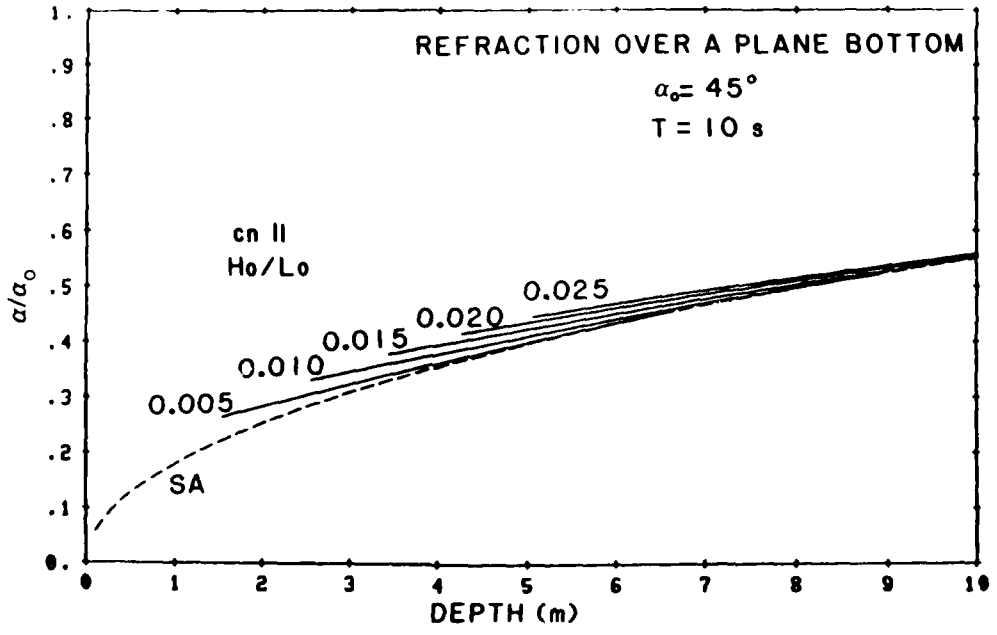

Figure 6.22. Refraction over a plane bottom (1:50), α_o = 45°, T = 10 s.

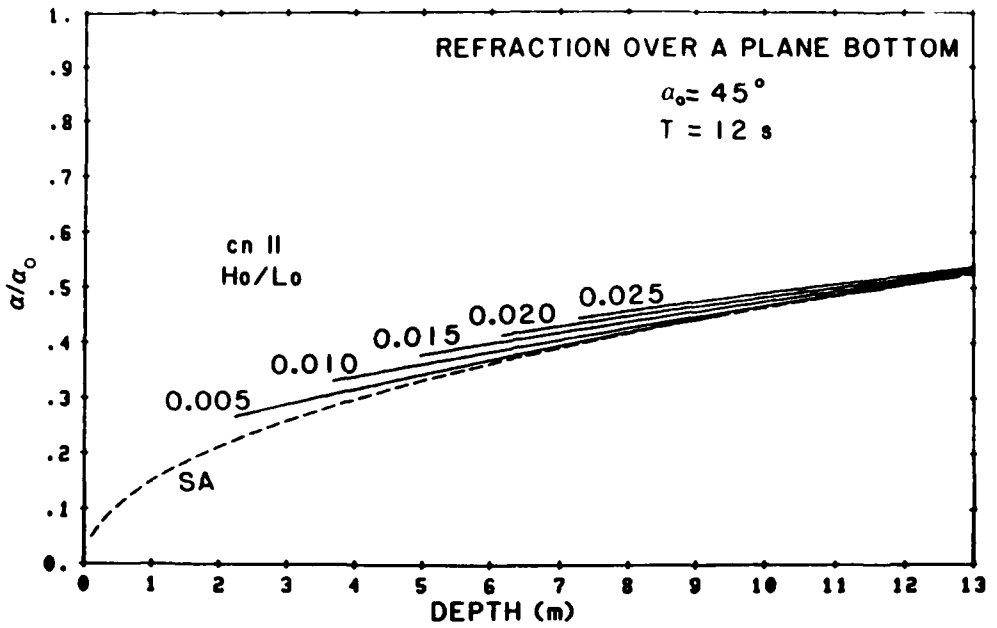

Figure 6.23. Refraction over a plane bottom (1:50), α_o = 45°, T = 12 s.

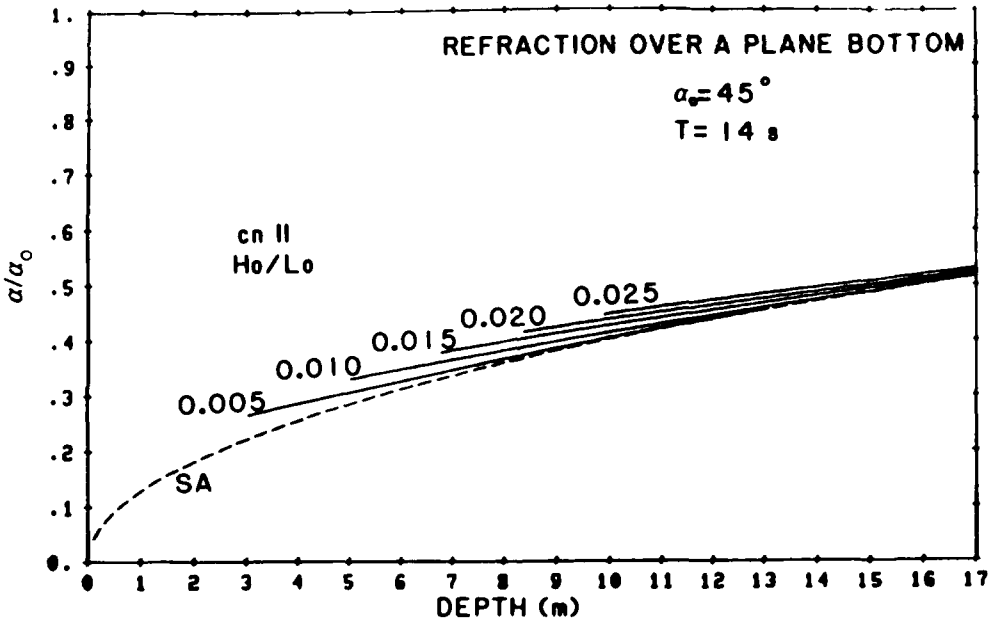

Figure 6.24. Refraction over a plane bottom (1:50), α_o = 45°, T = 14 s.

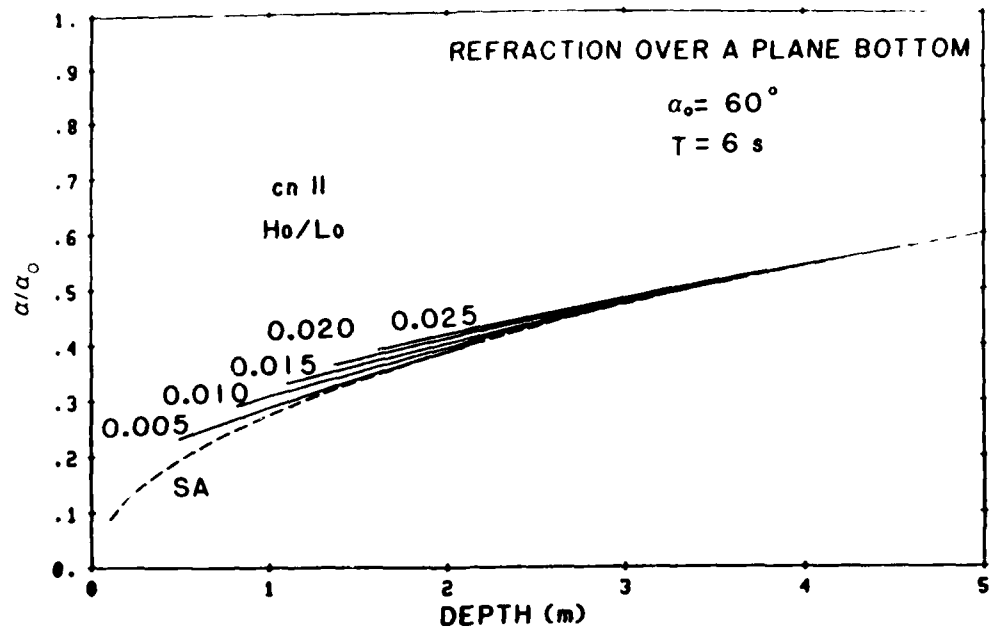

Figure 6.25. Refraction over a plane bottom (1:50), α_o = 60°, T = 6 s.

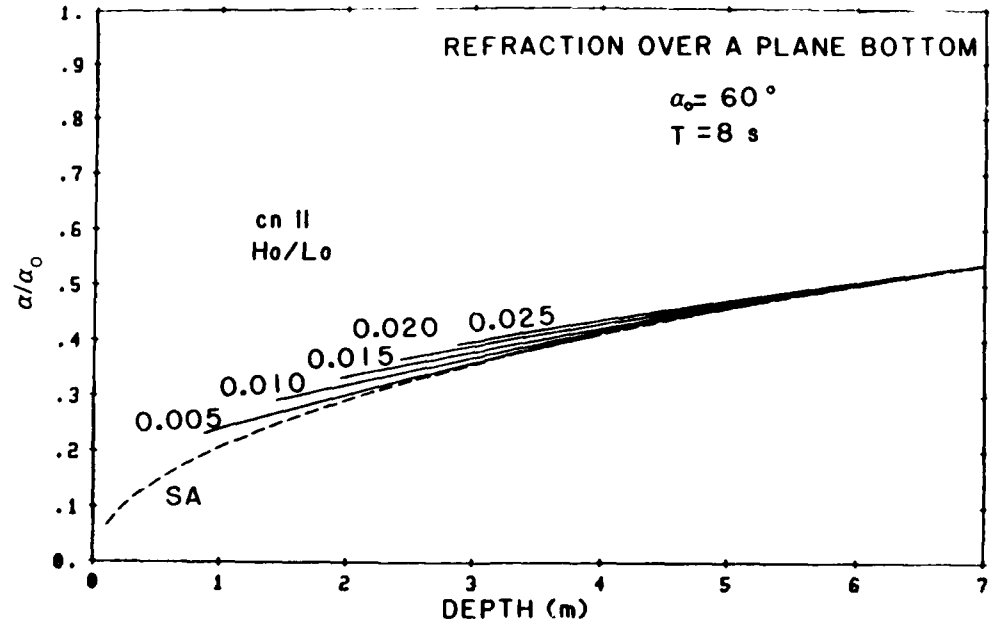

Figure 6.26. Refraction over a plane bottom (1:50), α_o = 60°, T = 8 s.

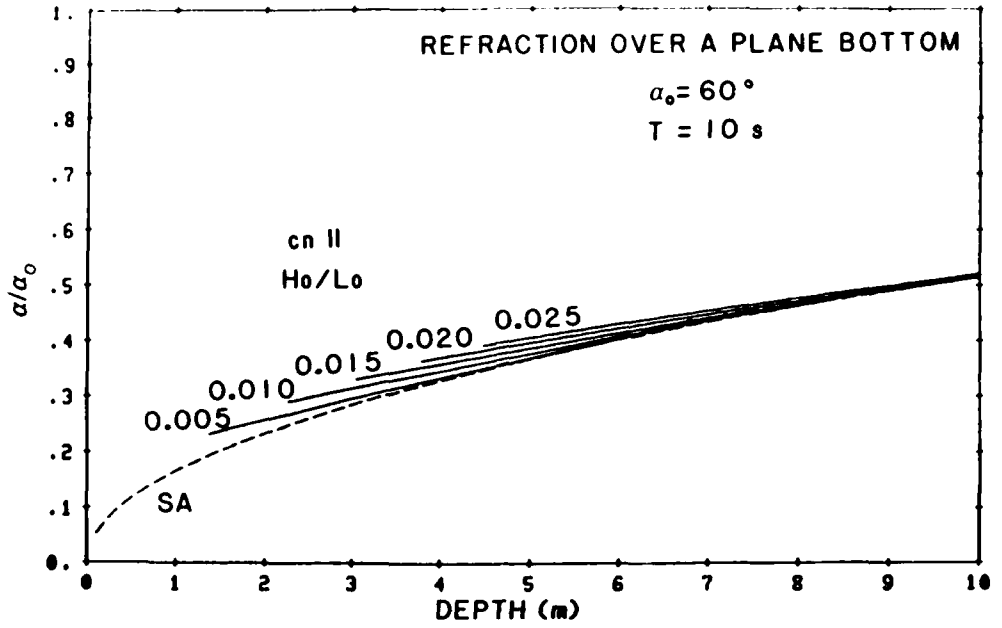

Figure 6.27. Refraction over a plane bottom (1:50), α_o = 60°, T = 10 s.

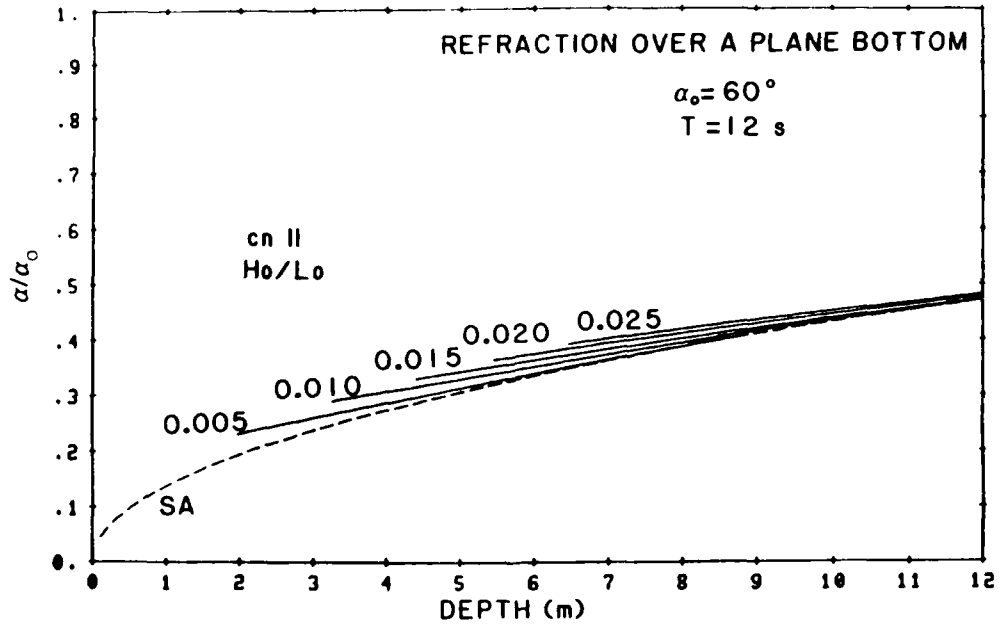

Figure 6.28. Refraction over a plane bottom (1:50), α_o = 60°, T = 12 s.

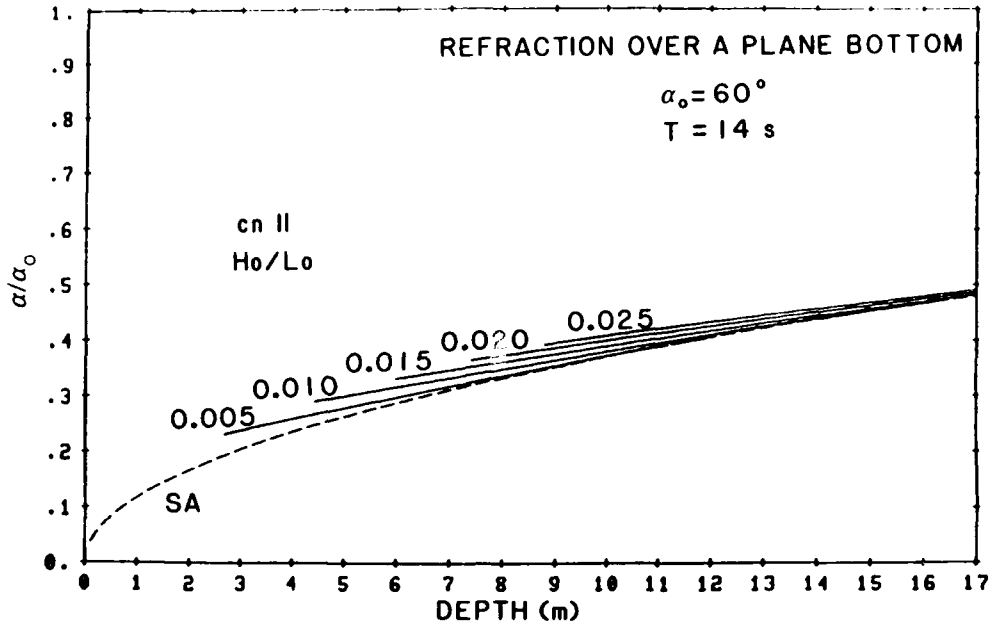

Figure 6.29. Refraction over a plane bottom (1:50), α_o = 60°, T = 14 s.

calculations, derived in Chapter IV and implemented for the numerical model in Chapter V should therefore still apply. These techniques were tested over an idealized non-planar bathymetry. As a measure of the performance of the numerical model, the results from the shoaling and refraction over an idealized bathymetry can be anticipated, and the model results can be compared to these expectations.

Model results for the shoaling and refraction of waves over a spherical shoal and an idealized trench are presented in Sections 6.3.1 and 6.3.2, respectively. In both cases the lateral boundaries were placed so that the lateral boundary conditions would not affect the results of the simulations.

6.3.1 Shoaling and refraction over a spherical shoal

A lens with the shape of a top section of a sphere was placed on a bottom with otherwise constant depth (9.9 m). The numerical grid was centered about the shoal. The maximum decrease in water depth caused by the spherical shoal was 2 m, and the radius of the shoal was 150 m. Waves of two deepwater wave steepnesses, H_o/L_o = 0.005 and H_o/L_o = 0.020, for a wave period of 12 s were simulated using the second-order cnoidal model. For comparison, a 12-s small amplitude wave was also simulated. Note that small-amplitude shoaling and refraction do not depend upon wave steepness; therefore, a single SA simulation can be used in comparisons with the two wave steepnesses simulated by the cnoidal model. A constant wave height and an angle normal to the shoreline were the inputs to the seaward boundary. The wave heights at the seaward boundary were determined from the small-amplitude shoaling simulations described in Section 6.1 . This implies a plane sloping bottom from deep water to the boundary depth of 9.9 m, where the bottom becomes horizontal except for the spherical disturbance.

The results from simulations employing second-order cnoidal wave theory are presented in Figures 6.30 and 6.31, for H_o/L_o equal to 0.005 and 0.020, respectively. Results are presented for three cross sections parallel to the shoreline. The cross sections are located fifty meters seaward of the center of the sphere, at the center of sphere, and fifty meters shoreward of the center of the sphere. There are three parts to each figure. At each of the three cross sections, Figures 6.30a and 6.31a show the longshore variation in depth, Figures 6.30b and 6.31b show the longshore variation in wave height, and Figures 6.30c and 6.31c

show the longshore variation wave angle. Note that in Figures 6.30a and 6.31a, the longshore variation of depth labeled "50 m before centerline" is identical to that labeled "50 m after centerline". The figures are orientated as if the observer were at sea and facing the shore. Positive and negative angles mean the wave is going to the left and right, respectively, as in Figure 5.1.

The following results were anticipated:

a. Calculated quantities should be symmetrical about a line running onshore-offshore at the center of the grid.

b. The wave angle should remain equal to zero on the centerline and at the lateral boundaries of each cross section.

c. At either lateral side of the shoal, the wave angle should be directed toward the middle of the grid.

d. The maximum wave angle should be located near the position of maximum change in the bathymetry in the longshore direction.

e. The maximum wave height should be located at the middle of the grid.

f. The minimum wave height should be located close to the edge of the spherical disturbance.

g. The trends in items c through e should increase as the wave propagated shoreward.

These anticipated results are confirmed by the results of the numerical simulations shown in Figures 6.30 and 6.31. The model simulates waves propagating over the spherical disturbance with no detectable numerical difficulties. Due to the absence of combined

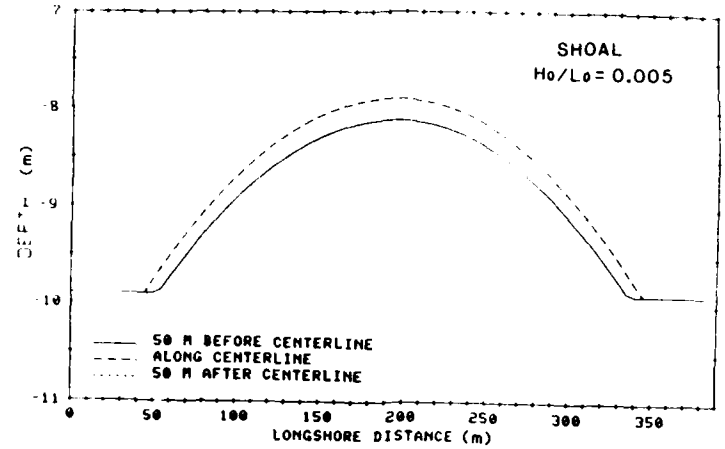

a. Depth

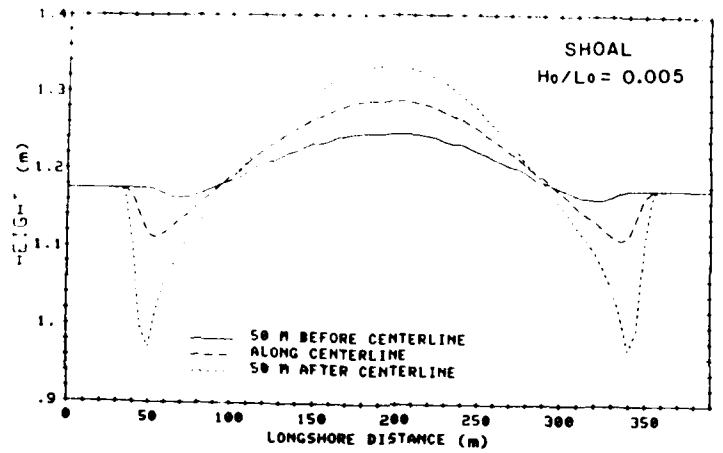

b. Wave Height

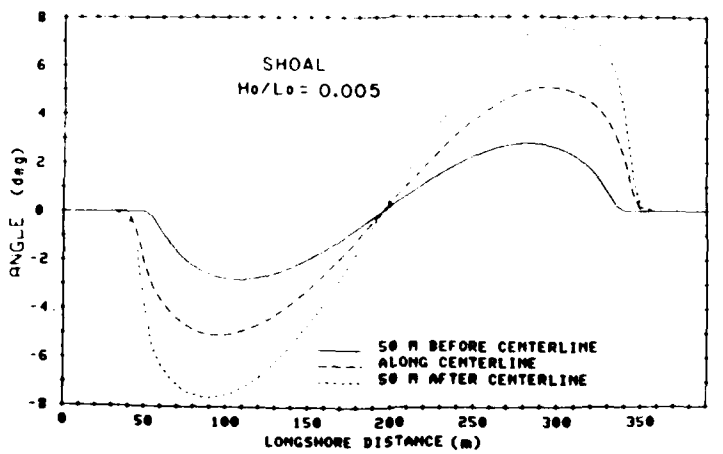

c. Wave Angle

Figure 6.30 Refraction over a spherical shoal, H_o/L_o = 0.005, T = 12 s

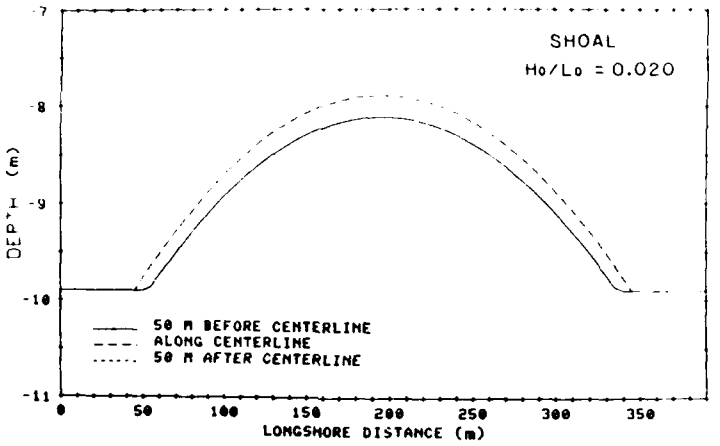

a. Depth

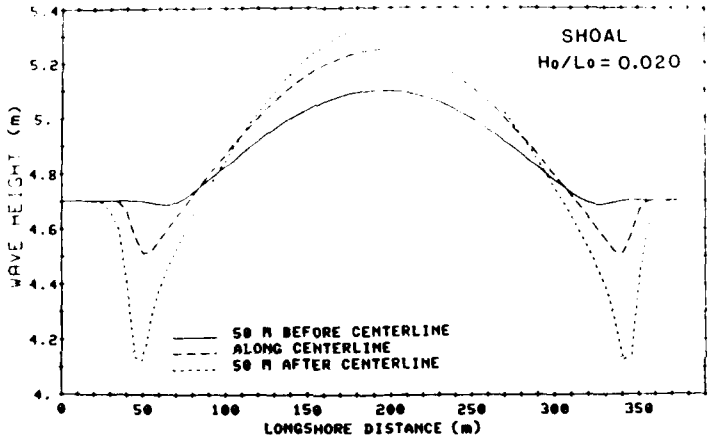

b. Wave Height

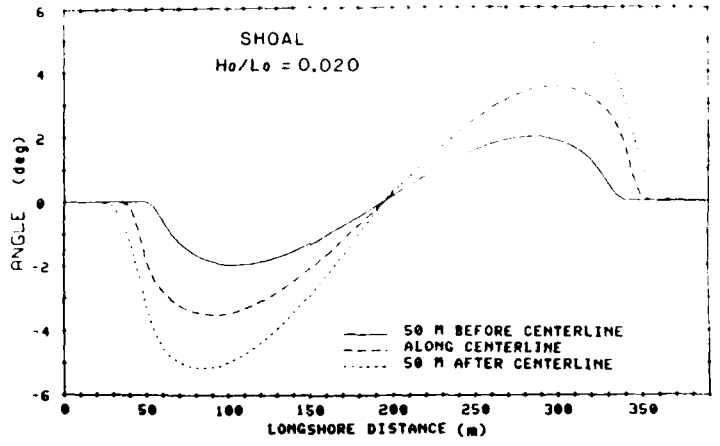

c. Wave Angle

Figure 6.31 Refraction over a spherical shoal, H_o/L_o = 0.020, T = 12 s

refraction-diffraction in the numerical model, results in the zone of convergence shoreward of the shoal will become increasingly inaccurate. The model did not "blow-up" during these runs, but did "blow-up" when a more severe shoal (5 m) was tested. For artificial bathymetries such as the spherical shoal, the area behind the shoal where energy will be focused is an obvious area where the limits of applicability of the model will be tested. If real bathymetries are modeled, these areas of inapplicability may not be as apparent. For every simulation, model results should be scrutinized to determine if regions exist where either unrealistically high or unrealistically low wave heights are calculated due to the absence of diffraction. These unrealistic values may not always cause the simulation to "blow-up," triggering a direct sign of model inapplicability.

Several interesting features can be seen in the Figures 6.30 and 6.31. There is less angle change with the steeper wave (Figures 6.31c). This reproduces the results of refraction over a plane bottom presented in Figures 6.15 to 6.29, where at a given depth, steeper waves refracted less than less steep waves. Looking at the maximum wave heights on each of the three curves of Figures 6.30b and 6.31b, the effects of shoaling vs. the effects of concentration of energy due to refraction can be seen. Recall from the results for shoaling over a plane bottom (Figures 6.8 to 6.12), that at a given depth the steeper wave experiences greater shoaling. On the seaward side of the shoal both refraction and shoaling cause an increase in wave height. On the shoreward side of the shoal, refraction continues to bring increasing amounts of energy towards the center, producing a

greater wave height. In contrast, the increasing depth as the wave propagates down the backside of the lens will cause "de-shoaling", a term coined here to describe wave height change resulting from wave propagation into deeper water. The concentration of energy towards the center of the shoal overwhelms the reduction of wave height due to this "de-shoaling," resulting in an increased wave height on the shoreward side of the shoal for both wave steepnesses. However, for the steeper wave (Figure 6.31b) with its greater "de-shoaling" and smaller refraction, the plot labeled "50 m after centerline" is much closer to the plot labeled "along centerline" than the corresponding plots on the less steep wave (Figure 6.30b).

A comparison between the results of the small-amplitude and second-order cnoidal models for the spherical shoal bathymetry is presented in Figure 6.32. This figure is similar to the previous two figures. Three plots - one each for depth, wave height, and wave angle are included. The slightly uneven nature of the curves for wave height results from round-off error in the number of digits retained for plotting. The results are shown for the cross section at the center of the shoal. Figure 6.32 echoes the results presented in Section 6.2; the curve for small-amplitude wave shows less shoaling but more refraction than do the curves for the second-order cnoidal waves. As would be expected, the results for the less steep second-order cnoidal wave are closer to the results for the small-amplitude wave than are the results from the steeper second-order cnoidal wave.

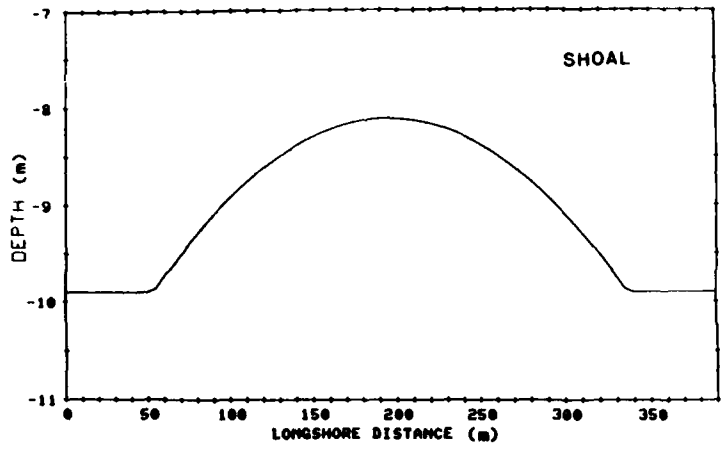

a. Depth

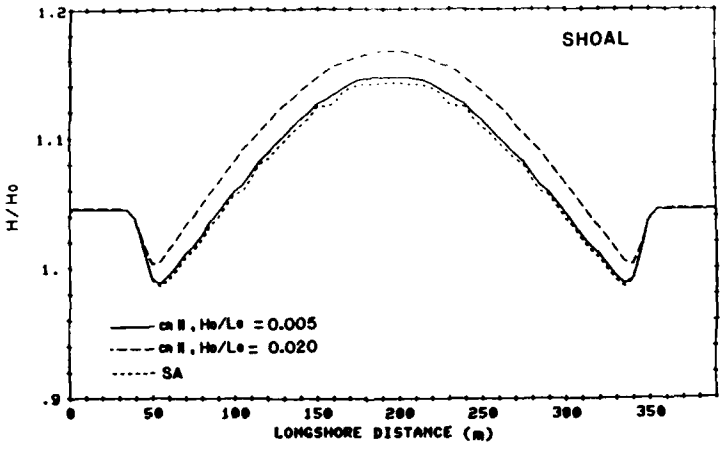

b. Wave Height

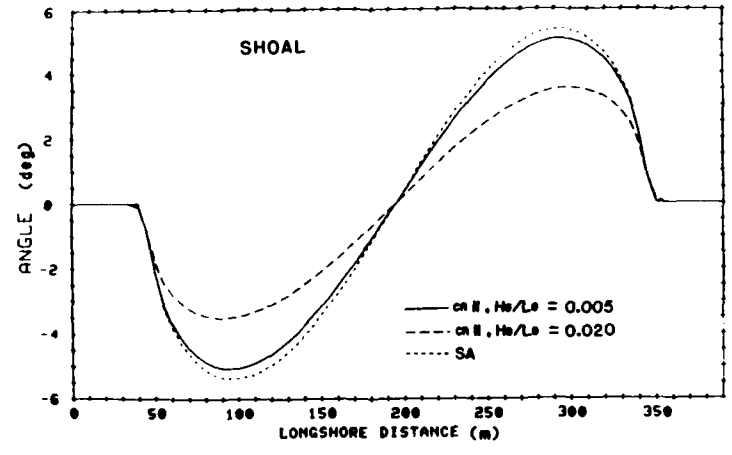

c. Wave Angle

Figure 6.32. Refraction over a spherical shoal, cnoidal - small-amplitude comparison at centerline of shoal

6.3.2 Shoaling and refraction over a trench

The trench bathymetry was calculated using Equation 5.1 (a = 0, b = 0.02, d = 1.0 . Unlike the spherical shoal example, the trench was superimposed on a bottom with slope of 1:50. A single trench was placed along the center of the grid with the trench axis in the onshore-offshore direction. The maximum increase in depth imposed on the sloping plane bottom by the trench was 2 m (for a total depth of 11 m) at the centerline of the grid 450 m offshore. The effect of the trench on the sloping bottom was linearly increased from 0 m at the seaward boundary (600 m offshore) to the maximum and then was linearly decreased to 0 m at the shoreline. This configuration represents an idealized rip channel, a feature commonly found along sandy coastlines. The seaward boundary was placed at a water depth of 12 m. The position of the seaward boundary allowed the comparison, at a range of depths, for simulations with deepwater wave steepnesses of 0.005 and 0.020 for a wave period of 12 s. The smaller wave was inside the cnoidal range (U > 10), and the larger wave was outside the point of wave breaking.

Simulations were conducted with both the small-amplitude and the second-order cnoidal models. A constant wave height and a wave direction normal to the shoreline ($\alpha = 0°$) were the inputs on the seaward boundary. The value of the wave height on the boundary was determined from the the small-amplitude shoaling simulations presented in Section 6.1 .

The results of simulations employing the second-order cnoidal model are presented in Figures 6.33 and 6.34, for $H_o/L_o = 0.005$ and $H_o/L_o = 0.020$, respectively. As with the Figures 6.30 and 6.31 for the

spherical shoal, there are three parts to each figure. Figures 6.33a and 6.34a show the longshore variation in depth at three cross sections (400, 350, and 300 m offshore for H_o/L_o = 0.005 and 500, 450, and 400 m offshore for H_o/L_o = 0.020) parallel to the shoreline. Note that the three cross sections shown for the steeper wave span the region of the maximum increase in depth due to the trench, whereas the cross sections shown for the less steep wave are all shoreward of the maximum trench location. Figures 6.33b and 6.34b are plots of the longshore variation in wave height corresponding to the three cross sections for the respective deepwater wave steepness. Similarly, Figures 6.33c and 6.34c are plots of the longshore variation of wave angle at each of the cross sections. As with Figures 6.30 and 6.31, Figures 6.33 and 6.34 are orientated as if the observer were at sea facing toward the shore.

The following results were anticipated:

a. Calculated quantities should be symmetrical about the centerline of the trench.

b. There should be no change in wave angle along the centerline of the trench.

c. At either side of the trench, the wave angle should be directed away from the centerline of the trench.

d. The maximum wave angle should be located near the position of maximum change in the bathymetry in the longshore direction.

e. The maximum wave height should be located near the lateral edges of the trench.

f. The minimum wave height would be located at the centerline of the trench.

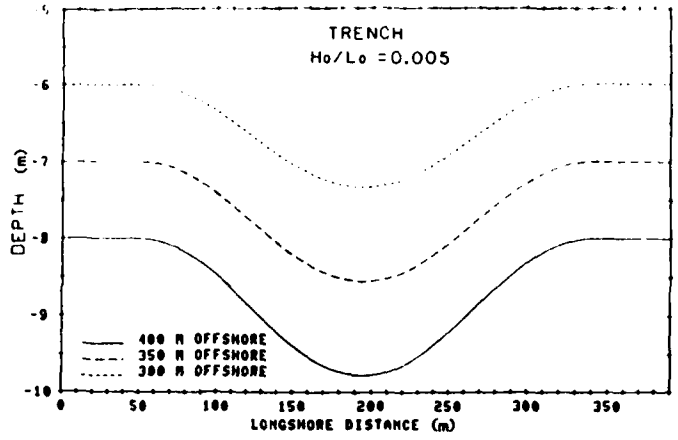

a. Depth

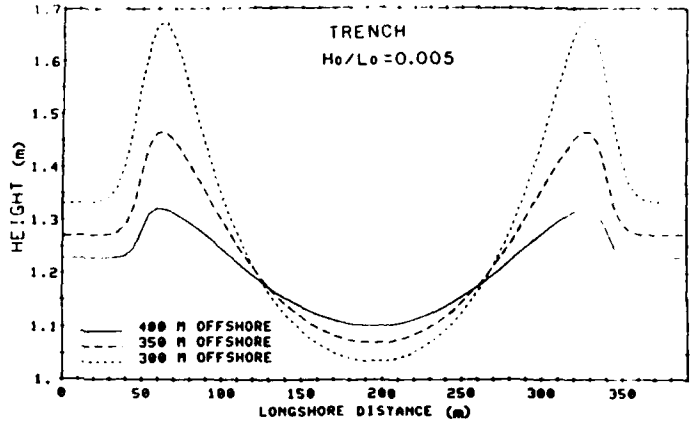

b. Wave Height

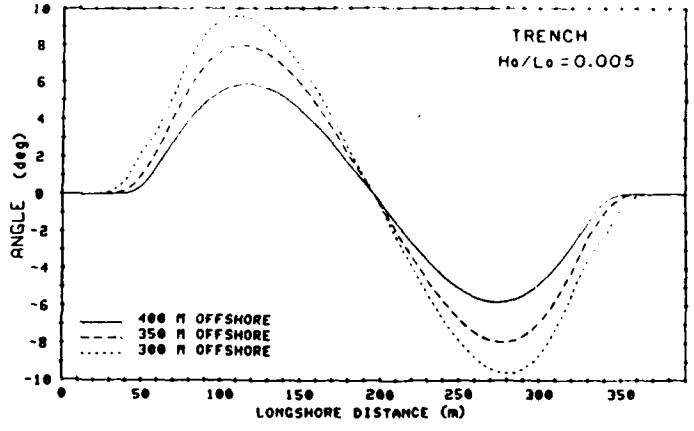

c. Wave Angle

Figure 6.33 Refraction over a trench H_o/L_o = 0.005, T = 12 s

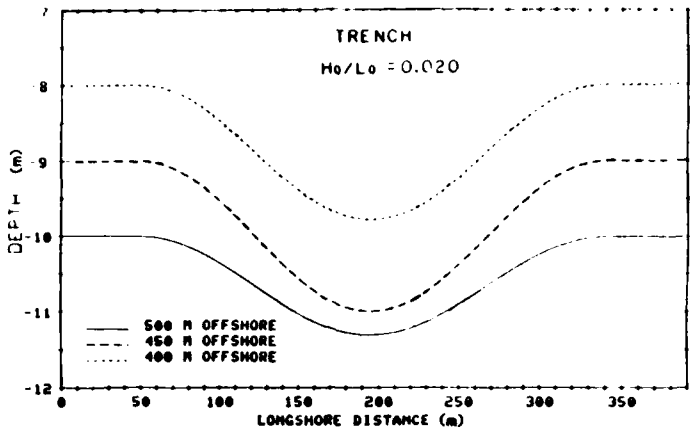

a. Depth

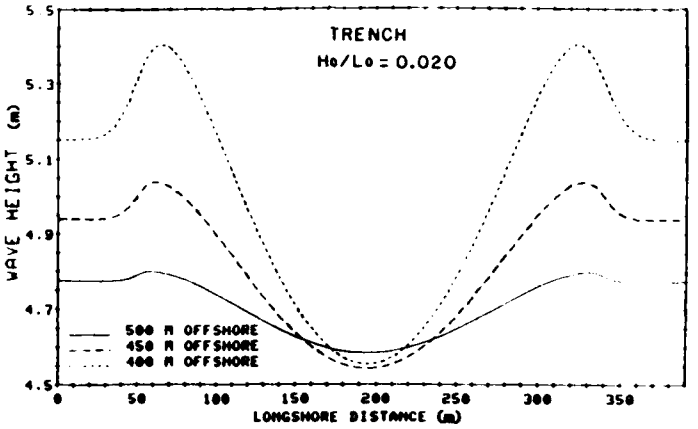

b. Wave Height

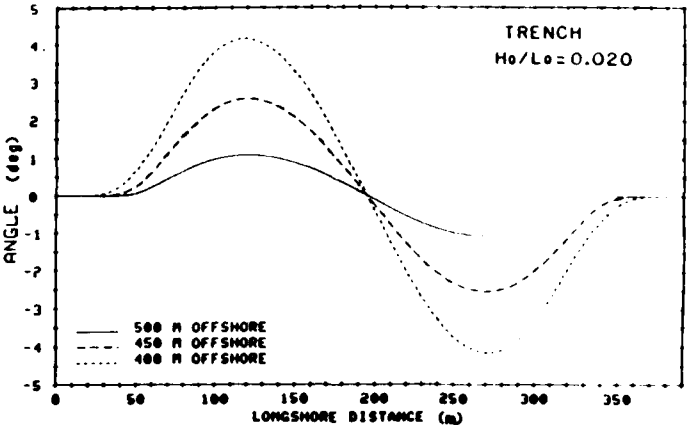

c. Wave Angle

Figure 6.34 Refraction over a trench H_o/L_o = 0.020, T = 12 s

g. The trends in items c through e would increase as the wave propagated shoreward.

These anticipated results are confirmed by the results of the numerical simulations shown in Figures 6.33 and 6.34. The model simulates waves propagating over the idealized trench with no detectable numerical difficulties.

A comparison between the results of the small-amplitude and second-order cnoidal models for the trench bathymetry is presented in Figure 6.35. The results shown are for the cross section 400 m offshore. Figure 6.35 is similar to the previous five figures. There are three parts to the figure, one plot each for depth, wave height, and wave angle. Figure 6.35 repeats the results presented in Section 6.2 and Figure 6.32; the curve for small-amplitude wave shows less shoaling but more refraction than does the curve for the second-order cnoidal wave. The dependence of wavelength on wave height can be seen in both the height and angle plots (Figures 6.35b and 6.35c). The refractive effect of the trench on the wave height and angle of the steeper second-order cnoidal wave extends further onto the constant depth regions at the lateral sides of the grid than for either the less steep cnoidal wave or the small-amplitude wave. Likewise, the refractive effect of the trench on the less steep cnoidal wave spreads onto these regions to a greater extent than for the small-amplitude wave. This tendency can be explained by the change in wavelength caused by changes in wave height. The wavelength determined by small-amplitude wave theory is constant over the constant depth regions, since wavelength is a function of only depth and wave period for small-amplitude waves. However, at a constant

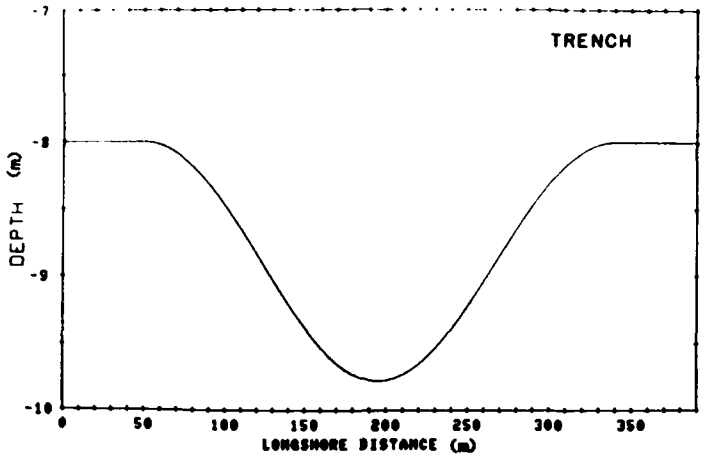

a. Depth

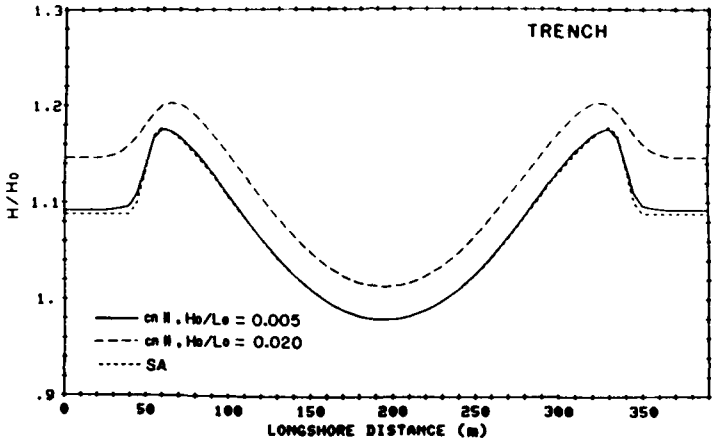

b. Wave Height

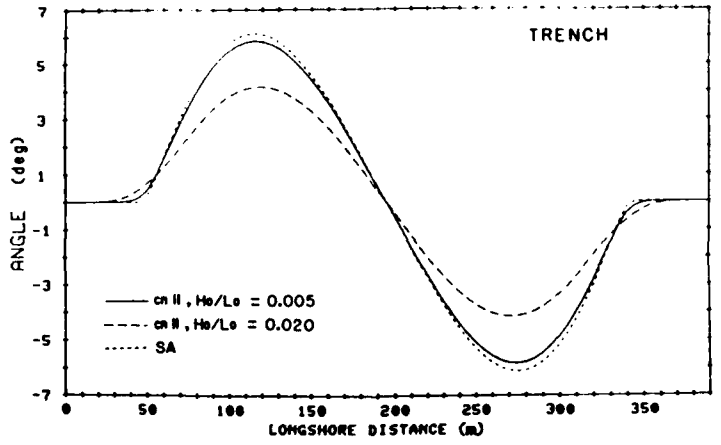

c. Wave Angle

Figure 6.35. Refraction over a trench, cnoidal - small-amplitude comparison at 400 m from shore

depth, the wavelength of a second-cnoidal wave increases with wave height (increasing ε). This increase of wavelength due to increasing wave height has the same effect on refraction as the increase in wavelength due to increasing depth. Thus, the finite-amplitude waves react as if the trench were laterally extended. The steeper wave shows this effect more than the less steep wave since the steeper wave has a greater value of ε.

The change in wave height and angle with deepwater wave steepness predicted by second-order wave theory but unaccounted for by small-amplitude wave theory (as shown in Figures 6.30 to 6.35) is a convincing argument for the use of a finite-amplitude wave theory to calculate wave transformation.

6.4 Comparison of Computer time between Small-Amplitude and Second-Order Simulations

The presentation of results would not be complete without commenting on the costs of modeling finite-amplitude shallow water waves using second-order cnoidal wave theory. None of the models used to produce results for this report were tuned for maximum efficiency. Array sizes were larger than necessary, and many extra variables were calculated and stored for research purposes. Nevertheless, some conclusions can be reached regarding the relative costs of small-amplitude vs. finite-amplitude wave modeling. The simulations were run on a VAX 750 mini-computer, computing power which is presently equalled or exceeded at most universities and many consulting firms. The ratio of CPU time between the second-order cnoidal and small-amplitude simulations was approximately 3.5 : 1 . For a simulation on a 100 by

100 grid this difference amounted to computing times of just over a minute for the small-amplitude model and less than four minutes for the second-order cnoidal model. Interestingly the first-order cnoidal simulations required slightly more computer time than the second-order cnoidal simulations, because the greater shoaling predicted by first-order theory near to the breaking point required more iterations to converge.

If wave simulation required hours of computing time, than the 3.5 : 1 ratio would indeed be an obstacle to the use of second-order cnoidal theory. But an extra few minutes will not significantly raise the cost of either computer or human time. The extra expense incurred seems well worth the extra accuracy obtainable with a finite-amplitude wave theory.

CHAPTER VII

CONCLUSIONS AND SUGGESTIONS FOR FURTHER STUDY

The goal of this report was the development of a shallow water wave transformation model that employs second-order cnoidal wave theory and has the capability to directly calculate at numerical grid points. This model was proposed to be an improvement over existing methods for calculating the transformation of monocromatic finite-amplitude waves in shallow water. A secondary goal was to advance the use of cnoidal wave theory by deriving and demonstrating methods for its accurate and efficient calculation.

A significant difference was shown to exist between shoaling and refraction predicted by second-order cnoidal wave theory and that predicted by the more commonly used small-amplitude wave theory. The greater shoaling and lesser refraction predicted by second-order cnoidal wave theory have important implications for the calculation of many engineering quantities, in particular, for the calculation of wave-induced currents and sediment transport in the nearshore zone. Furthermore, although not as good as had been expected, the results of second-order cnoidal wave shoaling were found to better match experimental data than did the results of either small-amplitude or first-order cnoidal wave theories. The model performed excellently in modeling waves propagating over non-plane bathymetries. The method employed for the calculation of results directly at numerical grid points is an obvious improvement over the more cumbersome ray tracing method. The techniques

for the calculation of second-order cnoidal wave shoaling and refraction used in the numerical model result in simulations which should be well within any financial limits imposed in a study requiring wave modeling. Although the second-order cnoidal model requires more computer time than a model based on small-amplitude theory, the differences in time and cost are inconsequential compared to the increase in accuracy of the results.

There is one effort that remains before this finite-amplitude model can be used in a production mode; investigation into the connection with the companion deeper water model, which uses Stokes third-order theory, must be completed. At the completion of the connection of the two models, a model which can transform finite-amplitude waves from deep water into the breaking point will be available.

This combined cnoidal II - Stokes III wave model will be best suited for open coast simulations, modeling monochromatic waves over smoothly varying bathymetries. After the connection research is completed, the model will continue to be improved. The comparison of model results to the experimental shoaling data indicate that a third-order cnoidal model may provide an improvement over second-order cnoidal theory near the breaking point. Development of the necessary third-order cnoidal wave theory expressions, especially for the energy flux, would be an arduous task very well suited for a computer program using symbolic manipulation.

Additional numerical techniques and wave transformation mechanisms will be added to expand the range of situations for which the model is applicable. The incorporation of either a stretched or boundary fitted

numerical grid would enable large areas to be more economically and accurately modeled. Perhaps the first transformation mechanism which will be added is the inclusion of energy loss due to bottom friction. The major limitation of the present model is the incapability to model highly irregular bathymetries because of the formation of caustics, regions where the focusing of wave energy results in calculation of unreliable wave properties. Therefore, the addition of a combined refraction-diffraction calculation scheme would be a significant improvement that would greatly add to the versitility of the model. Finally, the capability to model a spectrum of shallow water waves must eventually be included. However, the inclusion of a spectral capability will require extensive research.

Model development is currently hampered by the lack of adequate laboratory and field data with which to verify numerical wave transformation models. Excellent shoaling data are available (and used in this thesis), but adequate data for refraction, especially data for wave angles, are not available. When the time comes to verify a spectral shallow water finite-amplitude wave transformation model for use over a complex bathymetry, if adequate data are not available, then it will be difficult to design the optimum model.

The ultimate finite-amplitude shallow water wave transformation model which would include all the significant wave transformation mechanisms, as well as model the random nature of the sea surface, is not clearly in sight. It is hoped that this report may be a step in the direction of that final goal.

REFERENCES

Abramowitz, M., and Stegun, I. A., eds. 1972. Handbook of Mathematical Functions, Dover Publications, New York, 1046 pp.

Airy, G. B. 1845. "Tides and Waves," Encyclopaedia Metropolitana, Volume 192, pp. 241-396.

Berkhoff, J. C. W. 1972. "Computation of Combined Refraction-Diffraction," Proceedings of the 13th Coastal Engineering Conference, ASCE, pp. 471-490.

Boussinesq, J. 1872. "Theorie des Ondes at de Remous qui se Propagent le Long d'un Canal Rectangulaire Horizontal, en Communiquant au Liquide Contentu dans ce Canal des Vitesses Sensiblement Paralleles de la Surface au Fond," Journal de Mathematiques Pures et Appliquees.

Buhr Hansen, J., and Svendsen, I. A. 1979. "Regular Waves in Shoaling Water Experimental Data," Series Paper No. 21, Institute of Hydrodynamics and Hydraulic Engineering, Technical University of Denmark.

Byrd, P. F., and Friedman, M. D. 1954. Handbook of Elliptic Integrals for Engineers and Physicists, Springer-Verlag, Berlin, 355 pp.

Chappelear, J. E. 1962. "Shallow Water Waves" Journal of Geophysical Research, Vol. 67, No. 12, pp. 4693-4704.

Chu, H. 1975. "Numerical Model for Wave Refraction by Finite Amplitude Wave Theories," Proceedings Symposium on Modeling Techniques, Modeling 75, ASCE, pp. 1082-1100.

Cialone, M. A., and Kraus, N. C. 1987. "A Numerical Model for Shoaling and Refraction of Third-Order Stokes Waves Over an Irregular Bottom," Miscellaneous Paper CERC-87-10, US Army Engineer Waterways Experiment Station, Vicksburg, MS.

Cokelet, E. D. 1977. "Steep Gravity Waves in Water of Arbitrary Uniform Depth," Philosophical Transactions of the Royal Society London, A286, pp. 182-230.

Dean, R. G. 1965. "Stream Function Representation of Nonlinear Ocean Waves," Journal of Geophysical Research, Vol. 70, No. 18, pp. 4561-4572.

Dean, R. G. 1974. "Evaluation and Development of Water Wave Theories for Engineering Application," Volume I, Special Report No. 1, US Army Coastal Engineering Research Center.

Dean, R. G., and Dalrymple, R. A. 1984. Water Wave Mechanics for Engineers and Scientists, Prentice-Hall, Inc., Englewood Cliffs, New Jersey, 353 pp.

Ebersole, B. A. 1985. "Refraction-Diffraction Model for Linear Water Waves," Journal of Waterways, Port, Coastal, and Ocean Engineering, ASCE, Vol. 111, No. 6, pp. 939-953.

Fenton, J. D. 1985. "A Fifth-Order Stokes Wave Theory for Steady Waves," Journal of Waterways, Port, Coastal, and Ocean Engineering, Vol. 111, No. 2, ASCE, pp. 216-234.

Friedrichs, K. O. 1948. Appendix on the Derivation of Shallow Water Wave Theory, Committee of Pure Applied Mathematics No. 1, pp. 81-85.

Goda, Y. 1983. "A Unified Nonlinearity Parameter of Water Waves," Report of the Port and Harbour Research Institute, Vol. 22, No. 3, Japan.

Headland, J. R., and Chu, H. 1985. "A Model for the Refraction of Linear and Cnoidal Waves," Proceedings of the 19th Coastal Engineering Conference , ASCE, pp. 1118-1131.

Ippen, A. T., ed. 1966. Estuary and Coastal Hydrodynamics, McGraw-Hill, New York, 744 pp.

Isobe, M. 1985. "Calculation and Application of First-Order Cnoidal Wave Theory," Coastal Engineering, Vol. 9, pp. 309-325.

Isobe, M., and Horikawa, K. 1982. "Study on Water Particle Velocities of Shoaling and Breaking Waves," Coastal Engineering in Japan, Vol. 25, pp. 109-123.

Isobe, M., and Kraus, N. C. 1983a. "Derivation of a Third-Order Stokes Wave Theory," Hydraulics Lab. Report No. YNU-HY-83-1, Department of Civil Engineering, Yokohama National University, 37 pp.

Isobe, M., and Kraus, N. C. 1983b. "Derivation of a Second-Order Cnoidal Wave Theory," Hydraulics Lab. Report No. YNU-HY-83-2, Department of Civil Engineering, Yokohama National University, 43 pp.

Isobe, M., Nishimura, H., and Horikawa, K. 1982. "Theoretical Considerations on Perturbation Solutions for Waves of Permanent Type," Bulletin of the Faculty of Engineering, Yokohama National University, Vol. 31, pp. 29-57.

Keller J. B. 1948. "The Solitary Wave and Periodic Waves in Shallow Water," Communication of Pure and Applied Mathematics, Vol. 1, pp. 323-339.

Keulegan, G. H., and Patterson, G. W. 1940. "Mathematical Theory of Irrotational Translation Waves," Journal of Research of the National Bureau of Standards, Vol. 24, pp. 47-101.

Koh, R. C. Y., and Le Mehaute, B. 1966. "Wave Shoaling," Journal of Geophysical Research, Vol. 71, No. 8, pp. 2005-2012.

Korteweg, D. J., and de Vries, G. 1895. "On the Change of Form of Long Waves Advancing in a Rectangular Canal, and on a New Type of Long Stationary Waves," Philosophy Magazine, Series 5, Vol. 39, pp. 422-443.

Kraus, N. C., Cialone, M. A., and Hardy, T. A. 1987. Discussion of "Numerical Study of Finite Amplitude Wave Refraction," by I. S. Oh and C. E. Grosch, Journal of Waterways, Port, Coastal, and Ocean Engineering, Vol. 113, No. 2, pp. 199-201.

Laitone, E. V. 1960. "The Second Approximation to Cnoidal and Solitary Waves," Journal of Fluid Mechanics, Vol. 9, pp. 430-444.

Le Méhauté, B., and Webb, L. M. 1964. "Periodic Gravity Waves over a Gentle Slope at a Third Order of Approximation," Proceedings of the 9th Coastal Engineering Conference, ASCE, pp. 23-40.

Liu, P. L. 1985. "Wave-Current Interactions on a Slowly Varying Topography," Journal of Geophysical Research, Vol. 88, pp. 4421-4426.

Liu, P. L., and Ting-Kuei Tsay. 1985. "Numerical Prediction of Wave Transformation," Journal of Waterway, Port, Coastal and Ocean Engineering, ASCE, Vol. 111, No. 5, pp. 843-855.

Lozano, C., and Liu, P. L. 1980. "Refraction-Diffraction Model for Linear Surface Water Waves," Journal of Fluid Mechanics, Vol. 101, pp. 705-720.

McCowan, J. 1891. "On the Solitary Wave," Philosophy Magazine, Series 5, Vol. 32, pp. 45-58.

Milne-Thomson, L. M. 1950. Jacobian Elliptic Function Tables, Dover Publications, New York, 123 pp.

Munk, W. H., 1949. "The Solitary Wave and its Application to Surf Problems," Annals New York Academy of Science, Vol. 51, pp. 376-424.

Munk, W. H., and Arthur, R. S. 1952. "Wave Intensity Along a Refracted Ray", US National Bureau of Standards, Gravity Waves, NBS. Circular 521, US Government Printing Office, Washington, D.C., pp. 95-109.

Neville, E. H. 1951. Jacobian Elliptic Functions, 2nd edition, Clarendon Press, Oxford.

Nishimura, H., Isobe, M., and Horikawa, K. 1977. "Higher Order Solutions of the Stokes and the Cnoidal Waves," Journal of the Faculty of Engineering, University of Tokyo, Series B, Vol. 34, pp. 267-293.

Noda, E. K., Sonu, C. J., Rupert, V. C., and Collins, J. I. 1974. "Nearshore Circulation Under Sea Breeze Conditions and Wave-Current Interactions in the Surf Zone," Technical Report No. 4, Tetra Tech, Inc., Pasadena, CA.

Oh, I. S., and Grosch, C. E. 1985. "Numerical Study of Finite Amplitude Wave Refraction," Journal of Waterway, Port, Coastal, and Ocean Engineering, ASCE, Vol. 111, No. 1, pp. 78-95.

Perlin, M., and Dean R. C. 1983. "An Efficient Algorithm for Wave Refraction/Shoaling Problems," Proceedings of Coastal Structures '83, ASCE, pp. 988-1010.

Phillips, O. M. 1977. The Dynamics of the Upper Ocean, 2nd edition, Cambridge University Press, London, 336 pp.

Radder, A. C. 1979. "On the Parabolic Equation Method for Water-Wave Propagation," Journal of Fluid Mechanics, Vol. 95, pp. 159-176.

Rayleigh, L. 1876. "On Waves," Philosophy Magazine, Series 5, Vol. 1, pp. 257-79.

Russell, J. S. 1844. "Report on Waves," 14th Meeting British Association of the Advancement of Science, pp. 311-90.

Sakai, T., and Battjes, J. A. 1980. "Wave Shoaling Calculated from Cokelet's Theory," Coastal Engineering, Vol. 4, No. 1, pp. 65-85.

Sarpkaya, T., and Isaacson, M. 1981. Mechanics of Wave Forces on Offshore Structures, Van Nostrand Reinhold Company, New York, New York, 651 pp.

Shore Protection Manual. 1984. 4th edition, 2 volumes, US Army Engineer Waterways Experiment Station, Coastal Engineering Research Center, US Government Printing Office, Washington, DC.

Shuto, N. 1974. "Nonlinear Long Waves in a Channel of Variable Section," Coastal Engineering in Japan, Vol. 17, pp. 1-12.

Skjelbreia, L., and Hendrickson J. 1960. "Fifth Order Gravity Wave Theory," Proceedings of the 7th Coastal Engineering Conference, ASCE, pp. 184-196.

Skovgaard, O., and Peterson, M.H. 1977. "Refraction of Cnoidal Waves," Coastal Engineering, Vol. 1, pp. 43-61.

Stokes, G. G. 1847. "On the Theory of Oscillatory Waves," Transactions of the Cambridge Philosophy Society, Vol. 8, pp. 441-455.

Svendsen, I. A. 1974. "Cnoidal Waves Over a Gently Sloping Bottom," Series Paper No. 6, Institute of Hydrodynamics and Hydraulic, Technical University of Denmark, 181 pp.

Svendsen, I. A., and Brink-Kjaer, O. 1972 "Shoaling of Cnoidal Waves," Proceedings of the 13th Coastal Engineering Conference, ASCE, pp. 365-383.

Vincent, C. L. 1982. "Shallow-Water Wave Modeling," First International Conference on Meteorology and Air-sea Interaction in the Coastal Zone, The Hague.

Walker, J., and Headland, J. 1982. "Engineering Approach to Nonlinear Wave Shoaling," Proceedings of the 18th Coastal Engineering Conference, ASCE, pp. 523-542.

Wang, J. D., and Le Mehaute, B. 1980. "Breaking Wave Characteristics on a Plane Beach," Coastal Engineering, Vol. 4, pp. 137-149.

APPENDIX A

EFFICIENT CALCULATION OF ELLIPTIC INTEGRALS AND JACOBIAN ELLIPTIC FUNCTIONS

This appendix contains two sections. In Section A.1, expressions for the efficient calculation of elliptic integrals and Jacobian elliptic functions are derived based on the work of Isobe (1985). Section A.2 contains a short table of properties of the Jacobian elliptic functions.

A.1 Derivation of Expressions for the Efficient Calculation of Elliptic Integrals and the Jacobian Elliptic Functions

The elliptic modulus, κ , is a fundamental entity which enters in the definitions of the elliptic integrals and Jacobian elliptic functions. As is discussed in Chapter II, κ is used as the auxillary parameter for the perturbation expansion leading to cnoidal wave theory. In general, κ can have values ranging from 0 to 1 if the elliptic integrals are restricted to be real-valued. However, in cnoidal water wave theory, κ has a much smaller range. At $U = 25$, $\kappa \approx 0.92$ and, as the Ursell number increases, κ approaches 1.0. Computer subroutines from mathematics libraries and formulae found in references such as Byrd and Friedman (1954) and Abramowitz and Stegun (1972) are not conveniently used for this narrow range of κ values, because computer algorithms based upon these formulae can result in expensive or even inaccurate calculations. On the other hand, Isobe (1985) presented expressions for elliptic integrals and Jacobian elliptic functions (Equations 3.6 to 3.12) which converge quickly and accurately for the calculation of cnoidal wave theory. Derivations of these expressions

are not known to have not been published in English. Therefore, they will be presented in this appendix. The following derivations developed in the course of this research are based on concepts kindly supplied by Dr. Isobe (personal communication, 1985).

Several definitions are necessary for the derivations that follow. The complementary modulus, κ' , is defined from the following relationship:

$$\kappa^2 + \kappa'^2 \equiv 1 \tag{A.1}$$

The complete elliptic integral of the first kind, K , and its complement, K' , are defined as

$$K(\kappa) \equiv \int_0^{2\pi} \frac{d\phi}{(1 - \kappa^2 \sin^2 \phi)^{1/2}} \tag{A.2}$$

$$K'(\kappa) \equiv \int_0^{2\pi} \frac{d\phi}{(1 - \kappa'^2 \sin^2 \phi)^{1/2}} \tag{A.3}$$

The complete elliptic integral of the second kind, E_e , and its complement, E_e' are defined as

$$E_e(\kappa) \equiv \int_0^{2\pi} (1 - \kappa^2 \sin^2 \phi)^{1/2} \, d\phi \tag{A.4}$$

$$E_e'(\kappa) \equiv \int_0^{2\pi} (1 - \kappa'^2 \sin^2 \phi)^{1/2} \, d\phi \tag{A.5}$$

The nome, q, and the complementary nome, q', are defined as

$$q \equiv e^{-\pi(K'/K)} \tag{A.6}$$

$$q' \equiv e^{-\pi(K/K')} \tag{A.7}$$

Since extensive use will be made of equations from Abramowitz and Stegun, (1972, Chapters 16 and 17), the equation numbers from this source will be indicated in brackets (eg. [16.38.1]) for easy reference. Equations necessary for the calculation of elliptic integrals and the Jacobian elliptic functions are readily available. However, these expressions are often given in terms of q as in

$$\left(\frac{2K}{\pi}\right)^{1/2} = 1 + 2q + 2q^4 + 2q^9 + \ldots \qquad [16.38.5] \tag{A.8}$$

$$\left(\frac{2\kappa K}{\pi}\right)^{1/2} = 2q^{1/4}\,(1 + q^2 + q^6 + q^{12} + \ldots) \qquad [16.38.7] \tag{A.9}$$

$$\left(\frac{2\kappa' K}{\pi}\right)^{1/2} = (1 - 2q + 2q^4 - 2q^9 + \ldots) \qquad [16.38.8] \tag{A.10}$$

Cnoidal wave theory is valid for $U \gtrsim 10$ ($U = HL^2/D^3$, Equation 2.23). At $U \approx 10$, q and q' are almost equal ($q \approx q' \approx 0.043$). As a wave moves into shallower water, the Ursell number increases and the values of q' and q become smaller and larger, respectively. At $U = 100$, $q \approx 0.10$ and $q' \approx 0.00017$; at $U = 500$, $q \approx 0.60$ and $q' \approx 0.0000000039$. Consequently, for the range of Ursell numbers applicable to cnoidal theory, expressions using power series based on q' will converge much more rapidly than expressions based on q. The

purpose of this appendix is to derive expressions, as functions of q', which are needed for the practical and efficient calculation of cnoidal wave theory.

From Equations A.2 and A.3, it can be seen that

$$K(\kappa) = K'(\kappa') \qquad [16.1.2] \quad (A.11)$$

With this result and using Equations A.6 and A.7, Equations A.8 to A.10 can be written in terms of q'. After minor algebraic manipulations, the results are

$$K' = \frac{\pi}{2}\left(1 + 2q' + 2q'^4 + \ldots\right)^2 \qquad (A.12)$$

$$\kappa' = 4q'^{1/2}\left[\frac{\left(1 + q'^2 + q'^6 + \ldots\right)^2}{\left(1 + 2q' + 2q'^4 + \ldots\right)^2}\right] \qquad (A.13)$$

$$\kappa = \frac{\left(1 - 2q' + 2q'^4 + \ldots\right)^2}{\left(1 + 2q' + 2q'^4 + \ldots\right)^2} \qquad (A.14)$$

An expression relating E_e and K is given as

$$\frac{E_e}{K} = \frac{1}{3}\left(1 + \kappa'^2\right) + \left(\frac{\pi}{K}\right)^2\left\{\frac{1}{12} - 2\left[\frac{q^2}{\left(1 - q^2\right)^2} + \frac{q^4}{\left(1 - q^4\right)^2} + \ldots\right]\right\} \qquad [17.3.23] \quad (A.15)$$

The last term of this equation can be simplified using a binomial series. The result is

$$\frac{E_e}{K} = \frac{1}{3}\left(1 + \kappa'^2\right) + \left(\frac{\pi}{K}\right)^2 \left[\frac{1}{12} - 2\left(q^2 + 3q^4 + \ldots\right)\right] \qquad (A.16)$$

As was the case for K and K' (Equation A.11), E_e and E'_e are related by

$$E_e(\kappa) = E'_e(\kappa') \qquad (A.17)$$

Substituting Equation A.17 into Equation A.16 and using Equation A.11 yields

$$\frac{E'_e}{K'} = \frac{1}{3}\left(1 + \kappa^2\right) + \left(\frac{\pi}{K'}\right)^2 \left[\frac{1}{12} - 2\left(q'^2 + 3q'^4\right)\right] \qquad (A.18)$$

Equations A.12 and A.14 are substituted for K' and κ on the right hand side of Equation A.18. After carrying out the multiplications, combining terms, and neglecting terms of q'^5 and higher (in application to cnoidal wave theory, the largest value of q'^5 is approximately 0.0000005), Equation A.18 becomes

$$\frac{E'_e}{K'} = \frac{\left(1 + 8q'^2 - 8q'^4 + \ldots\right)}{\left(1 + 2q' + 2q'^4 + \ldots\right)^4} \qquad (A.19)$$

Substituting Equation A.12 into the left-hand side of Equation A.19, E'_e is given as

$$E'_e = \frac{\pi}{2}\left[\frac{\left(1 + 8q'^2 - 8q'^4\right)}{\left(1 + 2q' + 2q'^4\right)^2}\right] \qquad (A.20)$$

Using Equations A.7 and A.12, an expression for K is

$$K = -\frac{K'}{\pi} \ln q'$$

$$= -\frac{\ln q'}{2} (1 + 2q' + 2q'^4 + \ldots)^2 \qquad (A.21)$$

An expression for E_e in terms of q is

$$E_e = \frac{1}{K'} \left(\frac{\pi}{2} - E_e' K + K K' \right) \qquad [17.3.13] \quad (A.22)$$

Substituting expressions for E_e', K', and K (Equations A.20, A.12, and A.21) into Equation A.22 results in

$$E_e = \frac{\left[1 - \left(-\frac{\ln q'}{2} \right)(1 + 8q'^2 - 8q'^4) + \left(-\frac{\ln q'}{2} \right)(1 + 2q' + 2q'^4)^4 \right]}{(1 + 2q' + 2q'^4)^4} \qquad (A.23)$$

The above derivation provided expressions in terms of q' for the elliptic integrals (K, K', E_e, E_e'), the elliptic modulus (κ), and the complementary modulus (κ'). Next, expressions in terms of q' will be derived for the Jacobian elliptic functions; $cn\theta$, $sn\theta$, $dn\theta$.

Similar to the relationship between the cn and the cosine functions (Chapter III), the Jacobian elliptic functions sn and dn are analogous to the sine and tangent functions. In addition to the three Jacobian elliptic functions used directly to specify cnoidal wave theory (i.e., cn, sn, and dn), three other Jacobian elliptic functions are needed in the derivations which follow. These quantities can be expressed as $sc\theta = sn\theta/cn\theta$, $nc\theta = 1/cn\theta$ and $dc\theta = dn\theta/cn\theta$. For more

information the reader is referred to Abramowitz and Stegun (1972, Chapter 16).

The Jacobian elliptic functions $cn\theta$, $sn\theta$, and $dn\theta$ can be expressed in terms of κ', by using Jacobi's imaginary transform:

$$sn(i\theta;\kappa) = isc(\theta;\kappa') \qquad [16.20.1] \quad (A.24)$$

$$cn(i\theta,\kappa) = nc(\theta;\kappa') \qquad [16.20.2] \quad (A.25)$$

$$dn(i\theta,\kappa) = dc(\theta;\kappa') \qquad [16.20.3] \quad (A.26)$$

These three equations can be rewritten using the following relationship:

$$\theta = i(-i\theta) \qquad (A.27)$$

Substituting Equation A.27 into A.24 to A.26 yields

$$sn(\theta;\kappa) = isc(-i\theta,\kappa') \qquad (A.28)$$

$$cn(\theta;\kappa) = nc(-i\theta,\kappa') \qquad (A.29)$$

$$dn(\theta;\kappa) = dc(-i\theta,\kappa') \qquad (A.30)$$

A general expression for Jacobian elliptic functions is

$$pm\theta = \frac{T_p(\theta)}{T_m(\theta)} \qquad [16.36.3] \quad (A.31)$$

In which, p and m can be any of the symbols, s, c, d, or n. The three elliptic functions of interest, $cn\theta$, $sn\theta$, and $dn\,\theta$ can be

expressed in terms of κ' using Equations A.28 to A.31. This results in

$$sn(\theta;\kappa) = isc(-i\theta;\kappa') = i\,\frac{T_s(-i\theta;\kappa')}{T_c(-i\theta;\kappa')} \tag{A.32}$$

$$cn(\theta;\kappa) = nc(-i\theta;\kappa') = \frac{T_n(-i\theta;\kappa')}{T_c(-i\theta;\kappa')} \tag{A.33}$$

$$dn(\theta;\kappa) = dc(-i\theta;\kappa') = \frac{T_d(-i\theta;\kappa')}{T_c(-i\theta;\kappa')} \tag{A.34}$$

To use these three equations to evaluate $sn(\theta,q)$, $cn(\theta,q)$ and $dn(\theta,q)$ requires expressions in terms of $i\theta$ and q' for the theta functions, T_s, T_c, T_d, and T_n. However, these expressions are not available and must be derived from the following equations for the theta functions given in terms of θ and q.

$$T_s(\theta,q) = \left(\frac{2\pi q^{1/2}}{\kappa\kappa' K}\right)^{1/2}\left(\sin\beta - q^2\sin 3\beta + q^6\sin 5\beta + \ldots\right) \quad [16.38.1] \tag{A.35}$$

$$T_c(\theta;q) = \left(\frac{2\pi q^{1/2}}{\kappa K}\right)^{1/2}\left(\cos\beta + q^2\cos 3\beta + q^6\cos 5\beta + \ldots\right) \quad [16.38.2] \tag{A.36}$$

$$T_d(\theta;q) = \left(\frac{\pi}{2K}\right)^{1/2}\left(1 + 2q\cos 2\beta + 2q^4\cos 4\beta + \ldots\right) \quad [16.38.3] \tag{A.37}$$

$$T_n(\theta;q) = \left(\frac{\pi}{2\kappa' K}\right)^{1/2} \left(1 - 2q \cos 2\beta + 2q^4 \cos 4\beta + \ldots\right) \qquad [16.38.4] \quad (A.38)$$

where

$$\beta = \frac{\pi\theta}{2K} \qquad (A.39)$$

Using the following relationships between trigonometric functions and hyberbolic functions,

$$\cos(-i\theta) = \cosh(-\theta) = \cosh\theta \qquad (A.40)$$

$$\sin(-i\theta) = -\sin i\theta = -i \sinh\theta \qquad (A.41)$$

Equations A.35 to A.38 can be expressed in terms of q'. This results in the following four equations:

$$T_s(-i\theta;q') = -i\left(\frac{2\pi q'^{1/2}}{\kappa'\kappa K'}\right)\left(\sinh\beta' - q'^2 \sinh 3\beta' + q'^6 \sin 5\beta' + \ldots\right)$$

$$= -i\left(\frac{2\pi q'^{1/2}}{\kappa'\kappa K'}\right) T_1(\beta') \qquad (A.42)$$

$$T_c(-i\theta;q') = \left(\frac{2\pi q'^{1/2}}{\kappa' K'}\right)^{1/2}\left(\cosh\beta' + q'^2 \cosh 3\beta' + q'^6 \cosh 5\beta' + \ldots\right)$$

$$= \left(\frac{2\pi q'^{1/2}}{\kappa' K'}\right)^{1/2} T_4(\beta') \qquad (A.43)$$

$$T_d(-i\theta;q') = \left(\frac{\pi}{2K'}\right)^{1/2}\left(1 + 2q' \cosh 2\beta' + 2q'^4 \cosh 4\beta' + \ldots\right)$$

$$= \left(\frac{\pi}{2K'}\right)^{1/2} T_3(\beta') \qquad (A.44)$$

$$T_n(-i\theta;q') = \left(\frac{\pi}{2\kappa K'}\right)^{1/2}\left(1 - 2q' \cosh 2\beta' + 2q'^4 \cosh 4\beta' + \ldots\right)$$

$$= \left(\frac{\pi}{2\kappa K'}\right)^{1/2} T_2(\beta') \qquad (A.45)$$

where

$$\beta' = \frac{\pi\theta}{2K'} \qquad (A.46)$$

$$T_1(\beta') = \sinh \beta' - q'^2 \sinh 3\beta' + q'^6 \sinh 5\beta' + \ldots \qquad (A.47)$$

$$T_2(\beta') = 1 - 2q' \cosh 2\beta' + 2q'^4 \cosh 4\beta' + \ldots \qquad (A.48)$$

$$T_3(\beta') = 1 + 2q' \cosh 2\beta' + 2q'^4 \cosh 4\beta' + \ldots \qquad (A.49)$$

$$T_4(\beta') = \cosh \beta' + q'^2 \cosh 3\beta' + q'^6 \cosh 5\beta' + \ldots \qquad (A.50)$$

The next three expressions will be used to simplify the derivation which follows.

$$T_{02} \equiv T_2(0) = 1 - 2q' + 2q'^4 - \ldots \qquad (A.51)$$

$$T_{03} \equiv T_3(0) = 1 + 2q' + 2q'^4 + \ldots \qquad (A.52)$$

$$T_{04} \equiv T_4(0) = 1 + q'^2 + q'^6 + \ldots \qquad (A.53)$$

From Equations A.32 to A.34, A.42 to A.45, A.13, A.14, and A.51 to A.53, compact notation is developed for $cn(\theta,q)$, $sn(\theta,q)$, and $dn(\theta,q)$. The result is

$$sn(\theta,q) = isc\,(-i\theta,q')$$

$$= i\,\frac{T_s\,(-i\theta,q')}{T_c\,(-i\theta,q')}$$

$$= \left(\frac{1}{\kappa}\right)^{1/2} \frac{T_1(\beta')}{T_4(\beta')}$$

$$= \left(\frac{1 + 2q' + 2q'^4}{1 - 2q' + 2q'^4}\right) \frac{T_1(\beta')}{T_4(\beta')}$$

$$= \frac{T_{03}}{T_{02}}\ \frac{T_1(\beta')}{T_4(\beta')} \qquad ;\ |\theta| \le K \qquad (A.54)$$

$$cn(\theta,q) = nc(-i\theta,q')$$

$$= \frac{T_n(-i\theta,q')}{T_c(-i\theta,q')}$$

$$= \left(\frac{\kappa'}{4q'^{1/2}\kappa}\right)^{1/2} \frac{T_2(\beta')}{T_4(\beta')}$$

$$= \left(\frac{1 + q'^2 + q'^6}{1 - 2q' + 2q'^4}\right) \frac{T_2(\beta')}{T_4(\beta')}$$

$$= \frac{T_{04}}{T_{02}}\ \frac{T_2(\beta')}{T_4(\beta')} \qquad ;\ |\theta| \le K \qquad (A.55)$$

$$dn(\theta,q) = dc(-i\theta,q')$$

$$= \frac{T_d(-i\theta,q')}{T_c(-i\theta,q')}$$

$$= \left(\frac{\kappa'}{4q'^{1/2}}\right)^{1/2} \frac{T_3(\beta')}{T_4(\beta')}$$

$$= \left(\frac{1 + q'^2 + q'^6}{1 + 2q' + 2q'^4}\right)\frac{T_3(\beta')}{T_4(\beta')}$$

$$= \frac{T_{04}}{T_{03}} \frac{T_3(\beta')}{T_4(\beta')} \qquad ; |\theta| \leq K \qquad (A.56)$$

With these expressions, the elliptic functions can be calculated for $|\theta| > K$ using the following three expressions:

$$cn(\theta + 2nK;\kappa) = (-1)^n cn(\theta;\kappa) \qquad (A.57)$$

$$sn(\theta + 2nK;\kappa) = (-1)^n sn(\theta,\kappa) \qquad (A.58)$$

$$dn(\theta + 2nK;\kappa) = dn(\theta;\kappa) \qquad (A.59)$$

where

$$n = 0,1,2...$$

The elliptic integrals can be written using this compact notation defined in Equations A.47 to A.53. Thus, Equations A.14, A.13, A.21, A.12, A.23, and A.20 become

$$\kappa = \left(\frac{T_{02}}{T_{03}}\right)^2 \qquad (A.60)$$

$$\kappa' = 4q'^{1/2} \left(\frac{T_{04}}{T_{03}} \right)^2 \tag{A.61}$$

$$K = \left(T_{03}\right)^2 \frac{(-\ln q')}{2} \tag{A.62}$$

$$K' = \frac{\pi}{2} \left(T_{03}\right)^2 \tag{A.63}$$

$$E_e = \frac{1}{\left(T_{03}\right)^2} \left\{ 1 - \left[s - \left(T_{03}\right)^4 \right] \left(- \frac{\ln q'}{2} \right) \right\} \tag{A.64}$$

$$E'_e = \frac{\pi}{2} \left[\frac{S}{\left(T_{03}\right)^2} \right] \tag{A.65}$$

where

$$S = 1 + 8q'^2 - 8q'^4 \tag{A.66}$$

These expressions (Equations A.54 to A.65) are the equations for the efficient calculation of cnoidal wave theory first presented by Isobe (1985). These equations are used in the numerical model described in this thesis.

A.2 A Table of Properties of Jacobian Elliptic Functions

The following table is based on a table from Isobe and Kraus (1983b, Appendix B). It is included here for easy reference.

Relations between squares of the elliptic functions:

$$sn^2\,\theta + cn^2\,\theta = 1 \tag{A.67}$$

$$\kappa^2\,sn^2\,\theta + dn^2\,\theta = 1 \tag{A.68}$$

Derivatives of the elliptic functions:

$$\frac{d}{d\theta}(sn\,\theta) = cn\,\theta\,dn\,\theta \tag{A.69}$$

$$\frac{d}{d\theta}(cn\,\theta) = -\,sn\,\theta\,dn\,\theta \tag{A.70}$$

$$\frac{d}{d\theta}(dn\,\theta) = -\kappa^2 sn\,\theta\,cn\,\theta \tag{A.71}$$

Derivatives of even powers of the cn function:

$$\frac{d^2}{d\theta^2}(cn^{2n}\,\theta) = \kappa^2\Big[2n(2n-1)\lambda cn^{2n-2}\,\theta + (2n)^2(1-\lambda)cn^{2n}\,\theta - 2n(2n+1)cn^{2n+2}\theta\Big] \tag{A.72}$$

$$\frac{d^2}{d\theta^2}(cn^2\,\theta) = \kappa^2\Big[2\lambda + 4(1-\lambda)cn^2\theta - 6cn^4\theta\Big] \tag{A.73}$$

$$\frac{d^2}{d\theta^2}(cn^4\theta) = \kappa^2\Big[12\lambda cn^2\theta + 16(1-\lambda)cn^4\theta - 20cn^6\theta\Big] \tag{A.74}$$

$$\frac{d^4}{d\theta^4}(cn^2\theta) = \kappa^4\Big[8\lambda(1-\lambda) + 8(2-13\lambda+2\lambda^2)cn^2\theta - 120(1-\lambda)cn^4\theta + 120cn^6\theta\Big] \tag{A.75}$$

where

$$\lambda = \frac{(1-\kappa^2)}{\kappa^2} \tag{A.76}$$

The derivations of the equations for the surface profile, η, (Chapter 2); the energy flux, F, and energy, E, (Appendix B) require the time-averaged values of even powers of the cn function. Since a cnoidal wave is periodic in both time and space, then

$$\overline{cn^m\theta} \equiv \frac{1}{T}\int_0^T cn^m\theta \, d\theta = \frac{1}{L}\int_0^L cn^m\theta \, d\theta \qquad (A.77)$$

From Figure 3.2, it can be seen, for $m = 2, 4, 6...$, that

$$\frac{1}{L}\int_0^L cn^m\theta \, d\theta = \frac{1}{K}\int_0^K cn^m\theta \, d\theta \qquad (A.78)$$

For second-order cnoidal wave theory, the calculation of three of these quantities (for $m = 2$, 4, and 6) is needed.

Integrals of even powers of the cn function:

$$\begin{aligned}\int_0^K cn^2\theta d\theta &= \int_0^{\pi/2} \frac{\cos^2\phi}{\sqrt{1-\kappa^2\sin^2\phi}}\, d\phi \\ &= \frac{1}{\kappa^2}\left[\int_0^{\pi/2} \frac{1-\kappa^2\sin^2\phi}{\sqrt{1-\kappa^2\sin^2\phi}}\, d\phi - \int_0^{\pi/2} \frac{1-\kappa^2}{\sqrt{1-\kappa^2\sin^2\phi}}\, d\phi\right] \\ &= \frac{1}{\kappa^2}E_e - \frac{1-\kappa^2}{\kappa^2}K \qquad (A.79)\end{aligned}$$

From Equation A.72,

$$\int_0^K cn^{2n+2}\,\theta\,d\theta = \frac{2n-1}{2n+1}\lambda\int_0^K cn^{2n-2}\,\theta\,d\theta$$

$$+ \frac{2n}{2n+1}(1-\lambda)\int_0^K cn^{2n}\,\theta\,\dot{d}\theta \qquad \text{(A.80)}$$

Finally,

$$\overline{c_1} = \overline{cn^2\theta} = \frac{1}{K}\int_0^K cn^2\,\theta\,d\theta = -\lambda + \mu \qquad \text{(A.81)}$$

$$\overline{c_2} = \overline{cn^4\theta} = \frac{1}{K}\int_0^K cn^4\theta\,d\theta = \frac{1}{3}(-\lambda + 2\mu + 2\lambda^2 - 2\lambda\mu) \qquad \text{(A.82)}$$

$$\overline{c_3} = \overline{cn^6\theta} = \frac{1}{K}\int_0^K cn^6\,\theta\,d\theta = \frac{1}{15}(-4\lambda + 8\mu - 7\lambda\mu + 3\lambda^2 + 8\lambda^2\mu - 8\lambda^3) \qquad \text{(A.83)}$$

where

$$\mu = \frac{E_e}{\kappa^2 K} \qquad \text{(A.84)}$$

APPENDIX B

DERIVATION OF EXPRESSIONS FOR ENERGY FLUX, ENERGY, AND GROUP VELOCITY FOR SECOND-ORDER CNOIDAL WAVES

This appendix contains the derivation of energy-related expressions needed for the calculation of shoaling and refraction of second-order cnoidal waves. Corresponding results for first-order cnoidal waves are derived in the process. Section B.1 contains a derivation of an expression for energy flux of second-order cnoidal waves. Section B.2 contains a derivation of an expression for the average energy per unit surface area of second-order cnoidal waves. Finally, in Section B.3 the derivations of the first two sections are used to derive an expression for the group velocity of second-order cnoidal waves.

B.1 Energy Flux of Second-Order Cnoidal Waves

From Phillips (1977, p. 63), the average energy flux, F, in the direction of wave propagation, per unit surface area, is

$$F = \rho \overline{\int_{-D}^{\eta} u \left[\frac{1}{2} (u^2 + w^2) + gz + \frac{p}{\rho} \right] dz} \qquad (B.1)$$

The overbar denotes averaging over wavelength as in Appendix A (Equation A.77). Note that energy flux is a vector quantity, but since F is defined in the direction of wave propagation, the vector notation has been omitted for convenience. Direct evaluation of this equation using second-order cnoidal wave expressions for the variables would be tedious. However, a less complicated expression for F can be derived (Isobe and Horikawa, 1982). Using the Bernoulli equation for unsteady motion,

$$\frac{p}{\rho} + \frac{1}{2}(u^2 + w^2) + gz - \phi_t = \frac{p_B}{\rho} \tag{B.2}$$

Equation B.1 becomes

$$F = \rho \overline{\int_{-D}^{\eta} u\left(\phi_t + \frac{p_B}{\rho}\right) dz} \tag{B.3}$$

For waves of permanent form, the horizontal wave particle orbital speed, u, can be expressed as

$$u = u(x - Ct, z) \tag{B.4}$$

Since $u = \frac{\partial \phi}{\partial x}$ and $w = \frac{\partial \phi}{\partial z}$, the most general expression for the velocity potential, ϕ, is

$$\begin{aligned} \phi &= \phi(x - Ct, z) + f(t) \\ &= \phi(X, z) + f(t) \end{aligned} \tag{B.5}$$

where $X = x - Ct$.

Evaluating the time derivitive of ϕ, using

$$\begin{aligned} \phi_t &= \phi_X X_t + f_t \\ &= -C\phi_X + f_t \end{aligned} \tag{B.6}$$

and

$$\begin{aligned} \phi_x &= \phi_X X_x \\ &= \phi_X \end{aligned} \tag{B.7}$$

it can be seen that

$$\phi_t = Cu + f_t \tag{B.8}$$

Sustituting Equation B.8 into Equation B.3 yields

$$F = \rho \overline{\int_{-D}^{\eta} u\left(Cu + \frac{p_B}{\rho} + f_t\right) dz} \tag{B.9}$$

It can be shown that $f(t)$ can be chosen such that the Bernoulli constant, p_B/ρ, vanishes and such that f_t is not a function of t (see, eg., Isobe and Kraus, 1983b, Appendix C). Therefore, since Stokes' second definition of wave celerity (Equation 2.21) was used to derive the second-order cnoidal wave expressions (Chapter II), Equation B.9 simplifies to

$$F = \rho C \overline{\int_{-D}^{\eta} u^2 \, dz} \tag{B.10}$$

For use in the numerical model, this equation must be expressed in terms of the second-order cnoidal wave theory presented in Chapter II. The power series expansion of F, based on the perturbation parameter, $\varepsilon = H/D$ (Equation 2.44), will be developed. The expression for F will include the first two terms of the perturbation power series. In the course of the derivation, these two approximations will, at first, appear to be $O(\varepsilon^2)$ and $O(\varepsilon^3)$. However, the final form of the equation for F will show these first two approximations to be $O(1)$ and $O(\varepsilon)$. The third contribution to the power series of F (coefficients of ε^2) is not included because the third approximation is not complete for a second-order theory. This point will be illustrated during the derivation.

Repeating Equation 2.67, u can be expressed as

$$u = \sqrt{gD} \left[B_{00} + B_{10}c_1 + B_{20}c_2 - \frac{1}{2}\left(\frac{z + D}{D}\right)^2 (B_{01} + B_{11}c_1 + B_{21}c_2) \right] \tag{B.11}$$

The terms in this equation must be expanded and grouped into factors of a common power of ε. From Equations 2.75 to 2.80, Equation B.11 becomes

$$u = \sqrt{gD}\left[\varepsilon b_1 + \varepsilon^2 b_2 + \left(\varepsilon + \varepsilon^2 b_3\right) c_1 + \varepsilon^2 b_4 c_2 - \frac{1}{2}\left(\frac{z + D}{D}\right)^2 \left(\varepsilon^2 b_5 + \varepsilon^2 b_6 c_1 + \varepsilon^2 b_7 c_2\right)\right]$$

$$= \sqrt{gD}\left[\varepsilon(b_1 + c_1) + \varepsilon^2(b_2 + b_3 c_1 + b_4 c_2) - \frac{1}{2}\left(\frac{z + D}{D}\right)^2 \varepsilon^2(b_5 + b_6 c_1 + b_7 c_2)\right] \quad \text{(B.12)}$$

where

$$b_1 = \lambda - \mu \quad \text{(B.13)}$$

$$b_2 = \frac{1}{4}(\lambda - \mu - 2\lambda^2 + 2\mu^2) \quad \text{(B.14)}$$

$$b_3 = \frac{1}{4}(1 - 6\lambda + 2\mu) \quad \text{(B.15)}$$

$$b_4 = -1 \quad \text{(B.16)}$$

$$b_5 = \frac{3\lambda}{2} \quad \text{(B.17)}$$

$$b_6 = 3 - 3\lambda \quad \text{(B.18)}$$

$$b_7 = -\frac{9}{2} \quad \text{(B.19)}$$

Before making substitutions to write Equation B.12 in a more compact form, it will improve the clarity of the following manipulations to examine the variables in Equation B.12. The only z dependency is contained in the (z+D)/D term. The only terms which vary with wavelength are c_1 and c_2. The variables H and D are assumed not to vary over

wavelength as a basic assumption in the derivation of waves of permanent form in Chapter II. The b's, functions of elliptic functions (and, therefore, the Ursell parameter), are constant over both depth and wavelength.

Rewriting Equation B.12 in a more compact form results in

$$u = \sqrt{gD}\left[\varepsilon U_1 + \varepsilon^2\left(U_2 - \frac{1}{2}\,Y^2\,U_3\right)\right] \tag{B.20}$$

where

$$U_1 = b_1 + c_1 \tag{B.21}$$

$$U_2 = b_2 + b_3c_1 + b_4c_2 \tag{B.22}$$

$$U_3 = b_5 + b_6c_1 + b_7c_2 \tag{B.23}$$

$$Y = \frac{z + D}{D} \tag{B.24}$$

Squaring u and gathering coefficients of like powers of ε yields

$$u^2 = gD\left[\varepsilon^2U_1^2 + \varepsilon^3\left(2U_1U_2 - U_1U_3\,Y^2\right) + \varepsilon^4\left(U_2^2 - U_2U_3\,Y^2 + \frac{1}{4}\,U_3^2\,Y^4\right)\right] \tag{B.25}$$

Referring back to Equation B.10, u^2 must now be integrated over depth and then averaged over wavelength. The resulting equation

$$\overline{\int_{-D}^{\eta} u^2\,dz} = gD\left[\overline{\int_{-D}^{\eta} \varepsilon^2\,U_1^2\,dz} + \overline{\int_{-D}^{\eta} \varepsilon^3\left(2U_1\,U_2 - U_1\,U_3\,Y^2\right)dz} + \overline{\int_{-D}^{\eta} \varepsilon^4\left(U_2^2 - U_2\,U_3\,Y^2 + \frac{1}{4}\,U_3^2\,Y^4\right)dz}\right] \tag{B.26}$$

can be simplified to

$$\overline{\int_{-D}^{\eta} u^2 \, dz} = gD\left(\varepsilon^2 \langle \overline{u_1^2} \rangle + \varepsilon^3 \langle \overline{u_2^2} \rangle + \varepsilon^4 \langle \overline{u_3^2} \rangle\right) \qquad (B.27)$$

The three integrals on the right-hand side of Equation B.26 are represented by $\langle \overline{u_1^2} \rangle$, $\langle \overline{u_2^2} \rangle$, and $\langle \overline{u_3^2} \rangle$, respectively. The symbols, $\langle\ \rangle$ are used to denote integration over depth, from -D to η.

From Equation B.10, it is seen that Equation B.27 must be multiplied by ρC . The expression for wave celerity, C, repeated from Equation 2.65, is

$$C = \sqrt{gD}\left(C_0 + \varepsilon C_1 + \varepsilon^2 C_2\right) \qquad (B.28)$$

Now, using Equations B.27 and B.28, B.10 can be written

$$\frac{F}{\rho g D \sqrt{gD}} = \varepsilon^2 C_o \langle \overline{u_1^2} \rangle + \varepsilon^3\left(C_o \langle \overline{u_2^2} \rangle + C_1 \langle \overline{u_1^2} \rangle\right)$$

$$+ \varepsilon^4\left(C_o \langle \overline{u_3^2} \rangle + C_1 \langle \overline{u_2^2} \rangle + C_2 \langle \overline{u_1^2} \rangle\right) + \text{HOT} \qquad (B.29)$$

As was previously mentioned, only the first two terms of Equation B.29 are complete for a second-order theory. This can be seen by studying the equation for u (Equation B.12). A third-order theory would contribute terms to this equation which are coefficients of ε^3 . For u^2, the lowest terms unique to the third-order theory would be at the ε^4 level ($\varepsilon^3 \times \varepsilon^1$) . Therefore, the coefficient of ε^4 in Equation B.29 is not complete for a second-order theory. Keeping only the complete orders, Equation B.29 is rewritten as

$$\frac{F}{\rho g D \sqrt{gD}} = \varepsilon^2 C_0 \langle \overline{u_1^2} \rangle + \varepsilon^3 \left(C_0 \langle \overline{u_2^2} \rangle + C_1 \langle \overline{u_1^2} \rangle \right) + HOT \qquad (B.30)$$

Although it appears that only two orders remain in Equation B.30 [coefficients of $O(\varepsilon^2)$ and $O(\varepsilon^3)$], this is not the case. Both $\langle \overline{u_1^2} \rangle$ and $\langle \overline{u_2^2} \rangle$ are expressed as power series of ε . Therefore, to maintain only two levels of approximation in the evaluation of Equation B.30, it is necessary to truncate the contributions of $\langle \overline{u_1^2} \rangle$ and $\langle \overline{u_2^2} \rangle$. For the coefficient of ε^2 in Equation B.30, only the lowest two orders, [O(1) and $O(\varepsilon)$], of $\langle \overline{u_1^2} \rangle$ will be allowed. For the coefficient of ε^3 only the lowest order, [O(1)], of both $\langle \overline{u_1^2} \rangle$ and $\langle \overline{u_2^2} \rangle$ will be allowed.

From Equations B.27, B.26, and B.21 $\langle \overline{u_1^2} \rangle$ can be written as

$$\langle \overline{u_1^2} \rangle = \overline{\int_{-D}^{\eta} (b_1 + c_1)^2 \, dz}$$

$$= \overline{\int_{-D}^{\eta} b_1^2 + 2b_1c_1 + c_1^2 \, dz} \qquad (B.31)$$

Since there is no z dependency in this equation, the depth integration is easily accomplished. The result of the depth integration of $\langle \overline{u_1^2} \rangle$ is

$$\langle \overline{u_1^2} \rangle = \left(b_1^2 + 2b_1c_1 + c_1^2 \right) (\eta + D) \qquad (B.32)$$

An expression for η is needed to evaluate this equation. From Equation 2.66, η can be written as

$$\eta = D \left[\varepsilon (a_1 + c_1) + \varepsilon^2 (a_2 + a_3c_1 + a_4c_2) \right] \qquad (B.33)$$

where

$$a_1 = \lambda - \mu \tag{B.34}$$

$$a_2 = \frac{1}{4}(-2\lambda + \mu - 2\lambda^2 + 2\lambda\mu) \tag{B.35}$$

$$a_3 = -\frac{3}{4} \tag{B.36}$$

$$a_4 = \frac{3}{4} \tag{B.37}$$

The only terms which vary over wavelength are c_1 and c_2; noting from Equation A.81 to A.83 that $c_2 = c_1^2$ and $c_1 c_2 = c_3 = c_1^3$, then Equation B.32 becomes

$$\langle \overline{u_1^2} \rangle = D\left[b_1^2 + 2b_1\overline{c_1} + \overline{c_1^2} + \varepsilon\left(a_1 b_1^2 + 2a_1 b_1 \overline{c_1} + a_1\overline{c_1^2} + b_1^2\overline{c_1} + 2b_1\overline{c_1^2} + \overline{c_1^3}\right)\right] + \text{HOT} \tag{B.38}$$

Evaluating $\langle \overline{u_2^2} \rangle$ is more complicated than the evaluation of $\langle \overline{u_1^2} \rangle$ because $\langle \overline{u_2^2} \rangle$ has Y-terms, which are functions of depth. From Equations B.27, B.26, and B.21 to B.23, $\langle \overline{u_2^2} \rangle$ can be written as

$$\langle \overline{u_2^2} \rangle = \overline{\int_{-D}^{\eta} \left[2(b_1 + c_1)(b_2 + b_3 c_1 + b_4 c_2) - (b_1 + c_1)(b_5 + b_6 c_1 + b_7 c_2)\left(\frac{z + D}{D}\right)^2\right] dz} \tag{B.39}$$

Carrying out the depth integration yields

$$\langle \overline{u_2^2} \rangle = \overline{2(b_1 + c_1)(b_2 + b_3 c_1 + b_4 c_2)(\eta + D) - (b_1 + c_1)(b_5 + b_6 c_1 + b_7 c_2)\left(\eta + \frac{D}{3}\right)} + \text{HOT} \tag{B.40}$$

This equation can be simplified by neglecting higher-order contributions. Since $\langle \overline{U_2^2} \rangle$ is included only in the term representing the second approximation of F (Equation B.30), only terms of O(1) in $\langle \overline{U_2^2} \rangle$ will survive in the final expression for F. Inspecting the equation for η (Equation B.33), it can be seen that multiplication by η in Equation B.40 will increase the order of the result. The terms resulting from the multiplication of η are of higher order and are dropped, and Equation B.40 becomes

$$\langle \overline{u_2^2} \rangle = \overline{2\,(b_1 + c_1)\,(b_2 + b_3 c_1 + b_4 c_2)\,D} - \overline{(b_1 + c_1)\,(b_5 + b_6 c_1 + b_7 c_2)\,\frac{D}{3}} \qquad \text{(B.41)}$$

carrying out the multiplication this equation becomes

$$\langle \overline{u_2^2} \rangle = 2D\left(b_1 b_2 + b_1 b_3 \overline{c_1} + b_1 b_4 \overline{c_1^2} + b_2 \overline{c_1} + b_3 \overline{c_1^2} + b_4 \overline{c_1^3} \right) - \frac{D}{3}\left(b_1 b_5 + b_1 b_6 \overline{c_1} + b_1 b_7 \overline{c_1^2} + b_5 \overline{c_1} + b_6 \overline{c_1^2} + b_7 \overline{c_1^3} \right) \qquad \text{(B.42)}$$

Finally, all of the terms in the expression for F (Equation B.30) are ready to be assembled. Substituting Equations B.38 and B.42 into B.30 gives

$$\begin{aligned} \frac{F}{\rho g D \sqrt{gD}} &= C_0 D \epsilon^2 \left(b_1^2 + 2 b_1 \overline{c_1} + \overline{c_1^2} \right) \\ &+ \epsilon^3 \Big[C_0 D \left(a_1 b_1^2 + 2 a_1 b_1 \overline{c_1} + a_1 \overline{c_1^2} + b_1^2 \overline{c_1} + 2 b_1 \overline{c_1^2} + \overline{c_1^3} \right) \\ &+ 2 D C_0 \left(b_1 b_2 + b_1 b_3 \overline{c_1} + b_1 b_4 \overline{c_1^2} + b_2 \overline{c_1} + b_3 \overline{c_1^2} + b_4 \overline{c_1^3} \right) \\ &- \frac{D}{3} C_0 \left(b_1 b_5 + b_1 b_6 \overline{c_1} + b_1 b_7 \overline{c_1^2} + b_5 \overline{c_1} + b_6 \overline{c_1^2} + b_7 \overline{c_1^3} \right) \\ &+ C_1 D \left(b_1^2 + 2 b_1 \overline{c_1} + \overline{c_1^2} \right) \Big] \end{aligned} \qquad \text{(B.43)}$$

For use in the numerical model, this expression for F is put in terms of λ and μ . Substituting Equations B.34, B.13 to B.19 , A.81 to A.83, and 2.65 into Equation B.43 yields

$$\frac{F}{\rho g D^2 \sqrt{gD}} = \varepsilon^2 \left(-\lambda + 2\mu + 4\lambda\mu - \lambda^2 - 3\mu^2\right) \frac{1}{3}$$
$$+ \varepsilon^3 \left(-4\lambda + 8\mu + 53\lambda\mu - 12\lambda^2 - 60\mu^2\right.$$
$$\left. + 53\lambda^2\mu - 120\lambda\mu^2 - 8\lambda^3 + 75\mu^3\right) \frac{1}{30} \qquad \text{(B.44)}$$

The apparent order of this equation can be reduced by using the following relationship based on the definition of ε (Equation 2.44)

$$H^2 = D^2\varepsilon^2 \qquad \text{(B.45)}$$

Substituting this equation into Equation B.44 results in the final expression for F. The energy flux for first-order cnoidal wave theory is proportional to F_0; whereas, the εF term is the contribution for second-order cnoidal wave theory.

$$F = H^2 \rho g \sqrt{gD} \left(F_0 + \varepsilon F_1\right)$$
$$= H^2 \rho g \sqrt{gD} \left(-\lambda + 2\mu + 4\lambda\mu - \lambda^2 - 3\mu^2\right) \frac{1}{3}$$
$$+ \varepsilon \left(-4\lambda + 8\mu + 53\lambda\mu - 12\lambda^2 - 60\mu^2\right.$$
$$\left. + 53\lambda^2\mu - 120\lambda\mu^2 - 8\lambda^3 + 75\mu^3\right) \frac{1}{30} \qquad \text{(B.46)}$$

B.2 Energy of Second-Order Cnoidal Waves

The average wave energy per unit surface area, E, can be expressed as the sum of the average potential energy, E_p , and the average kinetic energy, E_k .

$$E = E_k + E_p \tag{B.47}$$

The two contributions in this equation will be evaluated in the next two sections.

B.2.1 Kinetic Energy

The equation for average kinetic energy per unit surface area is

$$E_k = \frac{\rho}{2} \overline{\int_{-D}^{\eta} u^2 \, dz} + \overline{\int_{-D}^{\eta} w^2 \, dz} \tag{B.48}$$

The quantities necessary for expressing the first integral in this equation were developed in the previous section. From Equation B.27, the depth integration of u^2 averaged over wavelength is

$$\overline{\int_{-D}^{\eta} u^2 \, dz} = gD \left(\varepsilon^2 \langle \overline{u_1^2} \rangle + \varepsilon^3 \langle \overline{u_2^2} \rangle \right) + HOT \tag{B.49}$$

As is the case for the derivation of F, E will be expressed up to and including the second approximation. Equation B.30 shows that $\langle \overline{u_1^2} \rangle$ will contain terms of O(1) and O(ε) and $\langle \overline{u_2^2} \rangle$ will contain terms of O(1).

Assembling these contributions from Equation B.38 and B.42 and inserting them into Equation B.49 results in

$$\overline{\int_{-D}^{\eta} u^2\,dz} = gD^2\Big\{\varepsilon^2\left(b_1^2 + 2b_1\overline{c_1} + \overline{c_1^2}\right) + \varepsilon^3\Big[a_1b_1^2 + 2a_1b_1\overline{c_1} + a_1\overline{c_1^2} + b_1^2\overline{c_1} + 2b_1\overline{c_1^2} + \overline{c_1^3} + 2\left(b_1b_2 + b_1b_3\overline{c_1} + b_1b_4\overline{c_1^2} + b_2\overline{c_1} + b_3\overline{c_1^2} + b_4\overline{c_1^3}\right) - \frac{1}{3}\left(b_1b_5 + b_1b_6\overline{c_1} + b_1b_7\overline{c_1^2} + b_5\overline{c_1} + b_6\overline{c_1^2} + b_7\overline{c_1^3}\right)\Big]\Big\} \quad (B.50)$$

Expressing this equation in terms of λ and μ and using Equation B.45 yields

$$\overline{\int_{-D}^{\eta} u^2\,dz} = gH^2\left[\frac{1}{3}\left(-\lambda + 2\mu + 4\lambda\mu - \lambda^2 - 3\mu^2\right) + \varepsilon\left(\lambda - 2\mu - 2\lambda\mu + 3\lambda^2 - 15\mu^2 - 2\lambda^2\mu - 30\lambda\mu^2 + 2\lambda^3 + 30\mu^3\right)\frac{1}{30}\right] \quad (B.51)$$

The second integral of Equation B.48 will require an evaluation similar to the evaluation of u^2 given in the derivation of F. Repeating Equation 2.68, the vertical water particle orbital speed, w, is given as

$$w = \sqrt{gD}\,4K\,\frac{D}{L}\,\mathrm{csd}\left[\left(\frac{z+D}{D}\right)\left(B_{10} + 2B_{20}c_1\right) - \frac{1}{6}\left(\frac{z+D}{D}\right)^3\left(B_{11} + 2B_{21}c_1\right)\right] \quad (B.52)$$

From Equations 2.76 to 2.80, B.13 to B.19, and B.24, Equation B.52 becomes

$$w = \sqrt{gD}\,4K\,\frac{D}{L}\,\mathrm{csd}\left\{\varepsilon Y + \varepsilon^2\left[Y\left(b_3 + 2b_4c_1\right) - \frac{1}{6}\,Y^3\left(b_6 + 2b_7c_1\right)\right]\right\} \quad (B.53)$$

This equation written in more compact form is

$$w = \sqrt{gD}\ 4K\ \frac{D}{L}\ \mathrm{csd}\left[\varepsilon Y + \varepsilon^2\left(YW_1 - \frac{1}{6}\ Y^3W_2\right)\right] \tag{B.54}$$

where

$$W_1 = b_3 + 2b_4c_1 \tag{B.55}$$

$$W_2 + b_6 + 2b_7c_1 \tag{B.56}$$

Squaring w and gathering coefficients of like powers of ε results in

$$w^2 = gD\ 16K^2\left(\frac{D}{L}\right)^2\ (\mathrm{csd})^2\left[\varepsilon^2Y^2 + \varepsilon^3 2Y\left(YW_1 - \frac{1}{6}\ Y^3W_2\right) + \varepsilon^4\left(YW_1 - \frac{1}{6}\ Y^3W_2\right)^2\right] \tag{B.57}$$

Equation B.57 must be integrated over depth and then averaged over wavelength. The resulting equation

$$\overline{\int_{-D}^{\eta} w^2\,dz} = gD\ 16K^2\ \left(\frac{D}{L}\right)^2\ \overline{(\mathrm{csd})^2}\left[\varepsilon^2\ \overline{\int_{-D}^{\eta} Y^2\,dz} + \varepsilon^3\ \overline{\int_{-D}^{\eta} 2Y\left(YW_1 - \frac{Y}{6}\ W_2\right)dz} + \varepsilon^4\ \overline{\int_{-D}^{\eta}\left(YW_1 - \frac{Y^3}{6}\ W_2\right)^2 dz}\right] \tag{B.58}$$

can be simplified to

$$\overline{\int_{-D}^{\eta} w^2\,dz} = gD\ 16K^2\left(\frac{D}{L}\right)^2\ \overline{(\mathrm{csd})^2}\left(\varepsilon^2\ \langle\overline{w_1^2}\rangle + \varepsilon^3\ \langle\overline{w_2^2}\rangle + \varepsilon^4\ \langle\overline{w_3^2}\rangle\right) \tag{B.59}$$

where the three integrals on the right-hand side of Equation B.58 are represented by $\langle\overline{w_1^2}\rangle$, $\langle\overline{w_2^2}\rangle$, and $\langle\overline{w_3^2}\rangle$.

Just as $\langle\overline{u_3^2}\rangle$ contributed only higher-order terms to F, $\langle\overline{w_3^2}\rangle$ contributes only higher-order terms to E_k. Futhermore, because of the term $(D/L)^2$ in Equation B.59, it will be shown that only $\langle\overline{w_1^2}\rangle$ will contain terms of sufficiently low order to contribute to E_k. From Equations 2.23 and 2.44 (U & ε), the following equation relates the Ursell parameter and the perturbation parameter.

$$\left(\frac{D}{L}\right)^2 = \frac{\varepsilon}{U} \tag{B.60}$$

Since the smallest value of U for which cnoidal wave theory is valid is approximately 10, $(D/L)^2 < \varepsilon$. This implies that $(D/L)^2$ contains a "hidden" ε, which will increase the order of Equation B.59. Substituting Equation 2.85 (dispersion relation) into Equation B.60 results in

$$\left(\frac{D}{L}\right)^2 = \frac{3}{16}\frac{1}{\kappa^2 K^2}\varepsilon + O(\varepsilon^2) \tag{B.61}$$

This expression is substituted into Equation B.59 resulting in Equation B.62.

$$\overline{\int_{-D}^{\eta} w^2\,dz} = gD\ 16K^2\frac{3}{16}\frac{1}{\kappa^2K^2}\overline{(csd)^2}\left(\varepsilon^3\langle\overline{w_1^2}\rangle + \varepsilon^4\langle\overline{w_2^2}\rangle + \varepsilon^5\langle\overline{w_3^2}\rangle\right) \tag{B.62}$$

Note that Equation B.62 is one order higher than Equation B.27, the

corresponding equation for the u^2 component of E_k. Maintaining a consistent contribution from both components requires that only the lowest order of Equation B.62 remain. Thus Equation B.62 becomes

$$\overline{\int_{-D}^{\eta} w^2 \, dz} = \frac{3gD}{\kappa^2} \overline{(csd)^2} \, \varepsilon^3 \, \langle \overline{w_1^2} \rangle \tag{B.63}$$

Therefore, only the lowest order term of $\langle \overline{w_1^2} \rangle$ will be represented. Referring to Equations B.24, B.59 and B.58, $\langle \overline{w_1^2} \rangle$ can be expressed as

$$\langle \overline{w_1^2} \rangle = \overline{\int_{-D}^{\eta} Y^2 \, dz}$$

$$= \frac{D}{3} + HOT \tag{B.64}$$

Substituting this equation into Equation B.63 yields

$$\overline{\int_{-D}^{\eta} w^2 \, dz} = \frac{gD^2}{\kappa^2} \overline{(csd)^2} \, \varepsilon^3 \tag{B.65}$$

Using Equation B.45, Equation B.65 can be written as

$$\overline{\int_{-D}^{\eta} w^2 \, dz} = H^2 \frac{g}{\kappa^2} \overline{(csd)^2} \, \varepsilon \tag{B.66}$$

Recall (from Equation 2.84) that the definition for csd is

$$csd = cn \, \theta \, sn \, \theta \, dn \, \theta \tag{B.67}$$

where, cn, sn, and dn are Jacobian elliptic functions and θ is defined

in Equation 4.2. These functions do not depend on z, but they are a function of x. Therefore, they must be averaged over wavelength. After squaring Equation B.67, the result can be expressed in quantities for which the average over wavelength is known. Using the following two identities repeated here from Equations A.67 and A.68.

$$sn^2\theta + cn^2\theta = 1 \tag{B.68}$$

$$\kappa^2 sn^2\theta + dn^2\theta = 1 \tag{B.69}$$

the square of Equation B.67 can be expressed as

$$\begin{aligned}(csd)^2 &= cn^2\theta - \kappa^2 cn^2\theta + 2\kappa^2 cn^4\theta - cn^4\theta - \kappa^2 cn^6\theta \\ &= c_1 - \kappa^2 c_1 + 2\kappa^2 c_2 - c_2 - \kappa^2 c_3 \end{aligned} \tag{B.70}$$

Substituting this equation into Equation B.66 yields

$$\overline{\int_{-D}^{\eta} w^2\, dz} = gH^2\left(\frac{\overline{c_1}}{\kappa^2} - \overline{c_1} + 2\overline{c_2} - \frac{\overline{c_2}}{\kappa^2} - \overline{c_3}\right)\epsilon \tag{B.71}$$

The definition of λ (rewritten from Equation 2.70)

$$\lambda = \frac{1 - \kappa^2}{\kappa^2} \tag{B.72}$$

can be used to simplify the terms of the above equation which have a κ^2 in the denominator

$$\frac{\overline{c_1}}{\kappa^2} = \lambda\overline{c_1} + \overline{c_1} \tag{B.73}$$

$$\frac{\overline{c_2}}{\kappa^2} = \lambda\overline{c_2} + \overline{c_2} \tag{B.74}$$

resulting in

$$\overline{\int_{-D}^{\eta} w^2\, dz} = gH^2\left(\lambda\overline{c_1} + \overline{c_2} - \lambda\overline{c_2} - \overline{c_3}\right)\epsilon \tag{B.75}$$

This equation is put in terms of λ and μ using Equations A.81 to A.83.

$$\overline{\int_{-D}^{\eta} w^2\, dz} = gH^2\,\frac{1}{15}\left(-\lambda + 2\mu + 2\lambda\mu - 3\lambda^2 + 2\lambda^2\mu - 2\lambda^3\right)\epsilon \tag{B.76}$$

Assembling the two components of E_k (Equations B.51 and B.76) results in Equation B.77, the average kinetic energy per unit surface area of a second-order cnoidal wave.

$$\begin{aligned} E_k &= \frac{\rho}{2}\,\overline{\int_{-D}^{\eta} w^2\, dz} + \overline{\int_{-D}^{\eta} w^2\, dz} \\ &= \rho g H^2\left[\frac{1}{6}\left(-\lambda + 2\mu + 4\lambda\mu - \lambda^2 - 3\mu^2\right)\right. \\ &\quad + \epsilon\left(-\lambda + 2\lambda\mu + 2\mu - 3\lambda^2 - 15\mu^2\right. \\ &\qquad \left.\left. + 2\lambda^2\mu - 30\,\lambda\mu^2 - 2\lambda^3 + 30\mu^3\right)\frac{1}{60}\right] \end{aligned} \tag{B.77}$$

B.2.2 Potential Energy of Second-Order Cnoidal Waves

The average potential energy per unit surface area is

$$E_p^* = \rho g\,\overline{\int_{-D}^{\eta} z\, dz} \tag{B.78}$$

The depth integration of this equation results in two terms.

$$E_p^* = \frac{1}{2}\rho g\overline{\eta^2} + \frac{1}{2}\rho g D^2 \tag{B.79}$$

The second term in this equation represents the potential energy of the still water column. Since we are interested in the portion of the potential energy due to the waves, only the first term of the above equation will be evaluated. Therefore, the potential energy per unit surface area due to waves is

$$E_p = \frac{1}{2}\rho g\overline{\eta^2} \tag{B.80}$$

Squaring η (Equation B.33) and keeping only the first two approximations results in

$$\eta^2 = D^2\left[\left(a_1^2 + 2a_1\overline{c_1} + \overline{c_1^2}\right)\varepsilon^2 + 2\left(a_1a_2 + a_1a_3\overline{c_1} + a_1a_4\overline{c_1^2} + a_2\overline{c_1} + a_3\overline{c_1^2} + a_4\overline{c_1^3}\right)\varepsilon^3\right] + \text{HOT} \tag{B.81}$$

Making use of Equations B.45, B.34 to B.37, and A.81 to A.83, Equation B.80 becomes

$$E_p = \rho g H^2\left[\frac{1}{6}\left(-\lambda + 2\mu + 4\lambda\mu - \lambda^2 - 3\mu^2\right) + \varepsilon\left(\lambda - 2\mu - 12\lambda\mu + 3\lambda^2 + 5\mu^2 - 12\lambda^2\mu + 10\lambda\mu^2 + 2\lambda^3\right)\frac{1}{20}\right] \tag{B.82}$$

B.2.3 Expression for Energy of Second-Order Cnoidal Waves

Combining E_k (Equation B.77) and E_p (Equation B.82) results in Equation B.83, the equation for the average wave energy per unit surface area.

As for F, the contribution for first-order wave cnoidal theory is proportional to E_0, and the contribution for second-order cnoidal wave theory is proportional to εE_1.

$$E = \rho g H^2 (E_0 + \varepsilon E_1)$$

$$= \rho g H^2 \left[\frac{1}{3} \left(- \lambda + 2\mu + 4\lambda\mu - \lambda^2 - 3\mu^2 \right) \right.$$

$$\left. + \varepsilon \left(\lambda - 2\mu - 17\lambda\mu + 3\lambda^2 - 17\lambda^2\mu + 2\lambda^3 + 15\mu^3 \right) \frac{1}{30} \right] \qquad \text{(B.83)}$$

B.3 Group Velocity of Second-Order Cnoidal Waves

The velocity of wave energy propagation; the group velocity, C_g, is defined (Phillips, 1977, p. 25) as

$$C_g \equiv \frac{F}{E} \qquad \text{(B.84)}$$

Using the results for F and E developed above (Equations B.46 and B.83), Equation B.84 becomes

$$C_g = \frac{\rho g H^2 \sqrt{gD} (F_0 + \varepsilon F_1)}{\rho g H^2 (E_0 + \varepsilon E_1)} \qquad \text{(B.85)}$$

The following algebraic manipulations on Equation B.85 will lead to a simplified form for C_g.

$$C_g = \sqrt{gD}\left(\frac{F_0 + \varepsilon F_1}{E_0 + \varepsilon E_1}\right)$$

$$= \frac{\sqrt{gD}}{E_0}\left(\frac{F_0 + \varepsilon F_1}{1 + \varepsilon \frac{E_1}{E_0}}\right)$$

$$= \frac{\sqrt{gD}}{E_0}\left(\frac{F_0 + \varepsilon F_1}{1 + \varepsilon \frac{E_1}{E_0}}\right)\left(\frac{1 - \varepsilon \frac{E_1}{E_0}}{1 - \varepsilon \frac{E_1}{E_0}}\right)$$

$$= \frac{\sqrt{gD}}{E_0}\left[\frac{F_0 + \varepsilon\left(F_1 - F_0 \frac{E_1}{E_0}\right) - \varepsilon^2 F_1 \frac{E_1}{E_0}}{1 + \varepsilon\left(\frac{E_1}{E_0} - \frac{E_1}{E_0}\right) - \varepsilon^2\left(\frac{E_1}{E_0}\right)^2}\right]$$

$$= \frac{\sqrt{gD}}{E_0}\left[\frac{F_0 + \varepsilon\left(F_1 - F_0 \frac{E_1}{E_0}\right)}{1}\right] + O(\varepsilon^2) \qquad \text{(B.86)}$$

From Equations B.46 and B.83,

$$E_0 = F_0 \qquad \text{(B.87)}$$

The final form for C_g is obtained by substituting Equation B.87 into B.86 yielding

$$C_g = \sqrt{gD}\left[1 + \varepsilon\left(\frac{F_1 - E_1}{E_0}\right)\right] \qquad \text{(B.88)}$$

Note from the expression for C, Equation B.28, that C and C_g, at the first approximation, are both equal to the shallow water wave speed of small-amplitude wave theory, $\sqrt{gD}$.

APPENDIX C

COMPUTER PROGRAM

```
      PROGRAM CNOIDAL

      PARAMETER (NX=110,NY=110,NZ=NX*NY)
      REAL LAM,MU,L,M
      COMMON /A1/ D(NY,NX), H(NY,NX), LAM(NY), MU(NY)
      COMMON /A2/ L(NY,NX), C(NY,NX), C0(NY), C1(NY), C2(NY),
     $            ALFA(NY,NX)
      COMMON /A3/ Q(NY,NX), U(NY,NX), DELQMAX(NX)
      COMMON /A4/ F(NY,NX), F0(NY), F1(NY), Eone(NY), Cg(NY,NX)
      COMMON /A5/ II,NI,JJ,NJ,IT,III
      COMMON /A6/ PI,DELHMAX,GAM,G,T,DXDY,A

      CHARACTER TITLE*20, ORDER*11, READDPT*3, READBC*3, BEACH*5,
     $          REDOF*3
      DIMENSION ITER(NX),LBP(NY)

C INNTIALIZE VARIABLES
      DATA Q/NZ*0.000000001/
      DATA PI /3.141592654/

C READ INPUT FILE
      OPEN (UNIT=1,NAME='INPUT.DAT',STATUS='OLD')
      READ(1,801) A,ALPHA,H0,T,G,RH0
      READ(1,801) DX,DY,SU,TOL
      READ(1,803) II,NI,JJ,NJ,IOUT,III
      READ(1,804) READDPT,BEACH,D1,B,M
      READ(1,805) READBC,NT
      DXDY = DX*DY
      GAM = RH0*G
      ALPHA = ALPHA*PI/180. + PI

C READ DEPTHS OR CALCULATE DEPTHS
C ADD DATUM CORRECTION (OR SURGE)
        IF(READDPT(1:3).EQ.'YES') THEN

          DO 5 I=1,NI
          READ(1,806) (D(J,I),J=1,NJ)
          DO 5 J=1,NJ
          D(J,I) = D(J,I) + SU
    5     CONTINUE

        ELSE

        RNY = FLOAT(NJ - JJ
        RNX = FLOAT(NI)
        PI2 = PI * 2.

          DO 6 I=1,NI
          RI = FLOAT(I
          DELX = RI * DX
          XX = RI   RNX

          DO 6 J=JJ,NJ
          RJ = FLOAT(J - JJ
          YY = RJ   RNY
          D(J,I) = SU + B + M*DELX    - D1*XX*COS(PI2*YY) + D1*XX
    6     CONTINUE

        ENDIF
```

```
C SET BOUNDARY CONDITIONS ON SEAWARD BOUNDARY.
      IF(READBC(1:3).EQ.'YES') THEN
      READ(1,955) (H(J,NI),J=JJ,NJ)
      READ(1,960) (ALFA(J,NI),J=JJ,NJ)
        DO 20 J=JJ,NJ
        ALFA(J,NI) = ALFA(J,NI) * PI/180. + PI
 20     CONTINUE
      ELSE
        DO 30 J=1,NJ
        ALFA(J,NI) = ALPHA
        H(J,NI) = HO
 30     CONTINUE
      ENDIF
      DO 12 J=JJ,NJ
      H(J,NI-1) = H(J,NI)
 12   CONTINUE

C CALCULATE ELLIPTIC QUANTITIES ON SEAWARD BOUNDARY.
      MM = 5
      CALL ELLIP(NI,MM)
C CALCULATE CELERITY AND WAVE LENGTH ON SEAWARD BOUNDARY.
      CALL LENGTH(NI)
C CALCULATE ENERGY FLUX ON SEAWARD BOUNDARY.
      NF = 0
      CALL EFLUX(NI,NF)
      NF = 1
C CALCULATE TRUE URSELL NUMBER ON BOUNDARY
      DO 50 J=JJ,NJ
      U(J,NI) = H(J,NI) * L(J,NI)**2 / D(J,NI)**3
 50   CONTINUE

C START OF LOOP TOWARD SHORE FROM BOUNDARY OR CONNECT POINT.
C LOOP ON ROWS OF CONSTANT I.
      DO 300 I=NI,II+1,-1
      IM = I-1

C ITERATION
        DO 200 IT=1,20
        ITER(IM)   = IT
        DELHMAX    = 0.0
        DELQMAX(IM) = 0.0

C CALCULATE ELLIPTIC QUANTITIES.
        MM = 2
        CALL ELLIP(IM,MM)
C CALCULATE CELERITY AND WAVE LENGTH.
        CALL LENGTH(IM)
C SOLVE FOR WAVE ANGLE
        CALL ANGLE(IM)
C CALCULATE WAVE HEIGHT
        CALL EFLUX(IM,NF)
C DO LATERAL BOUNDARIES
        ALFA(JJ,IM) = ALFA(JJ+1,IM)
        ALFA(NJ,IM) = ALFA(NJ-1,IM)
        F(JJ,IM)   = F(JJ+1,IM)
        F(NJ,IM)   = F(NJ-1,IM)
        H(JJ,IM)   = H(JJ+1,IM)
        H(NJ,IM)   = H(NJ-1,IM)

        IF(DELHMAX.LT.TOL) GOTO 201

 200    CONTINUE
 201  CONTINUE
```

```
C "BREAKING" CRITERION
C PLANE BEACH BREAKING CRITERION
          IF(BEACH(1:5).EQ.'PLANE') THEN

          HD = H(4,IM) / D(4,IM)
            IF(HD.GE.BREAK) THEN
            III = IM
            HDLAST = H(4,I) / D(4,I)
            HDDIFF = HD - HDLAST
            HD1 = (HD - BREAK) / HDDIFF
            HD2 = (BREAK - HDLAST) / HDDIFF
            H(4,IM) = HD1*H(4,I) + HD2*H(4,IM)
            D(4,IM) = HD1*D(4,I) + HD2*D(4,IM)
            ALFA(4,IM) = HD1*ALFA(4,I) + HD2*ALFA(4,IM)
            XB = FLOAT(IM) * DX + HD1 * DX
            GOTO 301
            ENDIF

          ELSE

C IRREGULAR BOTTOM
          HSTOP = 10
            DO 250 J=JJ,NJ
            HD = H(J,IM) / D(J,IM)
              IF(HD.GT.BREAK) THEN
              IF(IIII.EQ.10000) IIII = IM
              H(J,IM) = D(J,IM) * BREAK
              IF(LBP(J).EQ.0) LBP(J) = IM
              REDOF = 'YES'
              ENDIF
            HD = H(J,IM) / D(J,IM)
            HSTOP = AMIN1(HSTOP,HD)
  250       CONTINUE

            IF(HSTOP.GE.BREAK) THEN
            III = IM
            GO TO 301
            ENDIF

C IF HEIGHTS ARE TRUNCATED BY BREAKING CRITERION THEN RECALCULATE F.
            IF(REDOF(1:3).EQ.'YES') THEN
            CALL ELLIP(IM,MM)
            CALL LENGTH(IM)
            NF=0
            CALL EFLUX(IM,NF)
            NF=1
            ENDIF

          ENDIF

C SET WAVE HEIGHT ON NEXT I ROW TO HEIGHT AT CURRENT ROW IN
C PREPARATION FOR NEXT ITERATION
C ALSO CALCULATE TRUE URSELL NUMBER FOR OUTPUT.

        IMM = IM-1
          DO 275 J=JJ,NJ
          H(J,IMM) = H(J,IM)
          U(J,IM)  = H(J,IM) * L(J,IM)**2 / D(J,IM)**3
  275     CONTINUE

  300   CONTINUE
  301 CONTINUE
```

```
C       OUTPUT

        DO 325 I=II,NI
        DO 325 J=JJ,NJ
        ALFA(J,I) = (ALFA(J,I) - PI)*180./PI
  325   CONTINUE

      ALPHA = (ALPHA - PI)*180./PI

C SET WAVE HEIGHTS INSIDE BREAKING POINT TO ZERO FOR OUTPUT
        DO 400 I = 1,NI
        DO 400 J = JJ,NJ
          IF(LBP(J).GT.I) THEN
          H(J,I)     = 0.
          ALFA(J,I)  = 0.
          L(J,I)     = 0.
          Cg(J,I)    = 0.
          U(J,I)     = 0.
          ENDIF
  400   CONTINUE

        IF(A.EQ.0.0) THEN
        ORDER = 'CNOIDAL  I'
        ELSE IF(A.EQ.1.0) THEN
        ORDER = 'CNOIDAL II'
        ELSE
        ORDER = 'BONKERS'
        ENDIF

      WRITE(11,810) ORDER
      WRITE(11,815)
      WRITE(11,820) H0,T,ALPHA
      WRITE(11,825) DX,DY,TOL
      WRITE(11,830) SU,G,READBC
      WRITE(11,832) READDPT,B,M,D1,III,NI

      WRITE(11,815)
      WRITE(11,835) (ITER(I),I=II,NI)
      WRITE(11,815)
      WRITE(11,840) (DELQMAX(I),I=II,NI)
      WRITE(11,815)

        TITLE='WAVE HEIGHTS'
        CALL POUT(100.0,H,TITLE)

        TITLE='WAVE ANGLES '
        CALL POUT(10.0,ALFA,TITLE)

        IF(IOUT.GE.1) THEN
        TITLE='DEPTHS'
        CALL POUT(100.,D,TITLE)
        ENDIF

        IF(IOUT.GE.2) THEN
        TITLE='URSELL NUMBER'
        CALL POUT(1.0,U,TITLE)
        ENDIF

        IF(IOUT.GE.3) THEN
        TITLE='WAVE LENGTH'
        CALL POUT(10.,L,TITLE)
        ENDIF
```

```
      IF(IOUT.GE.4) THEN
      TITLE='WAVE CELERITY'
      CALL POUT(10.,C,TITLE)
      ENDIF

      IF(IOUT.GT.5) THEN
      TITLE='ENERGY FLUX'
      CALL POUT(0.01,F,TITLE)
      ENDIF

      IF(IOUT.GE.6) THEN
      TITLE='GROUP VELOCITY'
      CALL POUT(100.,Cg,TITLE)
      ENDIF

801 FORMAT(6F10.1)
803 FORMAT(6I10)
804 FORMAT(A6,T11,A5,T21,3F10.5)
805 FORMAT(A6,T11,I10)
806 FORMAT(8F10.4)
810 FORMAT(/,T20,A11,'REFRACTION AND SHOALING')
815 FORMAT(/)
820 FORMAT(' INPUT WAVE  =  ',F6.4,T30,'WAVE PERIOD = ',F6.3,T55,
   $        ' INPUT ANGLE =  ',F6.1)

825 FORMAT(' DELTA X =      ',F6.2,T30,'DELTA Y =      ',F6.2,T55,
   $        ' TOLERANCE =    ',F6.5)
830 FORMAT(' SURGE   =      ',F6.2,T30,'G       =      ',F6.3,T55,
   $        ' READ BC   =       ',A3)
832 FORMAT(' READ HEIGHTS =    ',A3,T30,'INTERCEPT =    ',F6.3,T55,
   $        ' SLOPE  =       ',F6.4,/,
   $        ' AMPLITUDE =    ',F6.3,T30,'PRINT START = ',I6,T55,
   $        ' PRINT STOP =   ',I6,/)

835 FORMAT(40I3)
840 FORMAT(10G10.3)
905 FORMAT(15X,8F12.8)
910 FORMAT(3I5,8F12.8,F12.5)
950 FORMAT(A8)
955 FORMAT(10F8.3)
960 FORMAT(10F8.1)

    END
```

```
C ***************************************************************************
      SUBROUTINE POUT(FACT,DUM,TITLE,IOUT)

      PARAMETER (NX=110,NY=110,NZ=NY*NX)
      COMMON /A5/ II,NI,JJ,NJ,IT,III
      DIMENSION KX(NY),DUM(NY,NX)
      CHARACTER TITLE*16,LINE*5

      LINE='-----'

      WRITE(11,900) TITLE
      WRITE(11,905) FACT

      NC = 20
      JMAX = NJ - JJ + 1
      JT   = JMAX/NC
      JTT  = MOD(JMAX,NC)
      IF(JTT.NE.0) JT=JT+1
      J1 = JJ
      J2 = J1+NC-1
      IF(J2.GT.NJ) J2=NJ

        DO 100 KK=1,JT
        WRITE(11,910) (J,J=J1,J2)
        WRITE(11,912) (LINE,J=J1,J2)
          DO 50 I=III,NI
            DO 40 J=J1,J2
            RND   = 0.5
            RND   = SIGN(RND,DUM(J,I))
            KX(J) = INT(FACT*DUM(J,I) + RND)
 40         CONTINUE
          WRITE(11,915) I,(KX(J),J=J1,J2)
 50       CONTINUE
C        WRITE(11,920)

        J1 = J1 + NC
        J2 = J2 + NC
        IF(J2.GT.NJ) J2=NJ

100     CONTINUE

900   FORMAT(/,T2,A16)
905   FORMAT(T2,'(MULTIPLIED BY ',F10.2,')')
910   FORMAT(/,' I/J :',20(2X,I3))
912   FORMAT(6X,20A5)
915   FORMAT(1X,I3,1X,':',20I5)
920   FORMAT('1')
      RETURN
      END
```

```
C ***************************************************************************
      SUBROUTINE ELLIP(I,MM)

      PARAMETER (NX=110,NY=110)
      REAL LAM,MU
      COMMON /A1/ D(NY,NX), H(NY,NX), LAM(NY), MU(NY)
      COMMON /A3/ Q(NY,NX), U(NY,NX), DELQMAX(NX)
      COMMON /A5/ II,NI,JJ,NJ,IT,III
      COMMON /A6/ PI,DELHMAX,GAM,G,T,DXDY,A

C STATEMENT FUNCTIONS FOR THE CALCULATION OF ELLIPTIC QUANTIES

      S(J,I)   = 1.0 + 8.0*Q(J,I)**2 - 8.0*Q(J,I)**4
      T02(J,I) = 1.0 - 2.0*Q(J,I)    + 2.0*Q(J,I)**4
      T03(J,I) = 1.0 + 2.0*Q(J,I)    + 2.0*Q(J,I)**4
      T04(J,I) = 1.0 +     Q(J,I)**2 +     Q(J,I)**6

        DO 101 J=JJ,NJ

        el     = H(J,I)/D(J,I)
        U(J,I) = G*H(J,I)*T*T / (D(J,I)*D(J,I))

C USE SUCCESSIVE UNDERRELAXATION PARAMETER (EXPONENTIAL FIT).

        R = EXP ( -0.61452 - 0.05249*U(J,I) )

          DO 30 M=1,MM
          LAM(J) = 16.0*Q(J,I)*(T04(J,I) / T02(J,I))**4
          Q1 = A* ( -1.0 - 2.0 * LAM(J) ) / 4.0
          QQ =EXP ( -SQRT ( 0.75*U(J,I)*(1. + el*Q1) ) / T02(J,I)**2 )
          DELQ = QQ - Q(J,I)
          QOLD = Q(J,I)
          Q(J,I) = QQ - (DELQ*R)
   30     CONTINUE

        DELQPC   = abs( ( QOLD - Q(J,I) ) ) / QOLD
        DELQMAX(I) = AMAX1(DELQMAX(I),DELQPC)

C CALCULATE NECESSARY ELLIPTIC QUANTITIES.

         LAM(J) = 16.0*Q(J,I)*(T04(J,I)/T02(J,I))**4
         MU(J)  = ( 2.0/ (-ALOG ( Q(J,I)) ) - S(J,I) + T03(J,I)**4) /
     $              T02(J,I)**4
  101    CONTINUE

         RETURN
         END
```

```
C ***************************************************************************
      SUBROUTINE LENGTH (I)

      PARAMETER (NX=110,NY=110)
      REAL LAM,MU,L
      COMMON /A1/ D(NY,NX), H(NY,NX), LAM(NY), MU(NY)
      COMMON /A2/ L(NY,NX), C(NY,NX), C0(NY), C1(NY), C2(NY),
     $            ALFA(NY,NX)
      COMMON /A5/ II,NI,JJ,NJ,IT,III
      COMMON /A6/ PI,DELHMAX,GAM,G,T,DXDY,A

        DO 102 J=JJ,NJ

        e1 = H(J,I)/D(J,I)
        e2 = e1*e1

        C0(J) = SQRT(G*D(J,I))
        C1(J) = ( 1.0 + 2.0*LAM(J) - 3.0*MU(J) )*0.5
        C2(J) = A * ( - 6.0 - 16.0*LAM(J) + 5.0*MU(J)
     $              - 16.0*LAM(J)**2 + 10.0*LAM(J)*MU(J)
     $              + 15.0*MU(J)**2 ) / 40.0
        C(J,I)    = C0(J)*( 1.0 + e1*C1(J) + e2*C2(J) )
        L(J,I)    = C(J,I)*T

  102   CONTINUE

      RETURN
      END

C ***************************************************************************
      SUBROUTINE ANGLE(I)
      PARAMETER (NX=110,NY=110)
      REAL L
      COMMON /A2/ L(NY,NX), C(NY,NX), C0(NY), C1(NY), C2(NY),
     $            ALFA(NY,NX)
      COMMON /A5/ II,NI,JJ,NJ,IT,III
      COMMON /A6/ PI,DELHMAX,GAM,G,T,DXDY,A

      IP = I+1
        DO 45 J=JJ+1,NJ-1
        JM = J-1
        JP = J+1
        ALFA(J,I) = ASIN( (SIN( ALFA(J,IP) ) / L(J,IP) - 0.5*DXDY*
     $  ( COS(ALFA(JP,IP)) / L(JP,IP) - COS(ALFA(JM,IP)) / L(JM,IP) ))
     $  * L(J,I) )

C CORRECT FOR ASIN FUNCTION
        ALFA(J,I) = PI - ALFA(J,I)
   45   CONTINUE

      RETURN
      END
```

```
C ***************************************************************************
      SUBROUTINE EFLUX(I,NF)

      PARAMETER (NX=110,NY=110)
      REAL LAM,MU,L
      COMMON /A1/ D(NY,NX), H(NY,NX), LAM(NY), MU(NY)
      COMMON /A2/ L(NY,NX), C(NY,NX), C0(NY), C1(NY), C2(NY),
     $            ALFA(NY,NX)
      COMMON /A4/ F(NY,NX), F0(NY), F1(NY), Eone(NY), Cg(NY,NX)
      COMMON /A5/ II,NI,JJ,NJ,IT,III
      COMMON /A6/ PI,DELHMAX,GAM,G,T,DXDY,A

        DO 103 J=JJ,NJ
        RL  = LAM(J)
        RM  = MU(J)
        RL2 = RL*RL
        RL3 = RL2*RL
        RM2 = RM*RM
        RM3 = RM2*RM
        e1 = H(J,I) / D(J,I)
        F0(J) = ( -RL + 2.0*RM + 4.0*RL*RM - RL2 - 3.0*RM2 ) / 3.0
        F1(J) = A * (  -4.0*RL  + 8.0*RM  + 53.0*RL*RM - 12.0*RL2
     $                 -60.0*RM2 + 53.0*RL2*RM - 120.0*RL*RM2
     $                 -8.0*RL3 + 75.0*RM3 ) / 30.0
        Eone(J) = A * ( RL - 2.0*RM - 17.0*RL*RM + 3.0*RL2
     $                 -17.0*RL2*RM + 2.0*RL3 + 15.0*RM3 ) / 30.0
        Cg2     = ( F1(J) - Eone(J) ) / F0(J)
        Cg(J,I) = C0(J) * ( 1.0 + e1 * A * Cg2 )
  103 CONTINUE
        IF(NF.EQ.0) THEN
          DO 104 J=JJ,NJ
          e1     = H(J,I) / D(J,I)
          F3     = GAM * C0(J) * ( F0(J) + e1*F1(J) )
          F(J,I) = H(J,I)**2 * F3
  104     CONTINUE
        ELSE
          IP = I+1
          DO 105 J=JJ+1,NJ-1
          JP = J+1
          JM = J-1
          e1 = H(J,I) / D(J,I)
          F3 = GAM * C0(J) * ( F0(J) + e1*F1(J) )
C         SOLVE FOR ENGERY FLUX (DEL DOT F)
          F(J,I) = ( F(J,IP) * COS(ALFA(J,IP)) + 0.5 * DXDY *
     $  ( F(JP,IP) * SIN(ALFA(JP,IP)) - F(JM,IP) * SIN(ALFA(JM,IP)) ) )
     $  / COS(ALFA(J,I))
          HNEW = SQRT( F(J,I)/F3 )
          DELPC  = ABS( HNEW - H(J,I) ) / H(J,I)
          H(J,I) = HNEW
          DELHMAX = AMAX1(DELHMAX,DELPC)
  105     CONTINUE
        ENDIF

      RETURN
      END
```

APPENDIX D

REFRACTION OF SECOND-ORDER CNOIDAL WAVES OVER A PLANE BOTTOM - PLOTS

This appendix contains plots of nondimension wave height vs. depth for the Refraction of second-order cnoidal waves over a plane bottom slope of 1:50. The plots contained in this appendix are companion plots to Figures 6.15 to 6.29, which are plots of nondimension wave angle vs. depth. For complete information on these simulations the reader is referred to Chapter VI, Section 6.2.2.

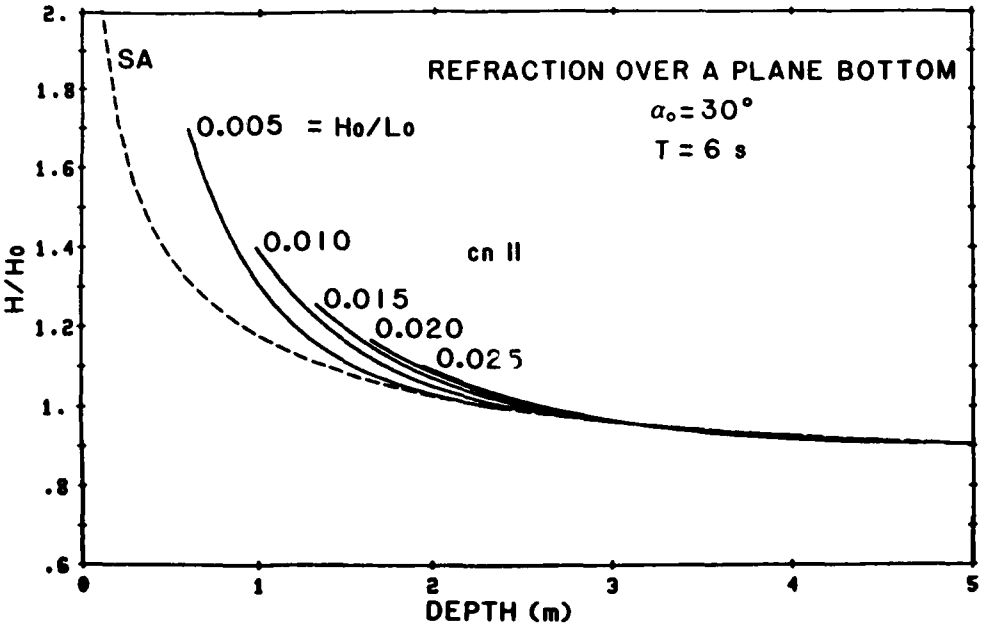

Figure D.1 Wave Height - Refraction over a plane bottom (1:50), α_o = 30°, T = 6 s

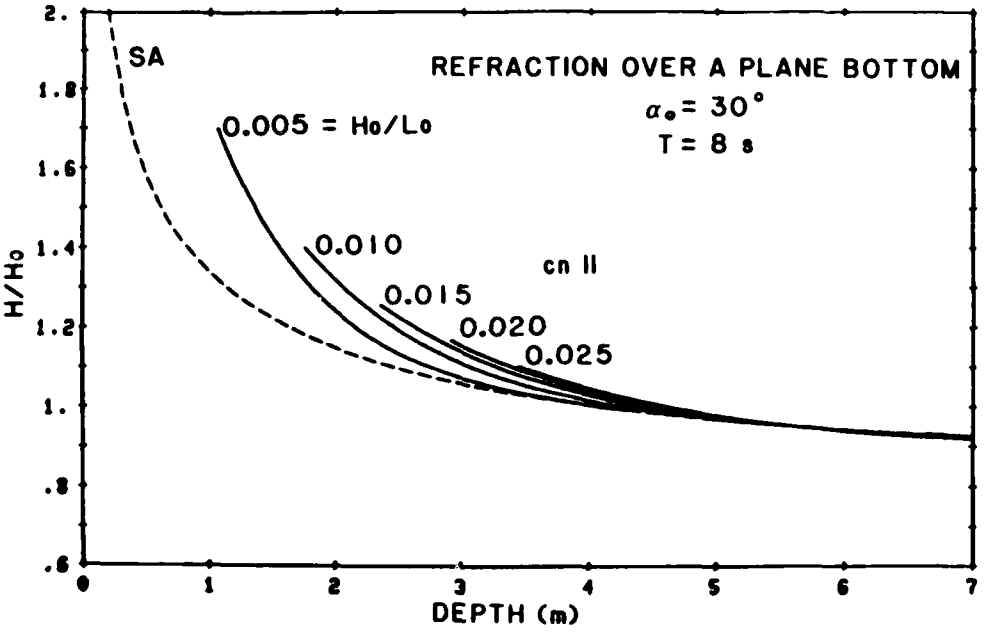

Figure D.2 Wave Height - Refraction over a plane bottom (1:50), α_o = 30°, T = 8 s

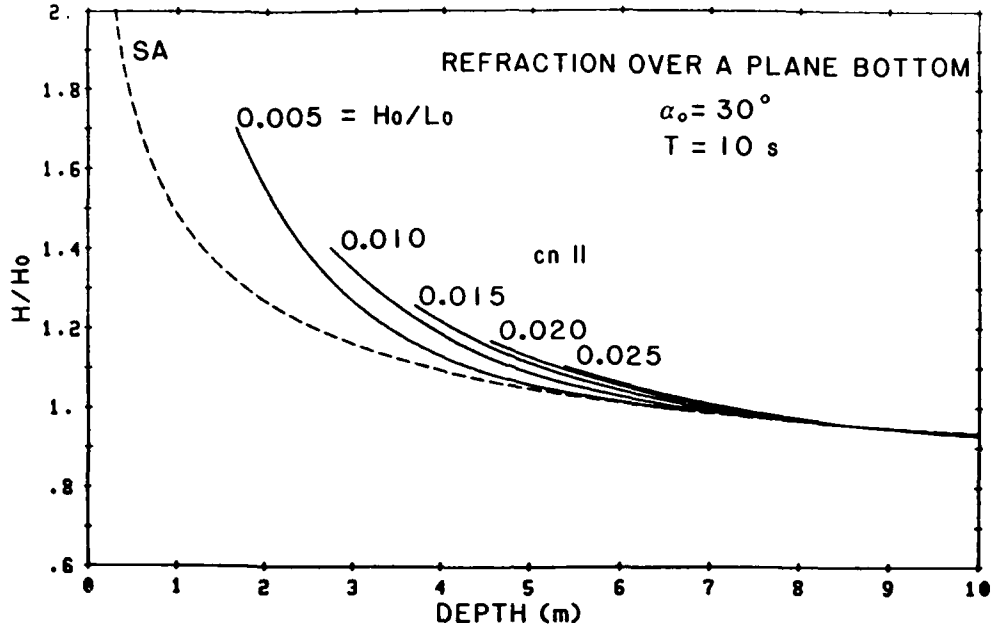

Figure D.3 Wave Height - Refraction over a plane bottom (1:50), α_o = 30°, T = 10 s

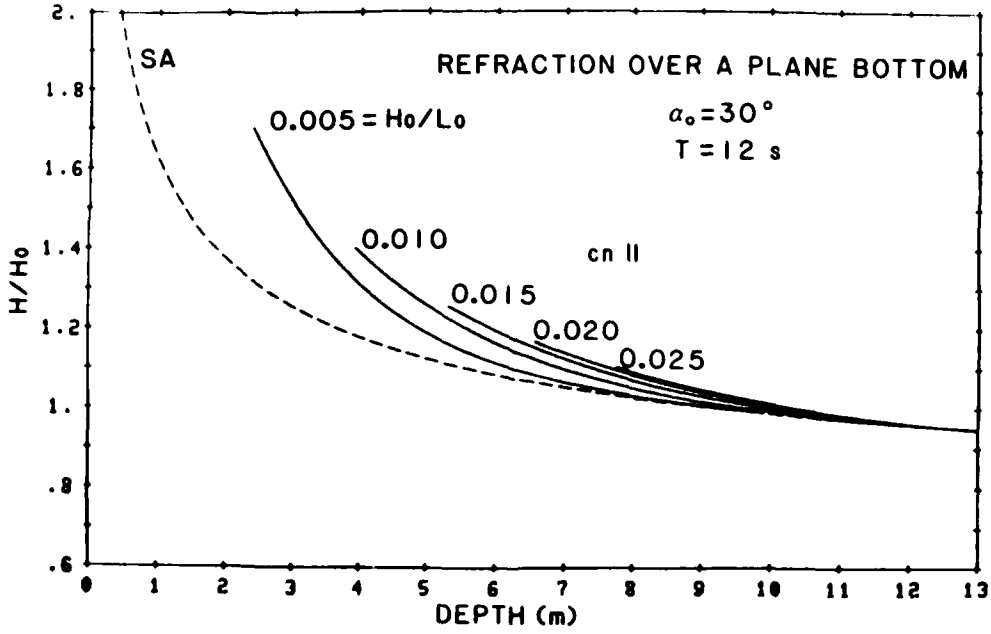

Figure D.4 Wave Height - Refraction over a plane bottom (1:50), α_o = 30°, T = 12 s

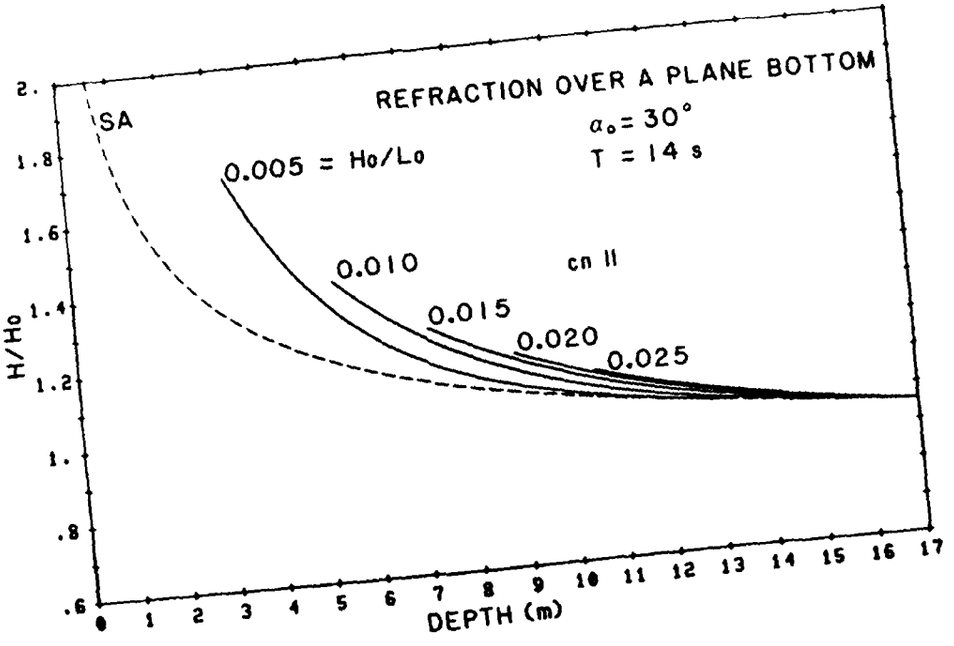

Figure D.5 Wave Height - Refraction over a plane bottom (1:50), α_o = 30°, T = 14 s

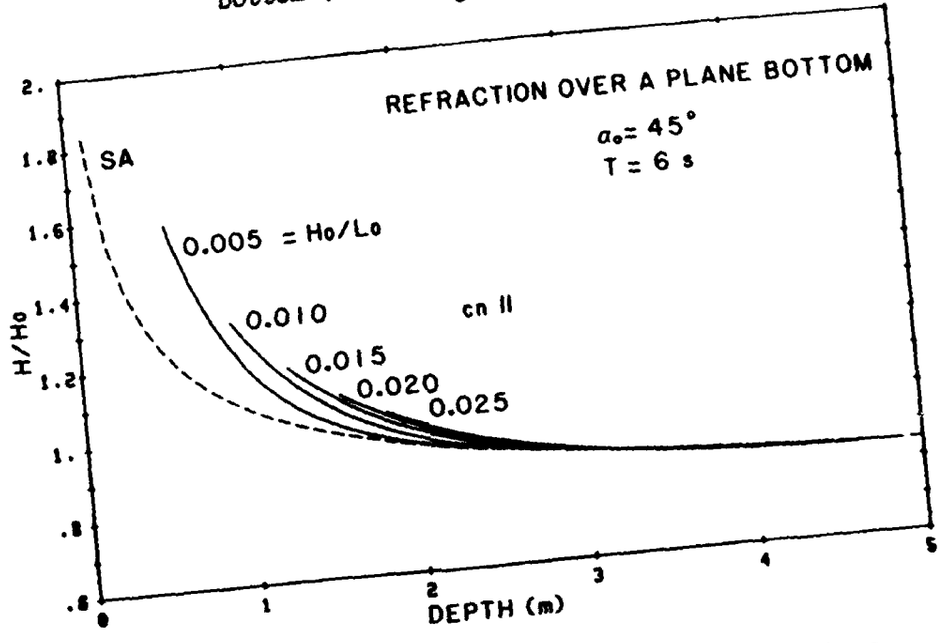

Figure D.6 Wave Height - Refraction over a plane bottom (1:50), α_o = 45°, T = 6 s

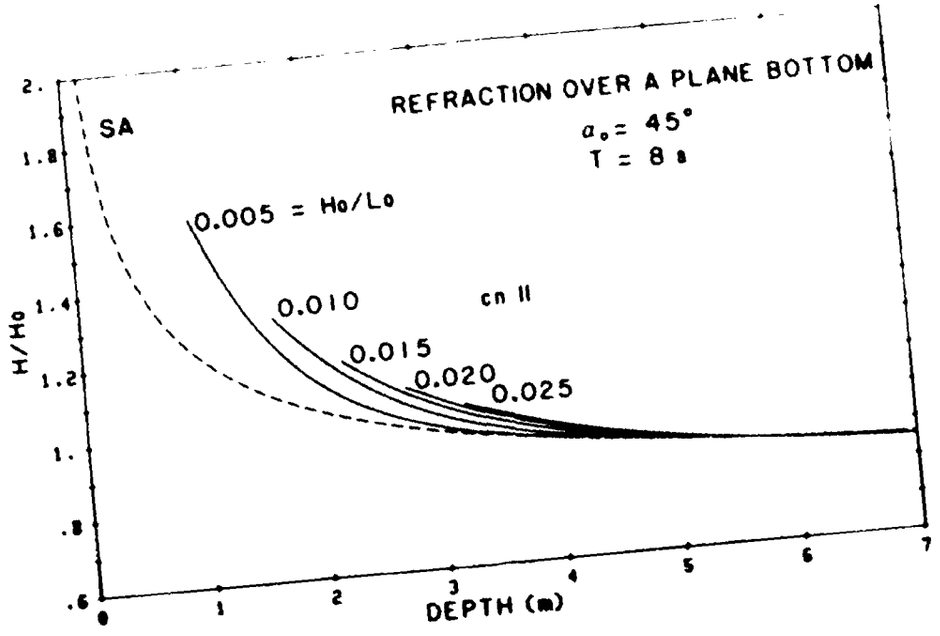

Figure D.7 Wave Height - Refraction over a plane bottom (1:50), α_o = 45°, T = 8 s

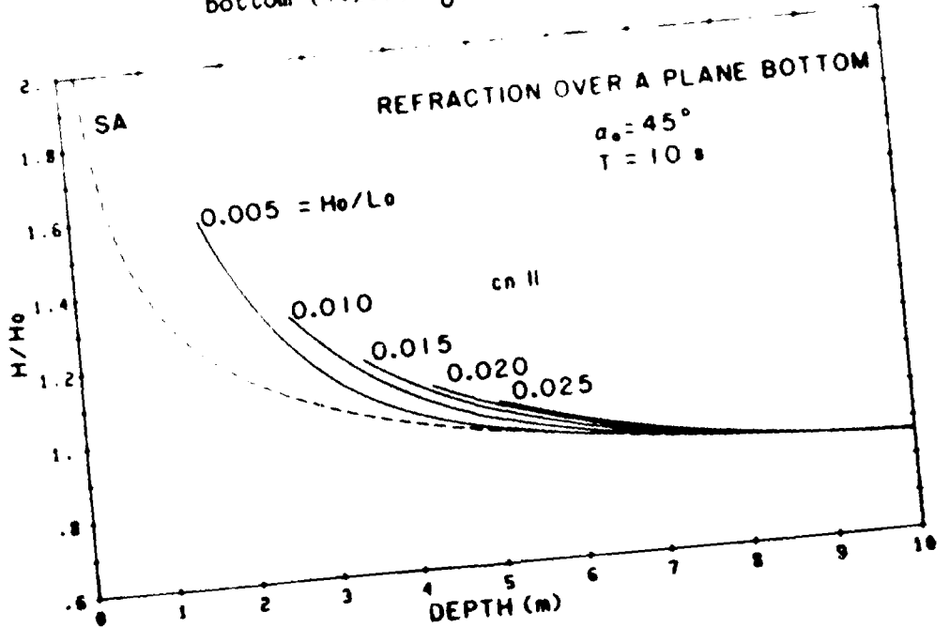

Figure D.8 Wave Height - Refraction over a plane bottom (1:50), α_o = 45°, T = 10 s

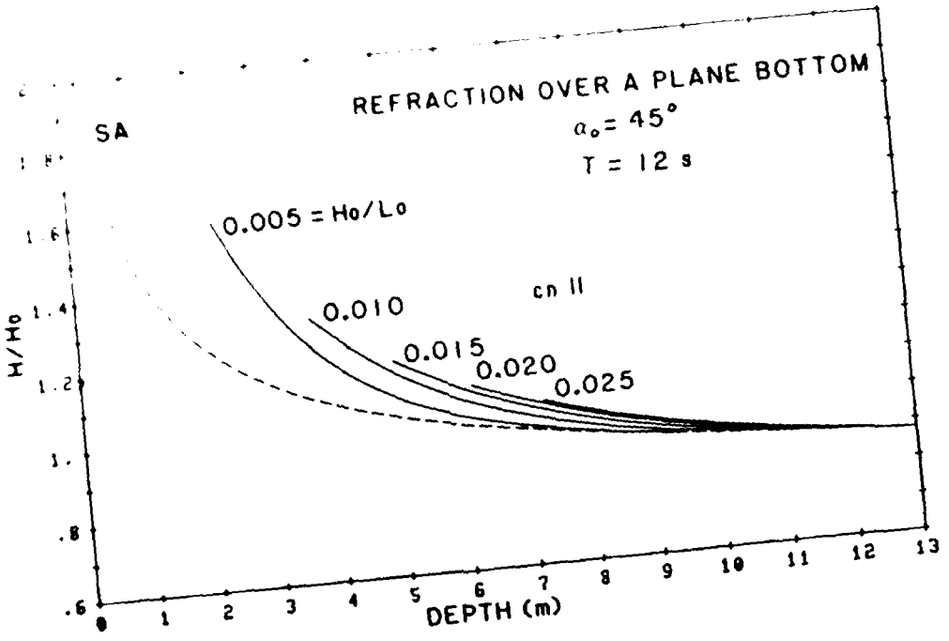

Figure D.9 Wave Height - Refraction over a plane bottom (1:50), α_o = 45°, T = 12 s

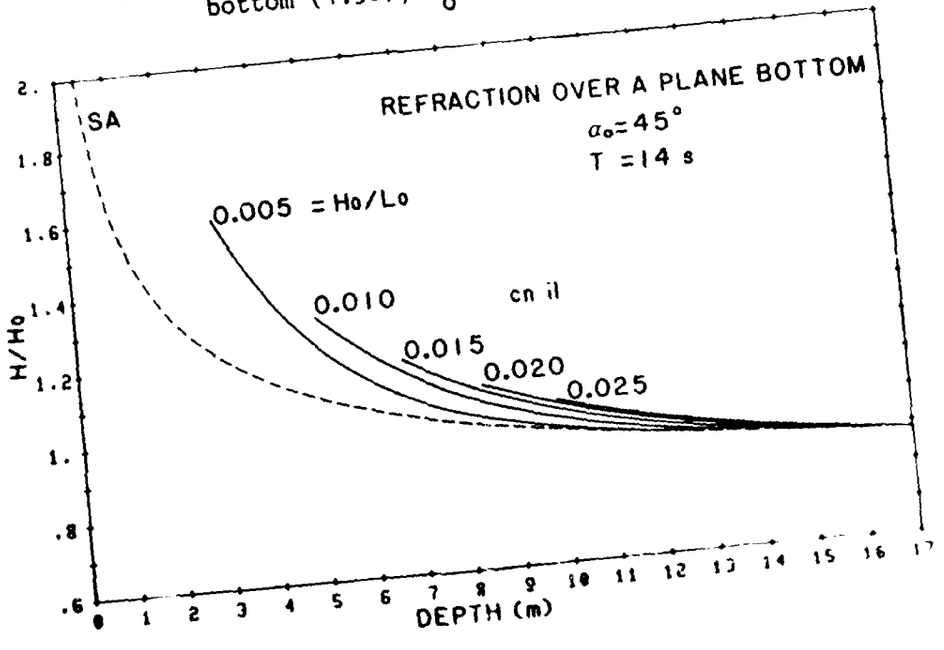

Figure D.10 Wave Height - Refraction over a plane bottom (1:50), α_o = 45°, T = 14 s

AD-A182 741 A NUMERICAL MODEL FOR SHOALING AND REFRACTION OF SECOND-ORDER CNOIDAL WAV (U) COASTAL ENGINEERING RESEARCH CENTER VICKSBURG MS T A HARDY ET AL MAY 86 3/3

UNCLASSIFIED CERC-MP-87-9 F/G 20/4 NL

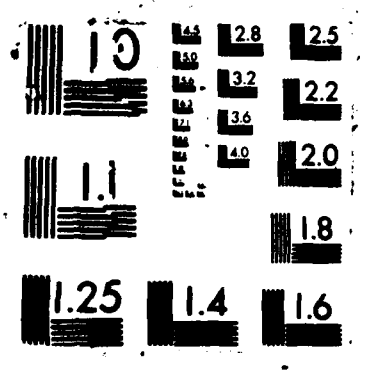
2.8
2.5
3.2
2.2
3.6
4.0
2.0
1.8
1.25
1.4
1.6

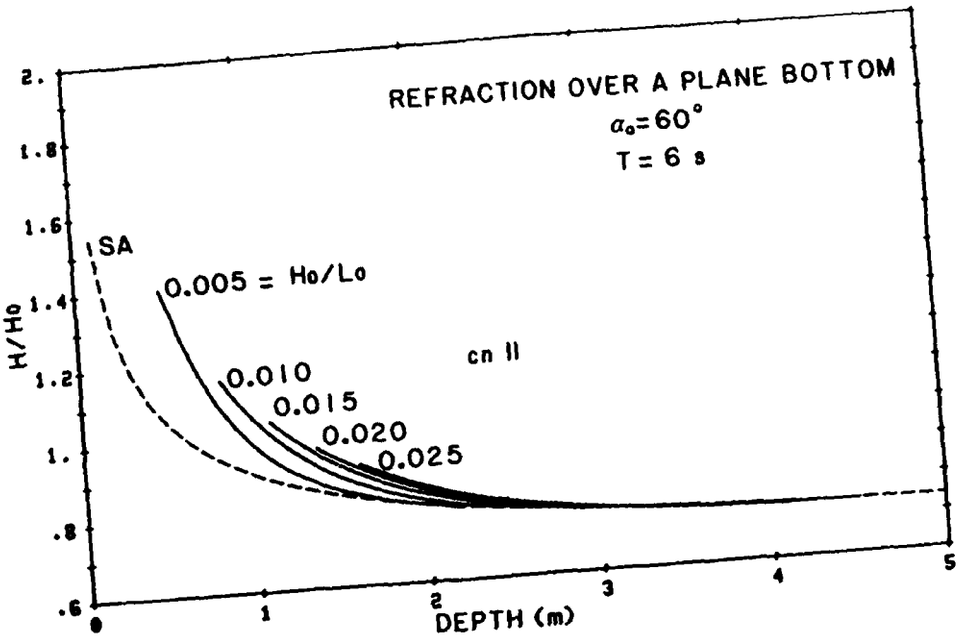

Figure D.11 Wave Height - Refraction over a plane bottom (1:50), α_o = 60° T = 6 s

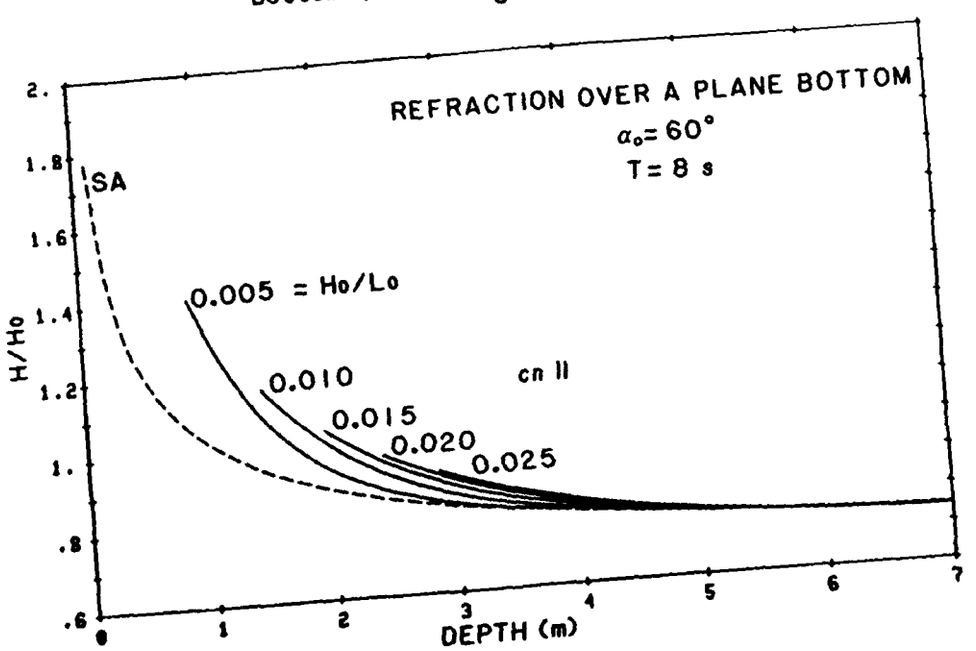

Figure D.12 Wave Height - Refraction over a plane bottom (1:50), α_o= 60°, T = 8 s

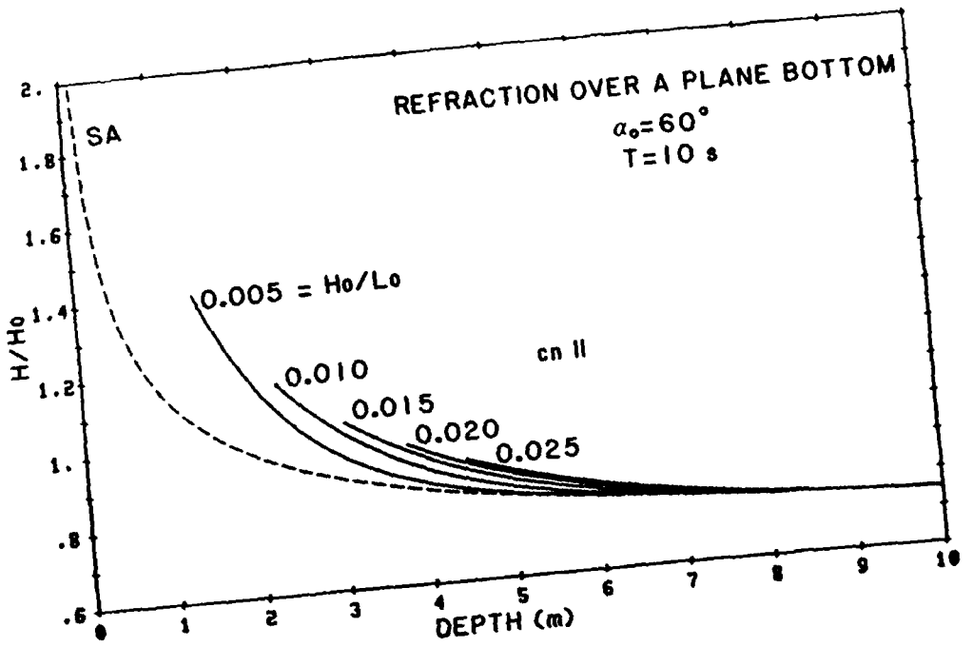

Figure D.13 Wave Height - Refraction over a plane bottom (1:50), α_o = 60°, T = 10 s

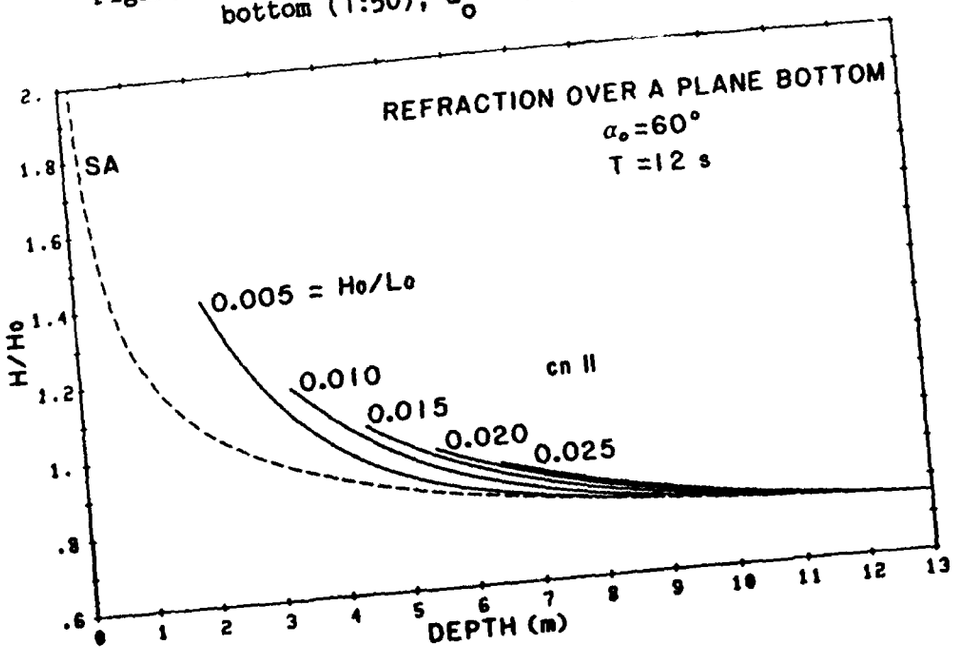

Figure D.14 Wave Height - Refraction over a plane bottom (1:50), α_o = 60°, T = 12 s

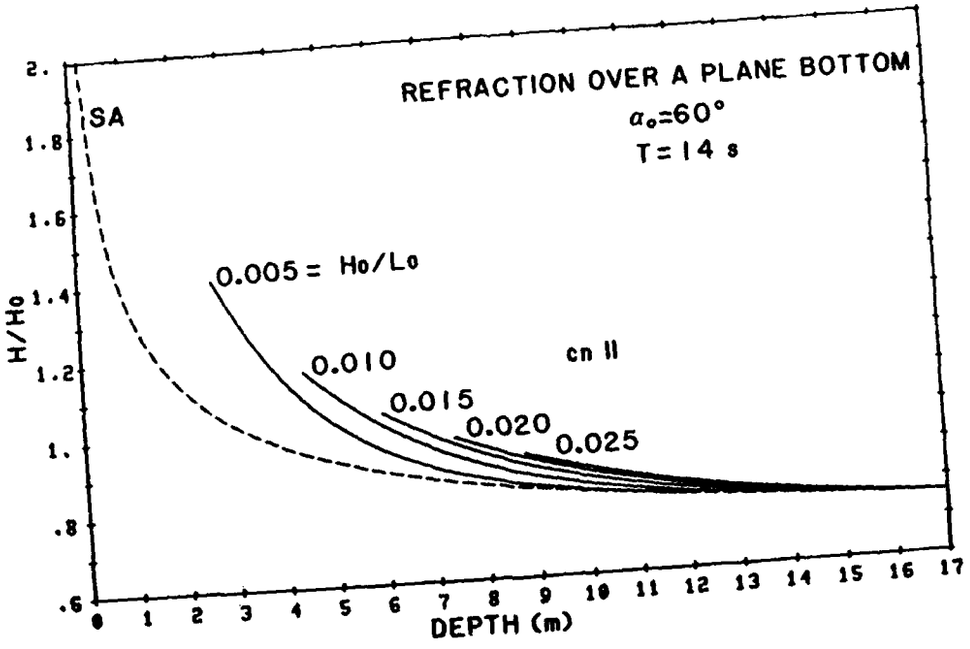

Figure D.15 Wave Height - Refraction over a plane bottom (1:50), α_o = 60°, T = 14 s

APPENDIX E

NOTATION

The following symbols are used in this thesis:

a	Depth at shoreline for calculated bathymetry
a_n	Term used to simplify η ($n = 0,1,2,3,4$)
A_n	Term in equation for η ($n = 0,1,2$)
b	Bottom slope of plane beach portion of calculated bathymetry
b_n	Term used to simplify u and w ($n = 1,2,3...7$)
b_{00}	Coefficient in zeroth-order of the stream function
B_{mn}	Term in equations for u and w ($m = 0,1,2$; $n = 0,1$)
c_n	$cn^n\theta$ ($n = 1,2,3$)
C	Wave celerity
C_g	Magnitude of group velocity
$\vec{C}_g$	Group velocity
C_n	Nth-order component of wave celerity ($n = 0,1,2...$)
d_n	Nth-order component in expansion of (D/L) ($n = 1,2,3...$)
D	Water depth measured to the stillwater level
d	Amplitude of cosine portion of rhythmic bathymetry
E	Average wave energy per unit surface area
E_n	Nth-order component to E ($n = 0,1$)
E_e	Complete elliptic integral of second kind
E'_e	$E(\kappa')$
E_k	Average kinetic energy per unit surface area due to waves
E_p	Average potential energy per unit surface area due to waves
E^*_p	E_p plus potential energy of still water

$f(t)$	Function added to Bernoulli equation to make Bernoulli constant vanish
F	Average wave energy flux in direction of wave propagation
$\overrightarrow{F}$	Average wave energy flux
F_n	Nth-order contributions to F (n = 0,1)
$F_{S\&I}$	Wave energy flux from Sarpkaya and Isaacson (1981)
$F_{j,i}$	Component of energy flux
g	Acceleration of gravity
H	Wave height
H_b	Wave height of breaking
H_o	Deepwater wave height
i	$=\sqrt{-1}$
$\hat{i}$	Unit vector in x-direction
$\hat{j}$	Unit vector in y-direction
k	Wave number, $2\pi/L$
k_{SA}	Wave number from small-amplitude wave theory
K	Complete elliptic integral of the first kind
K'	$K(\kappa')$
K_r	Refraction coefficient for small-amplitude waves
K_s	Shoaling coefficient for small-amplitude waves
L	Wavelength
L_{SA}	Wavelength from small-amplitude wave theory
L_o	Deep water wavelength
m	Number of nodes in x-direction
n	Number of nodes in y-direction
N	Nondimensional water surface elevation
N_n	Nth-order contribution to N (n = 1,2,3...)

p	Pressure
p_B	Bernoulli constant
P	Nondimensional pressure
P_B	Nondimensional Bernoulli constant
P_n	Nth-order component to expansion of P (n = 0,1,2...)
q	Nome of the theta function or Flow rate (used only in Chapter II)
q'	Complementary nome of the theta function
q'^*	Value of q before relaxation
Q	Nondimensional flow rate
Q_n	Nth-order component to expansion of Q (n = 0,1,2...)
R	Under-relaxation parameter
S	Quantity used in calculation of E
t	Time
T	Wave period
$T_i()$	Neville's notation for theta functions (i = c,d,n,s)
$T_i()$	Theta functions (i = 1,2,3,4)
T_{0i}	T(0) (i = 2,3,4)
u	Horizontal component of the orbital water particle velocity
$\vec{u}$	Oribital water particle velocity
$\langle\overline{u_n^2}\rangle$	Term used to simplify calculation of E and F (n = 1,2,3)
U	Ursell parameter
U_n	Term used to simplify calculation of F (n = 1,2,3)
w	Vertical component of the orbital water particle velocity
$\langle\overline{w_n^2}\rangle$	Term used to simplify calculation of E (n = 1,2,3)
W_n	Term used to simplify calculation of E (n = 1,2,3)
x	Horizontal coordinate

x_b	Location of wave breaking
Δx	Node spacing in x-direction
X	Nondimensional horizontal coordinate or = x-Ct (in Equations B.5 to B.1 only)
Δy	Node spacing in y-direction
y	horizontal coordinate
Y	= (z + D)/D
z	Vertical coordinate
Z	Nondimensional vertical coordinate
α	Angle of wave propagation
α_b	Wave angle at breaking
α_o	Deepwater wave angle
β	= $\pi\theta/2K$
β'	= $\pi\theta/2K'$
δ	Auxiliary parameter for the perturbation expansion
ε	= H/D, perturbation parameter
η	Water surface elevation
η_{SA}	η as determined from small amplitude wave theory
η_n	Nth-order components of η (n = 1,2,3...)
θ	Argument to the Jacobian elliptic functions
θ_{SA}	Small-amplitude wave phase function
κ	Modulus of the elliptic integral
κ'	Complementary modulus of the elliptic integral
λ	Term used to simplify elliptic calculations
μ	Term used to simplify elliptic calculations
ξ	The elliptic integral
π	The constant π

Π The unified nonlinearity parameter of Goda

ρ Density of water

ϕ Dummy argument of elliptic integral or
Velocity potential

Φ Nondimensional velocity potential

ψ Stream function

Ψ Nondimensional stream function

Ψ_n Nth-order contribution to the stream function (n = 0,1,2...)

Ω The portion of the wave phase used in deriving the wave angle equation

∇ Horizontal gradient operator

$\langle\rangle$ Denotes integration over depth from -D to η

$\overline{}$ Denotes integration over wavelength

END

8-87

DTIC